

**ISTANBUL TECHNICAL UNIVERSITY ★ ENERGY INSTITUTE**

**THE INVESTIGATION OF THE IRRADIATION EFFECT ON  
PMMA/MWCNTs POLYMER NANOCOMPOSITES**



**M.Sc. THESIS**

**Songül ULAĞ**

**Nuclear Researches Division**

**Radiation Science and Technology Programme**

**DECEMBER 2017**



**ISTANBUL TECHNICAL UNIVERSITY ★ ENERGY INSTITUTE**

**THE INVESTIGATION OF THE IRRADIATION EFFECT ON  
PMMA/MWCNTs POLYMER NANOCOMPOSITES**

**M.Sc. THESIS**

**Songül ULAĞ  
(302151002)**

**Nuclear Researches Division**

**Radiation Science and Technology Programme**

**Thesis Advisor: Prof. Dr. Nilgün BAYDOĞAN**

**DECEMBER 2017**



**İSTANBUL TEKNİK ÜNİVERSİTESİ ★ ENERJİ ENSTİTÜSÜ**

**PMMA/MWCNT POLİMER NANOKOMPOZİTLER ÜZERİNE RADYASYON  
ETKİSİNİN İNCELENMESİ**

**YÜKSEK LİSANS TEZİ**

**Songül ULAĞ  
(302151002)**

**Nükleer Araştırmalar Anabilim Dalı**

**Radyasyon Bilim ve Teknoloji Programı**

**Tez Danışmanı: Prof. Dr. Nilgün BAYDOĞAN**

**ARALIK 2017**



Songül Ulađ, M.Sc. student of ITU Institute of Energy student ID 302151002, successfully defended the thesis entitled “THE INVESTIGATION OF THE IRRADIATION EFFECT ON PMMA/MWCNTs POLYMER NANOCOMPOSITES”, which she prepared after fulfilling the requirements specified in the associated legislations, before the jury whose signatures are below.

**Thesis Advisor :**    **Prof. Dr. Nilgün BAYDOĐAN**    .....

Istanbul Technical University

**Jury Members :**    **Prof. Dr. Sema AKYIL ERENTÜRK**    .....

Istanbul Technical University

**Prof. Dr. Ayben KİLİSLİOĐLU**    .....

Istanbul University

**Date of Submission : November 17, 2017**

**Date of Defense : December 13, 2017**







*To Gökhan Ulaş,*



## FOREWORD

I would like to express my thankfulness to my advisor Prof. Dr. Nilgün Baydoğan for her patience, motivations and sparing her time during the preparation of this thesis.

I especially thanks to The Scientific and Technical Research Council of Turkiye (TUBITAK) for my scholar support at TUBITAK 1001 project with 115R017 project no and the financial support of ITU BAP at this MSc.Thesis Project with MYL-2017-40886 project no during this study.

I am grateful to the Prof.Dr. Adnan Tekin Materials Science and Production Technologies Applied Research Center (ATARC) personels for their supports also thankful to my laboratory colleagues Tayfun Bel, Güzde Kara, Emre Doğan, Abdullah Akın, Maihemuti Maimaitituersun for their supports.

I am thankful to Dr. Muhittin Okka and MSc. Sahip Kızıldaş and ITU TRIGA Mark-II Research and Training Reactor personels.

I especially thanks to my friends; Damla Fidan, Gülhan Kaya, Melis Pahalı, Sultan Güçlü for their friendships that give me confidence and strength.

I am deeply thankful to my sister Berna Ulağ for her special help to design the graphs in this thesis results section.

I would also like to thank my cousin Gülcan for her moral support and being willing to help me when I run into problems.

I am deeply thankful to my family for their constant support and unconditional love.

I am thankful to the memory of my father. Years may come and go but his memory will never be erased.

December 2017

Songül ULAĞ  
Physics Engineer



## TABLE OF CONTENTS

	<u>Page</u>
<b>FOREWORD</b> .....	<b>ix</b>
<b>TABLE OF CONTENTS</b> .....	<b>xi</b>
<b>ABBREVIATIONS</b> .....	<b>xiii</b>
<b>LIST OF TABLES</b> .....	<b>xv</b>
<b>LIST OF FIGURES</b> .....	<b>xix</b>
<b>SUMMARY</b> .....	<b>xxiii</b>
<b>ÖZET</b> .....	<b>xxvi</b>
<b>1. INTRODUCTION</b> .....	<b>1</b>
1.1 Polymers .....	1
1.1.1 Polymer fundamentals .....	1
1.1.2 Properties and applications of PMMA .....	3
1.1.2.1 Characteristic properties of PMMA.....	4
1.1.2.2 Application areas of PMMA .....	6
1.2 Nanotechnology and Nanomaterials.....	6
1.2.1 Properties of nanomaterials.....	7
1.2.2 Classification of nanomaterials .....	8
1.2.3 Multiwall carbon nanotube-derived nanomaterials .....	10
1.2.4 Properties of multiwall carbon nanotubes (MWCNTs).....	12
1.2.5 CNTs derived materials .....	13
1.3 Polymer Nanocomposites .....	13
<b>2. BACKGROUND AND LITERATURE REVIEW</b> .....	<b>14</b>
2.1 Synthesize of PMMA via ATRP .....	14
2.1.1. MMA monomer .....	15
2.1.2 Initiator .....	16
2.1.3 Catalyst .....	16
2.1.4 Ligand .....	17
2.1.5 Solvent .....	17
2.1.6 Temperature .....	17
2.2 ATRP Mechanism .....	18
2.3 Synthesize of Polymer/MWCNTs Nanocomposites .....	19
2.3.1 In-situ polymerization.....	19
2.3.2 Solution mixing .....	20
2.3.3 Melt compounding.....	21
2.4 Thermal Properties of Polymer .....	21
2.4.1 Thermogravimetric analysis.....	22
2.5 Mechanical Properties of Polymer Nanocomposite .....	22
2.5.1 Hardness.....	22
2.6 Ultrasonic Test .....	24
2.7 The Use of Gamma Transmission Technique at Polymers.....	26
2.8. The Use of Howitzer Technique with Pu-Be Neutron Source at Polymers.....	29
<b>3. EXPERIMENTAL</b> .....	<b>32</b>
3.1 Materials .....	32
3.2 Preparation of PMMA/ MWCNT Nanocomposite Sample .....	32
3.3 SEM Characterization.....	34
3.4 Fourier Transform Infrared Spectroscopy (FTIR) .....	36

3.5 X-Ray Diffraction (XRD) .....	37
3.6 Thermal Stability of PMMA/MWCNTs .....	38
3.7 Ultrasonic Test .....	38
3.8 Mechanical properties of PMMA/MWCNTs .....	40
3.8.1 Rockwell hardness .....	40
3.8.2 Density assesment of PMMA/MWCNTs nanocomposite by using pycnometer method.....	40
3.9 Application of Gamma Transmission Technique .....	41
3.10 Application of Pu-Be Neutron Howitzer (NH3).....	42
3.11 Absorbed Dose of PMMA/MWCNTs Nanocomposite .....	44
3.11.1 Irradiation conditions of the PMMA/MWCNTs nanocomposites .....	44
<b>4. RESULTS .....</b>	<b>46</b>
4.1 SEM Characterization.....	46
4.2 Fourier Transform Infrared Spectroscopy (FTIR) characterization .....	47
4.3 XRD Characterization .....	48
4.4 TGA Analysis .....	49
4.5 Mechanical Properties of PMMA/MWCNTs .....	51
4.5.1 Hardness .....	51
4.6 Gamma Transmission Technique and Pu-Be Neutron Source .....	52
4.6.1 Radiation process by using Cs-137 radioisotope .....	52
4.6.2 Radiation process by using Co-60 radioisotope .....	58
4.6.3 The application of the gamma transmission technique for the irradiated PMMA/MWCNTs nanocomposites at 50 kGy.....	64
4.6.4 The application of the neutron transmission technique for the unirradiated PMMA/MWCNTs nanocomposite by using Neutron Howitzer .....	72
4.6.5 The application of the neutron transmission technique for the irradiated PMMA/MWCNTs nanocomposites by using neutron Howitzer.....	76
4.7 Ultrasonic Test.....	81
<b>5. DISCUSSIONS .....</b>	<b>84</b>
<b>6. CONCLUSIONS .....</b>	<b>89</b>
<b>REFERENCES .....</b>	<b>91</b>
<b>CURRICULUM VITAE.....</b>	<b>95</b>

## ABBREVIATIONS

<b>ATRP</b>	: Atom Transfer Radical Polymerization
<b>Bu<sub>4</sub>NBr</b>	: Tetra-n-butylammonium bromide
<b>CREB</b>	: Cyclic amp-Response Element Binding protein
<b>CTE</b>	: Coefficient of Linear Thermal Expansion
<b>D</b>	: Dimension
<b>EBiB</b>	: Ethyl 2-bromoisobutyrate
<b>EGFR</b>	: Estimated Glomerular Filtration Rate
<b>FTIR</b>	: Fourier Transform Infrared Spectroscopy
<b>MWCNTs</b>	: Multi Wall Carbon Nanotubes
<b>MMA</b>	: Methyl Methacrylate
<b>PC</b>	: Polycarbonate
<b>PKA</b>	: Protein Kinase A
<b>PMDETA</b>	: 1, 1, 4, 7, 7- Pentamethyldiethylenetriamine
<b>PMMA</b>	: Poly (methyl methacrylate)
<b>PVC</b>	: Polyvinyl Chloride
<b>SEM</b>	: Scanning Electron Microscopy
<b>UV</b>	: Ultraviolet
<b>TGA</b>	: Thermal Gravimetric Analysis
<b>XRD</b>	: X-ray Diffraction





## LIST OF TABLES

	<b>Page</b>
<b>Table 1.1:</b> Thermal properties of PMMA.....	4
<b>Table 1.2:</b> Mechanical properties of PMMA.....	5
<b>Table 1.3:</b> Electrical properties of PMMA.....	5
<b>Table 1.4:</b> Main properties of PMMA .....	6
<b>Table 2.1:</b> Significant properties of MMA. ....	16
<b>Table 3.1:</b> Properties of the Pu-Be Neutron Howitzer (NH <sub>3</sub> ).....	43
<b>Table 3.2:</b> The properties of the Co-60 Radioisotope and irradiation conditions.....	45
<b>Table 4.1:</b> 5% weight loss temperatures of pure PMMA and PMMA/MWCNTs nanocomposites for unirradiated state. ....	50
<b>Table 4.2:</b> 5% weight loss temperatures of pure PMMA polymer and PMMA/MWCNTs polymer nanocomposites after irradiation process. ....	51
<b>Table 4.3:</b> Experimental results of pure PMMA against Cs-137 radioisotopes.....	53
<b>Table 4.4:</b> Experimental results of the gamma transmission properties of PMMA/MWCNTs 0.25 wt.% against Cs-137 radioisotopes.....	54
<b>Table 4.5:</b> Experimental results of the gamma transmission properties of 0.5 wt % PMMA/MWCNTs against Cs-137 radioisotopes. ....	55
<b>Table 4.6:</b> Experimental results of the gamma transmission properties of PMMA/MWCNTs 1 wt. % against Cs-137 radioisotopes .....	55
<b>Table 4.7:</b> Experimental results of the gamma transmission properties of PMMA/MWCNTs 2 wt. % against Cs-137 radioisotopes .....	56
<b>Table 4.8:</b> The compositions of the PMMA nanocomposite samples at different MWCNTs . ....	57
<b>Table 4.9:</b> The density values of the PMMA/MWCNTs samples.....	57
<b>Table 4.10:</b> The difference between the linear and mass attenuation coefficients.....	57
<b>Table 4.11:</b> Experimental results of the pure PMMA against the Co-60 radioisotope.....	58
<b>Table 4.12:</b> Experimental results of the gamma transmission properties of PMMA/MWCNTs 0.25 wt.% against Co-60 radioisotopes. ....	59
<b>Table 4.13:</b> Experimental results of the gamma transmission properties of PMMA/MWCNTs 0.5 wt.% against Co-60 radioisotopes. ....	60
<b>Table 4.14:</b> Experimental results of the gamma transmission properties of PMMA/MWCNTs 1wt. % against Co-60 radioisotopes.....	61
<b>Table 4.15:</b> Experimental results of the gamma transmission properties of PMMA/MWCNTs 2 wt.% against Co-60 radioisotopes.....	62
<b>Table 4.16:</b> The difference between the experimental and theoretical mass attenuation coefficients.....	63

<b>Table 4.17:</b>	Experimental results of the gamma transmission for the irradiated PMMA/MWCNTs at 0.5 wt.% for Cs-137 radioisotope. ....	64
<b>Table 4.18:</b>	Experimental results of the gamma transmission technique of irradiated PMMA/MWCNTs at 1wt.% MWCNTs for Cs-137 radioisotope. ....	65
<b>Table 4.19:</b>	Experimental results of the gamma transmission technique of the irradiated PMMA/MWCNTs at 2 wt. % .....	66
<b>Table 4.20:</b>	The density values of the irradiated PMMA/MWCNTs at 50kGy. ....	67
<b>Table 4.21:</b>	The linear and mass attenuation coefficients of irradiated PMMA/MWCNTs nanocomposite samples for Cs-137 radioisotope. ....	68
<b>Table 4.22:</b>	Experimental results of the gamma transmission technique of the irradiated PMMA/MWCNTs at 0.5 wt. % MWCNTs.....	68
<b>Table 4.23:</b>	Experimental results of the gamma transmission technique of the irradiated PMMA/MWCNTs at 1 wt. % MWCNTs .....	69
<b>Table 4.24:</b>	Experimental results of the gamma transmission technique of the irradiated PMMA/MWCNTs at 2 wt. % MWCNTs.....	70
<b>Table 4.25:</b>	The linear attenuation coefficient, $\mu_l$ and mass attenuation coefficient, $\mu_m$ of the irradiated PMMA/MWCNTs nanocomposite samples against Co-60.....	71
<b>Table 4.26:</b>	Experimental results of the PMMA/MWCNTs 0.25 wt. % against Pu-Be neutron source. ....	72
<b>Table 4.27:</b>	Experimental results of the PMMA/MWCNTs 0.5 wt. % against Pu-Be neutron source. ....	73
<b>Table 4.28:</b>	Experimental results of the PMMA/MWCNTs 1 wt. % against Pu-Be neutron source. ....	74
<b>Table 4.29:</b>	Experimental results of the PMMA/MWCNTs 2 wt. % against Pu-Be neutron source. ....	75
<b>Table 4.30:</b>	Experimental results of the irradiated PMMA/MWCNTs 0.5 wt. % for Pu-Be neutron source. ....	76
<b>Table 4.31:</b>	Experimental results of the irradiated PMMA/MWCNTs 1wt. % against Pu-Be neutron source. ....	77
<b>Table 4.32:</b>	Experimental results of the irradiated PMMA/MWCNTs 2 wt. % against Pu-Be neutron source. ....	78
<b>Table 4.33:</b>	The changes total macroscopic cross-sections of the unirradiated PMMA/MWCNTs nanocomposite samples for Pu-Be neutron source. ....	79
<b>Table 4.34:</b>	The changes total macroscopic cross-sections of irradiated PMMA/MWCNTs nanocomposite samples for Pu-Be neutron source. ....	80
<b>Table 4.35:</b>	Half-value layer (HVL) of unirradiated PMMA, PMMA/MWCNTs for Cs- 137, Co-60 Radioisotopes and Pu – Be NH <sub>3</sub> .....	80
<b>Table 4.36:</b>	Half-value layer (HVL) of the irradiated PMMA, PMMA/MWCNTs for Cs- 137, Co-60 Radioisotopes and Pu-Be NH <sub>3</sub> .....	81
<b>Table 4.37:</b>	The changes in Poisson's ratio, Shear modulus (G), Young's modulus(E) and Microhardness (H) with the rise of the amount of the MWCNTs in PMMA/MWCNTs nanocomposite samples. ....	83

**Table 5.1:** Comparison with literature of the produced PMMA/MWCNTs nanocomposites in this study.....88





## LIST OF FIGURES

	<u>Page</u>
<b>Figure 1.1:</b> Structure of thermoset and thermoplastic. ....	2
<b>Figure 1.2:</b> Structure of MMA monomer .....	3
<b>Figure 1.3:</b> The synthesis method of PMMA .....	3
<b>Figure 1.4:</b> Schematic structure of zero-dimensional nanoparticles .....	8
<b>Figure 1.5:</b> One-dimensional structures .....	8
<b>Figure 1.6:</b> The structure of two-dimensional nanomaterials .....	9
<b>Figure 1.7:</b> The schematic structure of 3-D nanomaterials .....	9
<b>Figure 1.8:</b> Different forms of carbon atoms. ....	10
<b>Figure 1.9:</b> Types of single-wall carbon nanotubes .....	10
<b>Figure 1.10:</b> Schematic structure of SWCNTs .....	11
<b>Figure 1.11:</b> Structure of a MWCNTs .....	11
<b>Figure 2.1:</b> The fundamental components of a ATRP polymerization method .....	14
<b>Figure 2.2:</b> Chemical structure of MMA .....	15
<b>Figure 2.3:</b> Illustration of nitrogen-based ligands. ....	17
<b>Figure 2.4:</b> Three main steps of ATRP mechanism .....	18
<b>Figure 2.5:</b> The image of in-situ polymerization process with steps .....	20
<b>Figure 2.6:</b> Schematic representation of the solution blending process. ....	20
<b>Figure 2.7:</b> Melt mixing process with its steps. ....	21
<b>Figure 2.8:</b> Tg effects on crystalline and amorphous region .....	22
<b>Figure 2.9:</b> The view of the Rockwell hardness test with steps. ....	24
<b>Figure 2.10:</b> Longitudinal and transverse (shear) waves .....	24
<b>Figure 2.11:</b> The schematic view of the photoelectric effects. ....	27
<b>Figure 2.12:</b> The picture of Compton scattering interaction with formulas. ....	27
<b>Figure 2.13:</b> The schematic outlook of pair production .....	28
<b>Figure 2.14:</b> The structure of the neutron according to the standart model. ....	29
<b>Figure 2.15:</b> The view of interactions between the neutron and nucleus. ....	30
<b>Figure 2.16:</b> The schematic illustration of neutron-proton reaction .....	31
<b>Figure 2.17:</b> The schematic illustration of neutron-alpha reaction. ....	31
<b>Figure 3.1:</b> The weight process was done inside this AtmosBag. ....	32
<b>Figure 3.2:</b> The AtmosBag that synthesis process was done. ....	33
<b>Figure 3.3:</b> The mixture is on the magnetic stirrer to complete the polymerization process fastly. ....	33
<b>Figure 3.4:</b> The picture of PMMA/MWCNTs test samples .....	34
<b>Figure 3.5:</b> The scanning electron microscope using this study .....	35
<b>Figure 3.6:</b> Symbolic representation of Bragg's law .....	38
<b>Figure 3.7:</b> The pulse echo technique using this study. ....	39
<b>Figure 3.8:</b> Rockwell hardness testing device .....	40
<b>Figure 3.9:</b> Schematic view of the application of the pycnometer method. ....	41

<b>Figure 3.10:</b>	Experimental set up of gamma transmission technique.....	42
<b>Figure 3.11:</b>	(a) The view of the Neutron Howitzer (b) The schematic view of thermal neutron port of Neutron Howitzer.....	44
<b>Figure 3.12:</b>	The settlement of the samples .....	45
<b>Figure 4.1:</b>	SEM images of pure PMMA at (a) 2500 x, (b) 10000 x, (c) 20000 x magnifications.....	46
<b>Figure 4.2:</b>	SEM images of MWCNTs at 2000 x, 5000 x, 10000 x, 20000x magnifications respectively.....	47
<b>Figure 4.3:</b>	FT-IR spectra of pure PMMA and PMMA/MWCNTs nanocomposites.....	48
<b>Figure 4.4:</b>	The view of XRD pattern of PMMA, MWCNTs, PMMA/MWCNTs.....	49
<b>Figure 4.5:</b>	The TGA results of PMMA and PMMA/MWCNTs nanocomposites for unirradiated and irradiated states.....	50
<b>Figure 4.6:</b>	The Rockwell hardness values of MWCNTs before and after irradiation.....	52
<b>Figure 4.7:</b>	The graph of thickness versus relative intensity in PMMA.....	53
<b>Figure 4.8:</b>	Relative intensity versus thickness graph of 0.25 wt.% PMMA/MWCNTs against Cs-137.....	54
<b>Figure 4.9 :</b>	Relative intensity-thickness graphs of 0.5 wt.% PMMA/MWCNTs.....	55
<b>Figure 4.10:</b>	Relative intensity-thickness graphs of 1 wt.% PMMA/MWCNTs ....	56
<b>Figure 4.11:</b>	Relative intensity-thickness graphs of 2 wt.% PMMA/MWCNTs.....	56
<b>Figure 4.12:</b>	The relative intensity of base PMMA for unirradiated state by using Co-60 radioisotope.....	59
<b>Figure 4.13:</b>	The changes in the relative intensity of PMMA/MWCNTs nanocomposite at 0.25 wt.% MWCNTs with the rise of the thickness.....	60
<b>Figure 4.14:</b>	The changes in the relative intensity of PMMA/MWCNTs nanocomposite at 0.5 wt.% MWCNTs with the rise of the thickness.....	61
<b>Figure 4.15:</b>	The changes in the relative intensity of PMMA/MWCNTs nanocomposite at 1 wt.% MWCNTs with the rise of the thickness.....	62
<b>Figure 4.16:</b>	The changes in the relative intensity of PMMA/MWCNTs nanocomposite at 2 wt.% MWCNTs with the rise of the thickness.....	63
<b>Figure 4.17:</b>	The changes in the relative intensity of PMMA/MWCNTs nanocomposite at 0.5 wt.% MWCNTs with the rise of the thickness.....	64
<b>Figure 4.18:</b>	The changes in the relative intensity of PMMA/MWCNTs nanocomposite at 1 wt.% MWCNTs with the rise of the thickness.....	66
<b>Figure 4.19:</b>	The changes in the relative intensity of PMMA/MWCNTs nanocomposite at 2 wt.% MWCNTs with the rise of the thickness.....	67

<b>Figure 4.20:</b>	The changes in the relative intensity of the irradiated PMMA/MWCNTs at 0.5 wt. % MWCNTs with the rise of thickness. ....	69
<b>Figure 4.21:</b>	The changes in the relative intensity of the irradiated PMMA/MWCNTs nanocomposite at 1 wt.% MWCNTs with the rise of the thickness .....	70
<b>Figure 4.22:</b>	The changes in the relative intensity of the irradiated PMMA/MWCNTs nanocomposite at 2 wt.% MWCNTs with the rise of the thickness. ....	71
<b>Figure 4.23:</b>	The changes in relative intensity at 0.25 wt.% PMMA/MWCNTs with the rise of the thickness. ....	73
<b>Figure 4.24:</b>	The changes in relative intensity at 0.5 wt. % PMMA/MWCNTs depending on their thickness. ....	74
<b>Figure 4.25:</b>	The changes in relative intensity at 1 wt. % PMMA/MWCNTs depending on their thickness. ....	75
<b>Figure 4.26:</b>	The changes in relative intensity at 2 wt. % PMMA/MWCNTs depending on their thickness. ....	76
<b>Figure 4.27:</b>	The changes in relative intensity at irradiated 0.5 wt. % PMMA/MWCNTs depending on their thickness. ....	77
<b>Figure 4.28:</b>	The changes in relative intensity at irradiated 1wt. % PMMA/MWCNTs depending on their thickness. ....	78
<b>Figure 4.29:</b>	The changes in relative intensity at irradiated 2wt. % PMMA/MWCNTs depending on their thickness. ....	79
<b>Figure 4.30:</b>	The picture of homogeneity of the 2 wt.% PMMA/MWCNTs nanocomposite sample. ....	81
<b>Figure 5.1:</b>	Schematic illustration of (A) a CNT bridging a crack, (B) telescopic failure of a CNT and (C) CNT fibre pullout experienced in CNT-reinforced polymers. ....	84
<b>Figure 5.2:</b>	SEM image of PMMA/MWCNTs nanocomposite in (a) the literature and (b) this study at 2 wt % MWCNTs . ....	85





## **THE INVESTIGATION OF THE IRRADIATION EFFECT ON PMMA/MWCNTs POLYMER NANOCOMPOSITES**

### **SUMMARY**

Poly (methyl methacrylate) (PMMA) is a transparent thermoplastic material that shows good mechanical properties, high resistance to abrasion and superior heat resistance. Mechanical, thermal and radiation shielding properties of PMMA can be enhanced by addition of multiwall carbon nanotubes (MWCNTs). Due to suitable structural properties of MWCNTs, PMMA is an ideal candidate for some applications such as sensor, solar cell, electronic and aerospace fields. Carbon nanotubes separate two parts which are single-wall carbon nanotubes and multi-wall carbon nanotubes. Single-wall carbon nanotubes (SWCNTs) have scale from 0.5 nm to 1.5 nm. On the other hand, multi-wall carbon nanotubes (MWCNTs) are bigger than 100 nm scale. The use of MWCNT in polymer results with higher mechanical properties than SWCNT in polymer. Besides, MWCNT in polymer gives more chemical resistance than SWCNT. MWCNT contained polymer nanocomposites can be utilized in a several industrial application areas such as automotive and aerospace due to their outstanding advantages such as high durability, high strength and light weight. PMMA is one of the thermoplastic polymers coming from the acrylate family. PMMA reinforced by carbon nanotubes has significant importance in many applications ranging from large scales to nanometer scales. It is considered as a candidate for the applications in new technologies depending on the improved mechanical, electrical, optical properties of polymer. There are three methods to produce PMMA reinforced by MWCNTs which are solution-mixing, melt compounding, in-situ polymerization. In this study, it was preferred to use Atom Transfer Radical Polymerization (ATRP) method to disperse MWCNTs in PMMA effectively. MWCNTs were selected as nanofiller to improve the mechanical and thermal properties of PMMA with the investigation of the changes in radiation shielding performance. Several analysis and tests were performed to examine the main characteristic properties of the PMMA/MWCNTs nanocomposites such as SEM, XRD, FTIR, TGA, hardness, ultrasonic test, gamma transmission technique and the behaviors of the PMMA/MWCNTs nanocomposite against neutrons. Further, PMMA/MWCNTs nanocomposite samples were irradiated at 50 kGy using Co-60 radioisotope. The irradiated polymer nanocomposite samples were characterized to examine the structural changes after irradiation treatment. The surface morphology of the PMMA/MWCNTs nanocomposite in SEM images indicated that ATRP method was efficient to get homogeneous dispersion of MWCNTs in the PMMA matrix. In addition, the results of the ultrasonic test supported the homogeneous structure of PMMA/MWCNTs nanocomposites at 2 wt.% MWCNTs. PMMA/MWCNTs nanocomposite presented three characteristic diffraction peaks in XRD analysis. The FTIR spectra of PMMA/MWCNT nanocomposites revealed the similar spectrum with pure PMMA, showing that interaction occurred between

MWCNTs nanocomposites and PMMA polymer matrix. TGA results of unirradiated nanocomposite at the addition of 2 wt. % MWCNTs exhibited that the 5% weight loss temperatures shifted from  $\sim 191$  °C to  $243$  °C with the improvement in the temperature (as  $\sim 52$  °C). The thermal stability of PMMA was enhanced with the rise of the amount of the MWCNTs from (0.25 to 2 wt. %) in PMMA/MWCNTs nanocomposite. The 5 % weight loss temperatures increased after irradiation process. In the ultrasonic test, the Shear modulus, Young's modulus and Microhardness values of pure PMMA were increased with the addition of 2 wt. % MWCNTs. The improvement in Rockwell hardness values between the pure PMMA and PMMA/MWCNTs at 2 wt. % MWCNTs is  $\sim 11$  %. The difference in Rockwell hardness values is almost  $\sim 3$  % for unirradiated and irradiated states of PMMA/MWCNTs at 2 wt. % MWCNTs. The linear attenuation coefficient values for Cs-137, Co-60 radioisotopes changed slightly with the rise of the MWCNTs amount and macroscopic cross sections for neutrons Pu-Be neutron source increased slightly.



## PMMA/MWCNT POLİMER NANOKOMPOZİTLER ÜZERİNE RADYASYON ETKİSİNİN İNCELENMESİ

### ÖZET

PMMA, mekanik özellikleri iyi, aşınmaya karşı direnci yüksek, üstün ısı direncine özelliklere sahip, termoplastik polimerler arasında kabul edilmektedir. PMMA'nın mekanik, termal ve radyasyon zırlama özellikleri, çeşitli nanopartiküller eklenerek iyileştirilebilmektedir. Böylece, PMMA, geliştirilen yapısal özelliklerinden dolayı, çeşitli uygulama alanlarındaki kullanımda, ideal bir malzeme olarak kabul edilebilmektedir. Bu uygulama alanları arasında; sensor, güneş hücresi, elektronik ve uzay uygulamaları mevcuttur. Polimer yapıya eklenen nanopartiküllerden olan karbon nanotüplerin, PMMA yapıya eklenmesi, bilimsel ve endüstriyel alanda ilgi çeken konular arasındadır. Karbon nanotüpleri, tek duvarlı karbon nanotüpleri ve çok duvarlı karbon nanotüpleri olarak iki kısma ayırmak mümkündür. Tek duvarlı karbon nanotüpler (SWCNT'ler), 0.5 nm'den 1.5 nm'ye kadar olan büyüklüğe sahip olabilmektedir. Çok duvarlı karbon nanotüpler ise (MWCNT'ler) 100 nm'den büyüktür. MWCNT'nin polimer içinde kullanılması, polimerde SWCNT kullanılması durumundan, daha yüksek mekanik özelliklere neden olur. Ayrıca, MWCNT, polimer yapıda, SWCNT'den daha fazla kimyasal direnç sağlamaktadır. MWCNT içeren polimer nanokompozitler, yüksek dayanım, yüksek mukavemet ve hafiflik gibi olağanüstü avantajlarından dolayı, otomotiv ve havacılık gibi bir çok endüstriyel uygulama alanlarında kullanılabilir. Bütün bu sebeplerden dolayı, bu yüksek lisans tez çalışmasında, PMMA yapının özelliklerinin geliştirilmesinde, MWCNTs kullanımı tercih edilmiştir. ATRP metodu kullanılarak, MWCNT nano katkı maddesinin PMMA polimer matrisinde homojen bir şekilde dağılması sağlanmıştır. Karbon nanotüp takviyeli PMMA, farklı büyüklüklerdeki, pek çok uygulamada önemli bir yere sahiptir. Çünkü, geliştirilen fiziksel özelliklerine bağlı olarak polimerler, yeni teknolojilerdeki uygulamalar için, uygun bir aday olarak görülmektedir. Polimerler, çok sayıda aynı veya farklı atomik grupların kimyasal bağlarla az veya çok düzenli bir biçimde bağlanarak oluşturduğu, uzun zincirli yüksek molekül ağırlıklı bileşiklerdir. Polimer, birden fazla mer'in (molekülün) ısı ve basınç altında birleşerek uzun zincirlerin meydana gelmesiyle oluşmaktadır. Monomer; polimerik madde içinde, tekrar eden en küçük moleküldür ve bu molekülün kimyasal ve fiziksel özellikleri, elde edilen polimerin karakteristik özelliklerini belirlemektedir. Çok sayıda aynı veya farklı monomerin, bir kimyasal işlemle, birbirleriyle birleşerek, uzun zincirler (makromoleküller) oluşturmasına polimerizasyon olayı denilmektedir. Polimerlerin çoğu, tek bir monomer çeşidinin dizilmesiyle oluşmaktadır ve bazıları, iki veya üç monomer çeşidinin bir araya gelmesinden oluşabilmektedirler. Polimerler, ekonomik ve hafif olup, kolay işlenebilir, yüksek kimyasal ve korozyon direncine sahiptir. Ayrıca, yüksek ısı ve elektriksel özelliklere sahip olacak şekilde, nanopartikül takviyesi ile polimerlerin bu özelliklerini geliştirmek mümkün olabilmektedir. Polimerlerin önemli başlıca yapısal

karakteristik özellikleri; polimer moleküllerinin rijitlik derecesi, polimer zincirleri arasındaki Van der Waals ve elektrostatik bağlar, kristalimsi bölgeler oluşturan zincirlerin dereceleri, zincirler arasındaki çapraz bağlanma dereceleri bu özellikler arasındadır. MWCNT takviyeli PMMA üretiminde, çözelti karıştırma, eriyik harmanlama, yerinde polimerizasyon olmak üzere, başlıca üç yöntem mevcuttur. Bu çalışmada, PMMA'daki MWCNT'lerin uygun bir şekilde dağıtılması için, Atom Transfer Radikal Polimerizasyon (ATRP) yöntemi kullanılması tercih edilmiştir. Bu tez çalışmasında, PMMA'nın mekanik, termal özelliklerini geliştirirken, radyasyon karşısındaki davranışlarını incelemek için, nanopartikül takviyesi olarak çok duvarlı karbon nanotüp (MWCNTs) seçilmiştir. Karbon nanotüp eklenmesiyle PMMA'nın karakteristik özelliklerinde oluşan değişimleri incelemek için; SEM, XRD, FTIR, TGA, setlik testi, ultrasonik test, gama ve nötron geçirgenlik testleri uygulanmıştır. Nanokompozitin maruz kaldığı radyasyon dozunun yapıya etkisini incelemek için, Co-60 radyoizotopu kullanılarak, PMMA/MWCNT nanokompozit örnekler, 50 kGy'lik doza maruz bırakılmıştır. Işınlanma işleminden sonra, polimer nanokompozitin yapısal karakterizasyonundaki değişikliği incelemek amacıyla, SEM, XRD, FTIR ve TGA analizleri yapılmıştır. PMMA/MWCNTs yapının SEM görüntüleri incelendiğinde, nanokompozit yapıdaki MWCNTs görüntülerinde bu nanopartiküllerin, yapıda homojen bir şekilde dağıldığı tespit edilmiştir ve nanopartiküllere ilişkin herhangi bir yığılma, topaklanma veya biraraya gelme görülmemektedir. Ayrıca, PMMA/MWCNTs nanokompozit örneklerin, XRD analizine ilişkin sonuçlar, PMMA/MWCNTs nanokompozitin karakteristik kırınım piklerini vermiş olup, FTIR analizlerinden elde edilen sonuçlar ise, bu nanopartiküllerin, nanokompozit yapıya uygun bir şekilde dahil olduğunu belirtmektedir. PMMA/MWCNTs nanokompozit örneklerin termal kararlılığı TGA analizi ile incelenmiştir. Bu analiz sonuçlarında, PMMA'ya MWCNTs eklenmesiyle PMMA'nın termal kararlılığının geliştiği tespit edilmiştir ve 2wt.% 'lik MWCNTs ilavesiyle termal kararlılığının daha iyi şekilde geliştiği belirlenmiştir. PMMA/MWCNTs nanokompozit örneklerin homojen yapısını ve üretim sırasında yapıda oluşabilecek habbe veya topaklanma gibi üretim kusuru olup olduğunu tespit etmek amacıyla, tahribatsız test metodlarından biri olan ultrasonik test yöntemi uygulanmıştır. Ultrasonik testlerde, polimer nanokompozit örnekler içerine gönderilen ses dalgalarından, polimer yapı içerisinde oluşan ses yankıları sonucu meydana gelen ekolar incelenmiştir. Tespit edilen ses pikleri periyodik aralıklarla tekrar etmekte olup, bu oluşan ses ekoları, ürettiğimiz nanokompozit örneklerin homojen bir yapıda olduğunu işaret etmektedir. Bu amaçla, boyuna dalgaların ve enine dalgaların hızlarını tespit etmek amacıyla iki farklı prob kullanılmıştır. Ayrıca, yoğunlukları piknometre metodu ile belirlenmiş, polimer nanokompozit örneklerin yapısı içerisinde ilerleyen boyuna dalga hızları ve enine dalga hızları belirlenerek, bu örneklerin elastik özellikleri tespit edilmiştir. PMMA/MWCNTs nanokompozit örneklerin, Kayma modülü, Young modülü, Poisson oranı ve Mikrosertlik değerleri hesaplanmıştır ve elde edilen sonuçlar, saf PMMA'nın elastik değerleri ile karşılaştırılmıştır. MWCNTs takviyesinin bu özellikleri değiştirdiği tespit edilmiştir. PMMA/MWCNTs nanokompozit örneklerin, sertlikleri, Rockwell sertlik testi yapılarak incelenmiştir ve nanokompozit örneklerin sonuçları, saf PMMA örneklerin test sonuçları ile karşılaştırıldığında, ağırlıkça % 2 wt.'lik MWCNTs ilavesiyle oluşturulan PMMA/MWCNTs nanokompozit örneğin, Rockwell sertliği değerinin arttığı belirlenmiştir. Dört farklı MWCNTs miktarları taşıyan (0.25, 0.50, 1.00, 2.00 wt.% MWCNTs), PMMA/MWCNTs nanokompozit örneklerin, gama radyasyonu zayıflatma değerlerinde oluşan değişimler, gamma geçirgenlik tekniği kullanılarak

incelenmiştir. Cs-137 ve Co-60 radyoizotopları kullanılarak üretilen nanokompozitlerin, lineer zayıflatma katsayısı değerleri, deneysel olarak elde edilmiştir ve nanokompozitlerin tespit edilen yoğunluk değerleri de kullanılarak, kütle zayıflatma katsayılarında oluşan değişimler tespit edilmiştir. Ayrıca, üretilen PMMA/MWCNTs nanokompozit örneklerin, kimyasal element konsantrasyon değerleri kullanılarak, XCOM programı ile malzemelerin teorik kütle zayıflatma katsayıları, Cs-137 ve Co-60 radyoizotopları için elde edilmiştir. Elde edilen deneysel değerler ile teorik değerler karşılaştırıldığında, deneysel sonuçların teorik sonuçlar ile uyumlu olduğu belirlenmiştir. Bu tez çalışmasında MWCNTs miktarı arttıkça nanokompozit örneklerin özelliklerinin değiştiği tespit edilmiştir. PMMA/MWCNT nanokompozitin XRD analizinde, üç karakteristik kırınım piki tespit edilmiştir. PMMA/MWCNTs nanokompozit takviyeli PMMA'nın FTIR spektrumu saf PMMA ile benzer spektrum göstermiştir, bu durum katkı maddesi ile PMMA polimer matrisi arasında etkileşimin olduğunu göstermiştir. Işınlanmamış örneklerin TGA sonuçları, % 2 wt. MWCNTs eklenerek üretilmiş PMMA/MWCNTs nanokompozitin, %5 kütle kaybı durumundaki sıcaklık değerinin, 191°C'den 243°C'ye çıktığını ve 52°C geliştiğini göstermiştir. PMMA/MWCNTs içerisinde MWCNTs miktarı arttıkça, yapının termal kararlılığının, saf PMMA'ya göre arttığı tespit edilmiştir. Ayrıca, PMMA/MWCNTs nanokompozitin termal kararlılığı, ışınlanan örneklerde artış göstermiştir. Ultrasonik testlere yönelik çalışmalarda, saf PMMA'nın Kayma Modülü, Young modülü ve mikrosertlik değerleri, % 2 wt. MWCNTs eklenmesi ile artmıştır. Saf PMMA ile %2 MWCNTs eklenerek üretilmiş PMMA/MWCNTs nanokompozitin Rockwell sertliği karşılaştırıldığında, % 2 wt. MWCNTs takviyesi ile Rockwell sertliğinin % 11 arttığı tespit edilmiştir. % 2 wt. MWCNTs eklenerek üretilmiş PMMA/MWCNTs nanokompozitin, ışınlanmadan önceki Rockwell sertlik değeri ile ışınlandıktan sonraki değeri arasındaki değişim ~ % 3'tür. Cs-137, Co-60 radyoizotopları ve Pu-Be nötron kaynağı ile yapılan incelemelerde, lineer zayıflatma katsayıları ve makroskopik kesit değerlerinde, MWCNTs miktarının artışı ile kısmen yavaşça artış mevcuttur.

Sonuç olarak, PMMA/MWCNTs nanokompozit örneklerde, yerinde polimerizasyon metoduyla, MWCNTs homojen bir şekilde dağılmış olup, nanokompozit örnekler içerisinde, habbe ya da çatlakların oluşmadığı ve MWCNTs'nin PMMA ile etkileşimin fiziksel özelliklerde gelişme ile sonuçlandığı belirlenmiştir. MWCNTs'nin, PMMA içerisine homojen bir şekilde yerleşerek, saf PMMA'nın fiziksel özelliklerini uygun şekilde geliştirdiği tespit edilmiştir.



## **1. INTRODUCTION**

Polymers have a significant role in many applications. Polymers are large molecules. They are consisting of a large number of repeated structural molecules calling monomers. Thus, polymers have high molecular weight compounds. The intermolecular forces between the monomers and different amounts of monomers determine the polymer's properties. If monomer lies parallel to each other, crystalline polymer structure forms. On the other hand, non-parallel connection forms the amorphous region in polymer structure. Polymers can be used in several applications at communication, transportation, clothing, packing and buildings. (Jenkins & Kawamura, 1976)

### **1.1 Polymers**

Polymer derives from the Greek alphabet and named polys+meros. Polys mean many and meros imply parts. Polymers are synthesized by using many different polymerization processes. In these processes, monomers are connecting to each other to form the polymers. The bonds between the molecules are covalent compounds of carbon. The repeat unit is called -mer. Number of 'mers' determine the degree of polymerization (DP). Polymers can show many different structures. Depending on the method of polymerization, polymers can be linear, branched, cross-linked, star, ladder and dendrimer structure. These differences determine the properties of the polymer. (Koo, 2006)

#### **1.1.1 Polymer fundamentals**

Polymers show different behaviours against heat. Due to the different reactions, polymers are classified as thermosets and thermoplastics.

Thermoplastics: These polymers melt when heated and re-solidify when cooled. They may show linear structure or branched chain. This group of polymers is recycleable even if they are used many times. This property enables polymers to

move freely when temperature changes. The examples of this group of polymers are polythene, polyesterne and PVC. (Olabisi & Adewale, 2015)

Thermosets: Thermosets have a cross-linked structure. Their thermal stability is very high so it is a rigid type of polymer. This polymer is hard and it does not melt when heated. There are some example materials, which show thermoset polymer behavior such as epoxy, resin, polyurethanes, bakelite, and vulcanized rubber.

Differences between thermoplastics and thermosets (Figure 1.1):

- 1) Thermosetting polymers are more resistant to heat than thermoplastic polymers.
- 2) Thermoset polymers are hard and they can be softened by adjusting the composition.
- 3) Thermoplastics tend to creep more than thermoset plastics.
- 4) Thermoplastics are resistant to some organic solvents.
- 5) Thermoplastics can be produced having transparency property.
- 6) Thermoplastics have straight chain but thermosets have cross-linked.

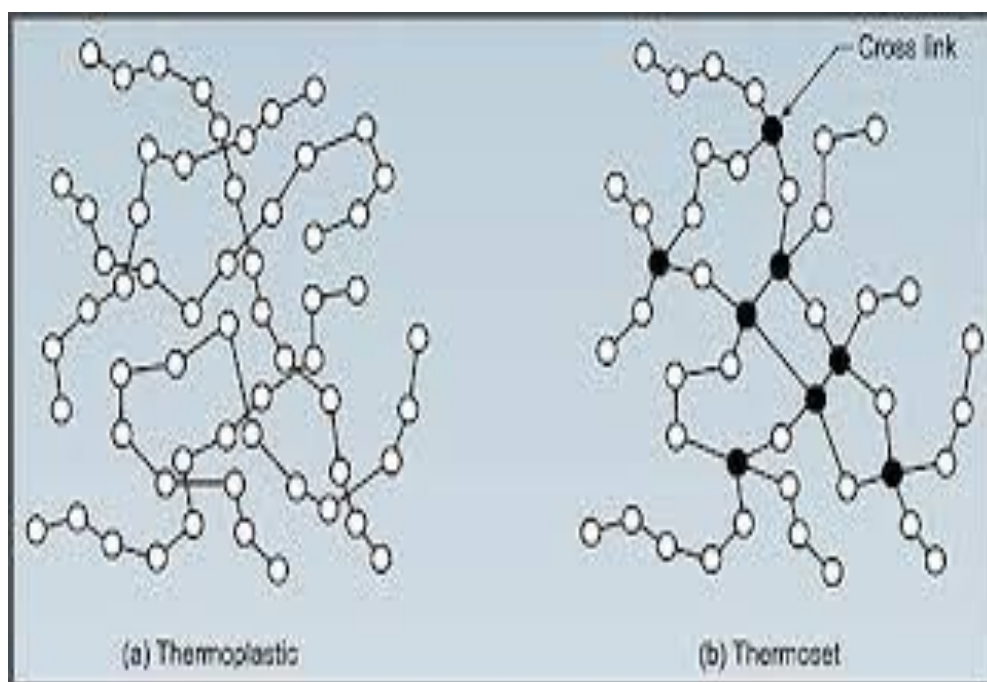


**Figure 1.1 :** Structure of thermoset and thermoplastic (Url-1).



### 1.1.2 Properties and applications of PMMA

Polymethyl methacrylate (PMMA) is a polymer which has  $(C_5H_8O_2)_n$  chemical formula. Methyl methacrylate (MMA) is the monomer of the PMMA. The method of polymerization of PMMA using MMA is radical polymerization technique.

PMMA is a kind of acrylic thermoplastic and has repeating unit as shown in the Figure 1.2:

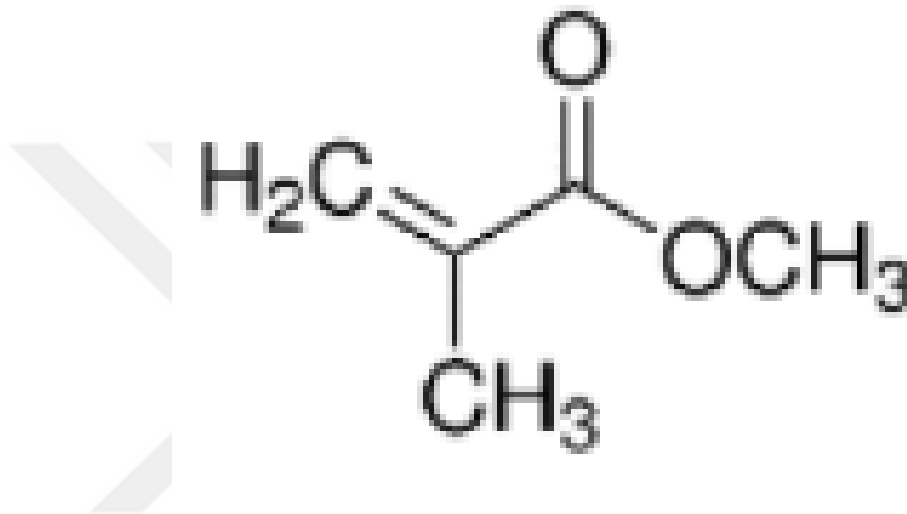


**Figure 1.2 :** Structure of a MMA monomer (Url-3).

Method of synthesis PMMA with MMA is radical polymerization method that is given in Figure 1.3 (Thakur V. & Thakur K, 2015).

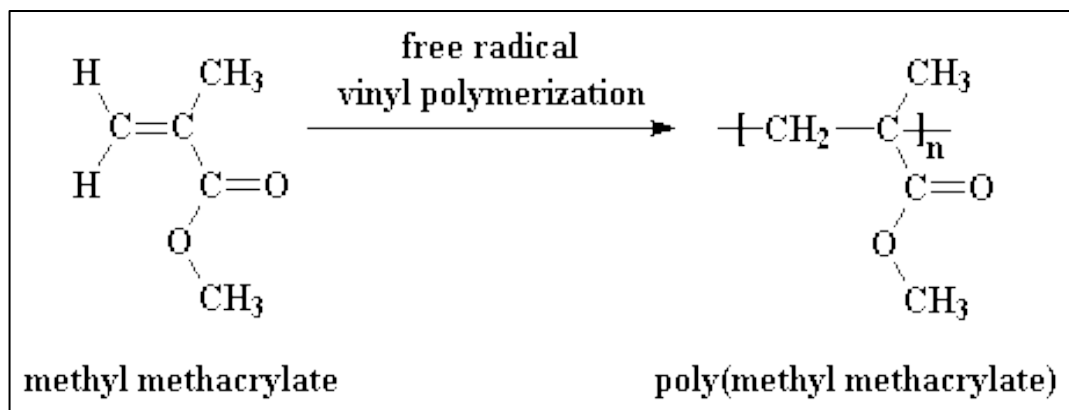


**Figure 1.3 :** Synthesis method of PMMA.

### 1.1.2.1 Characteristic properties of PMMA

PMMA has good properties, which provide common usage at large areas and their main properties are below:

- 1) Physical properties: PMMA is resistant to hardness and scratching. Its density is 1.18-1.20 g/cm<sup>3</sup> at room temperature. The density of PMMA is less than density of glass.
- 2) Optical properties: PMMA absorbs the damaging UV light. C=O group absorbs the UV radiation effectively (Tuna, 2016).
- 3) Thermal properties: The thermal stability of standard PMMA is 65°C. PMMA can tolerate temperatures as low as -70 °C (Url-4). Table 1.1 shows important thermal properties of PMMA clearly.

**Table 1.1 : Thermal properties of PMMA.**

Properties	Value
CTE, linear 20 °C	60-130 µm/m. °C
CTE, linear 20 °C Transverse to Flow	70-90 µm/m. °C
Specific Heat Capacity	1.46-1.47 J/g. °C
Thermal Conductivity	0.19-0.24 W/M.K
Maximum Service Temperature, Air	41-103 °C
Melting Point	130 °C
Softening Point	47-117 °C
Glass Temperature	100-105

- 4) Mechanical properties: PMMA has high mechanical strength, high Young's modulus and low elongation at break. It does not shatter on rupture. It is one of the hardest thermoplastics and is highly scratch resistant. It exhibits low moisture and water absorbing capacity, due to which products made have good dimensional stability. Both of these characteristics increase as the temperature rises. (Url-4)

Mechanical properties of PMMA were summarized in Table 1.2.

**Table 1.2 : Mechanical properties of PMMA.**

<b>Properties</b>	<b>Value</b>
Hardness, Rockwell M	63-97
Tensile Strength	47-79 MPa
Elongation at Break	1-30 %
Tensile Modulus	2.2-3.8 GPa
Flexural Modulus	3-3.5 GPa
Izod Impact, Notched	1.2-20 kJ/m <sup>2</sup>
Izod Impact, Unnotched	11kJ/m <sup>2</sup>
Tensile Creep Modulus, 1h	1800-2700 MPa
Tensile Creep Modulus, 1000h	1200-1800

- 5) Electrical properties: PMMA is very suitable for electrical devices with the suitable properties. It has low water absorption capacity and has good dielectric properties. (Table 1.3) Properties of dielectric constant depend on temperature, relative humidity of air and frequency. (Url-5)

**Table 1.3 : Electrical properties of PMMA.**

<b>Properties</b>	<b>Value</b>
Electrical Resistivity	$10^{14}$ - $10^{15}$ $\Omega$ .cm
Surface Resistance	$10^{14}$ - $10^{16}$ $\Omega$
Loss factor, 20 °C, 1000 Hz, 60% humidity	0.04
Dielectric Constant	2.8-4
Dielectric Constant, Low Frequency	3-4
Dielectric Strength	17.7-60 kV/mm
Dissipation Factor	0.03-0.55
Arc Resistance	100-180

- 6) Chemical properties: Organic solvents affect PMMA and it is being durable against many chemicals. Its hardenability resembles copper hardness. It can be drawn with brush and sandpaper.
- 7) Combustibility: PMMA is combustible.
- 8) Hydrolysis resistance: The hydrolysis resistance of PMMA is very high.
- 9) Weathering resistance: The change in transparency and color can affect PMMA in very small quantities. PMMA has effective weathering resistance.
- 10) Radiation resistance: PMMA has effective resistance against the ionization radiation that can cause radiation damage among the materials.

All of these properties can summarize as in Table 1.4. (Ellis & Smith, 2008)

**Table 1.4 : Main properties of PMMA.**

<b>Properties</b>	<b>Value</b>
Density	1.18-1.20 g/cm <sup>3</sup>
Water Absorption	0.3 – 2 %
Transmission, Visible	~ 92 %
Refractive Index	~ 1.49
Hardness, Rockwell M	63 - 97
Young's modulus	1.8-3.2 GPa
Tensile Strength	47 - 79 MPa
Compression strength	70-120 MPa
Electrical Resistivity	~ 10 <sup>15</sup> Ω.cm
Thermal Conductivity	~ 0.2 W/m.K
Glass Temperature	~ 105 °C
Softening Point	~ 115°C
Melting Point	~ 160 °C

### 1.1.3 Application areas of PMMA

PMMA has significant importance in several industrial fields including (Olabisi & Adewale, 2015):

- Optics: sunglasses, watch glasses, lenses, magnifying glasses.
- Vehicles: rear lights, indicators, warning triangles.
- Office equipment: writing equipments, pens.
- Medicine: pills, capsules, sterilise equipments.
- Electronic devices: lamp covers, switch parts, dials, control buttons.

## 1.2 Nanotechnology and Nanomaterials

Nanotechnology is a developing technology. It represents the smallest units of atoms and molecules. Nanotechnology aims to design and manufacture materials at nanoscale. Nanotechnology tries to produce new devices from these materials. Nanometre is one billionth of a meter (10<sup>-9</sup> m) and it consists of approximately three or four atoms combining with each other.

Technology focused on nanomaterials to make the particles, things, devices at the atomic and molecular scale. Unlike many conventional materials, nanomaterials show excellent properties.

### **1.2.1 Properties of nanomaterials**

Nanocomposites are materials formed by the dispersion of particles in a matrix at the nanometer scale. The properties of nanocomposites brought to the material are: It increases the elasticity module, heat resistance, hardness, yield strength, toughness of the materials. It prevents gas leakage to the material. It also reduces the flammability of the material.

Nanometaterials can diffuse easily at elevated temperatures. Further, nanomaterials can be sintered easily at lower temperatures and it takes shorter time than bigger particles. This property affects the agglomeration of nanomaterials. (Url-2)

Some specific properties of nanomaterials distinctive from properties of bulk materials were discussed below:

- The melting point of the nanomaterials is hundred of degrees lower than bulk materials. The reason of this situation is the surface to volume ratio is different between the bulk and nanoscale materials. The ratio has largest value when materials are nanoscale materials.
- Nanomaterials have better mechanical properties compared to the bulk materials. The strength of nanomaterials is nearly one or two times higher in magnitude than bulk that has single crystal structure.
- The hardness of the materials is increasing with decreasing particle size.
- Nanoparticles have fewer defects than bulk materials so electron scattering from the material reduces. Thus, the resistivity also decreases. (Url-5)

### **1.2.2 Classification of nanomaterials**

Nanomaterials can be classified four parts depending on number of dimensions. Nanomaterials at each dimension have different crystal structures. They were given below with their crystal structures.

- 1) Zero-dimensional nanomaterials (0-D): nanoparticles, spheres and clusters are the examples of zero dimensional nanomaterials shown in Figure 1.4 (Pokropivny et al., 2007).

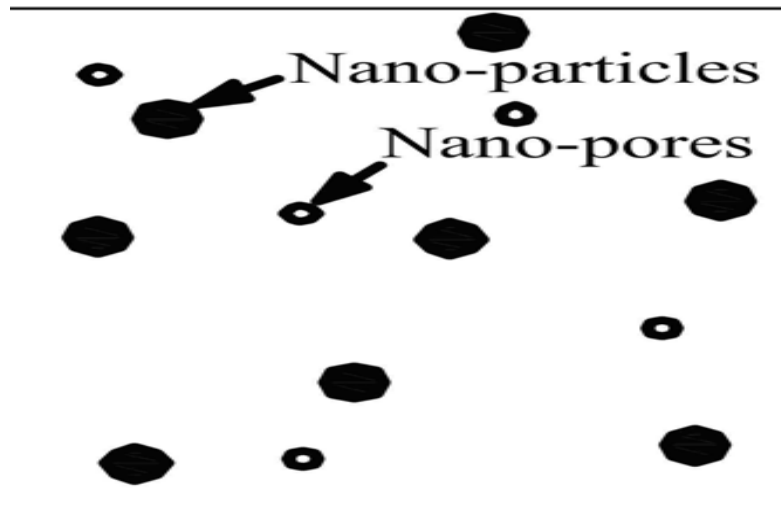


**Figure 1.4 :** Schematic structure of zero-dimensional nanoparticles.

- 2) One-dimensional nanomaterials (1-D): It can be called as quantum well. Nanofibers, wires, rods are the examples of 1-D nanomaterials (Figure 1.5) (Pokropivny et al., 2007).

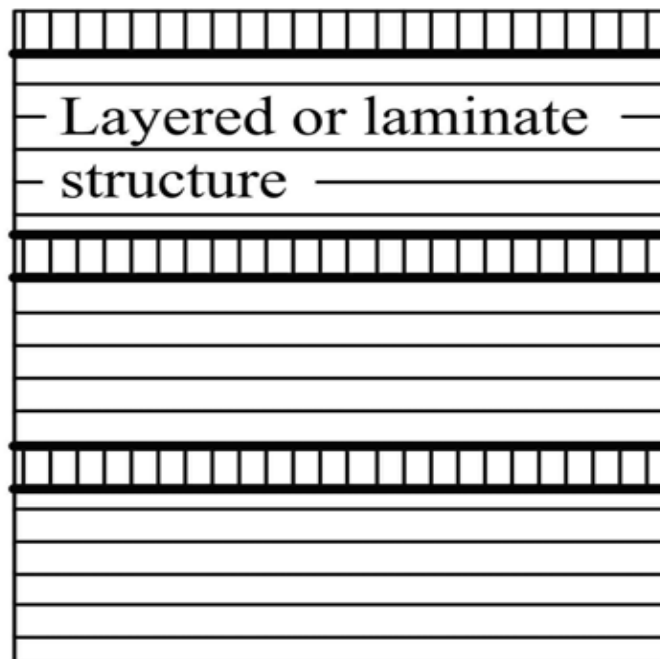


**Figure 1.5 :** One-dimensional structures.

- 3) Two-dimensional nanomaterials (2-D): It shows plate-like shapes. There are some examples that have 2-D structure including nanofilms, nanolayers, and nanocoatings. (Figure 1.6) (Pokropivny et al., 2007)

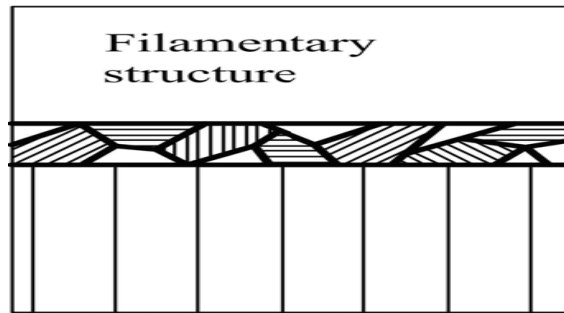


**Figure 1.6 :** The structure of two-dimensional nanomaterials.

- 4) Three-dimensional nanomaterials (3-D): Bulk nanomaterials get into this group. These materials have dimensions above 100 nm. Nanoparticles, nanowires, and nanotubes that consist multilayers can be given as examples of 3-D nanomaterials group. Figure 1.7 shows these nanomaterials. (Pokropivny et al., 2007)



**Figure 1.7 :** The schematic structure of 3-D nanomaterials.

### 1.2.3 Multiwall carbon nanotube-derived nanomaterials

Carbon materials can be found in many forms (Figure 1.8), including graphite, diamond, carbon fiber, fullerenes and carbon nanotubes. The reason why carbon creates such a different structure is that the carbon atom can form valence band in many different varieties. Within these forms,  $sp^2$ -bonded carbon atoms can occur carbon nanotubes. A carbon nanotube is the cylindrical rolling up sheets of the

graphene or graphite. The diameter of a carbon nanotube is at the nanometer scale. The length of a carbon nanotube may be greater than 1 micrometer. (Yetim, 2011)

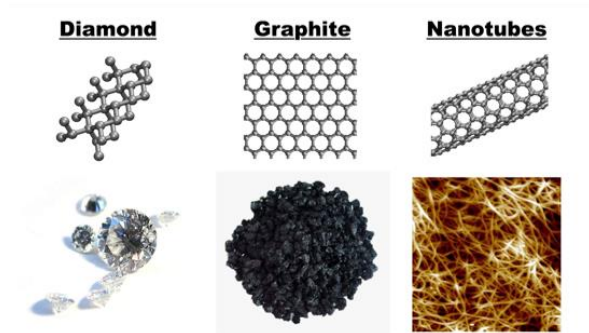


**Figure 1.8 :** Different forms of carbon atoms.

Carbon nanotubes separate two parts that are single-wall carbon nanotubes and multi-wall carbon nanotubes. Single-wall carbon nanotubes (SWCNTs) have scale from 0.5 nm to 1.5 nm. On the other hand, multi-wall carbon nanotubes (MWCNTs) are bigger than 100 nm scale.

Single-wall carbon nanotubes: Cylindrical rolling up sheets of the graphene or graphite to form a tube forms SWCNTs. SWCNTs can formed in three different designs depending on the way of the rolling up sheets of the graphene. These designs are armchair, chiral and zigzag which structures were given in Figure 1.9. (Yetim, 2011)



**Figure 1.9 :** Types of single-wall carbon nanotubes.

Schematic structure of SWCNTs was presented in Figure 1.10. The outer diameter of SWCNTs is 1-2 nm and inner diameter is 0.8-1.6 nm. The length of the single-wall carbon nanometers is 5-30  $\mu\text{m}$ . (Yetim, 2011)



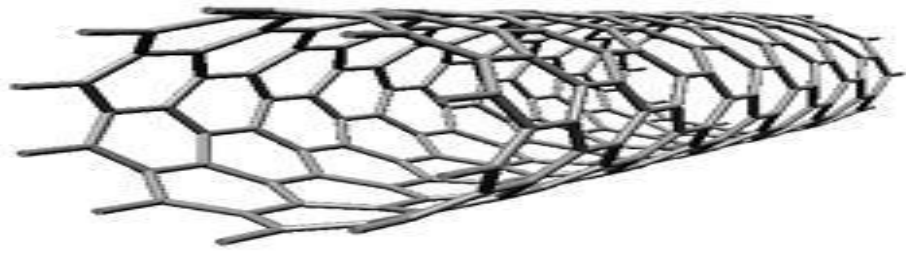


**Figure 1.10 :** Schematic structure of SWCNTs.

Multi-wall carbon nanotubes (MWCNTs): MWCNTs are other parts of the carbon nanotubes. They consist of multiple layers of graphite rolling in themselves. The differences between SWCNTs and MWCNTs are their rigidities, structures, diameters. MWCNT's outer diameter is smaller than 8 nm, inner diameter is between 2 to 5 nm. Besides, the length of the MWCNT is range from 10  $\mu\text{m}$  to 30  $\mu\text{m}$  (Yetim, 2011). Schematic structure of MWCNTs was presented in Figure 1.11.

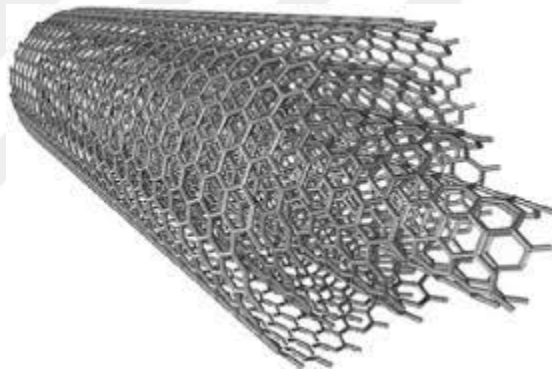


**Figure 1.11 :** Structure of MWCNTs.

The interlayer distance is approximately 0.34 nm (Ruoff et al., 2003). MWCNT contains fibrous particles longer than 5 micrometer with an aspect ratio of more than three. Dimension of the MWCNT is similar with mesotheliomagenic asbestos. It suggested that the MWCNT like a potent mesotheliomagenic asbestos fiber associate with generation of oxidative stress in this study. Hence, MWCNT causes the improvement in oxidative stress of CREB in human mesothelial cells via EGFR- and PKA dependent pathways. (Atsuya et al., 2012)

In this study, we focused on MWCNTs due to some properties that are interesting for the industry. These special properties are electrical conductivity, mechanical strength, thermal conductivity compared to some materials that have significant importance in industrial applications.

#### **1.2.4 Properties of multiwall carbon nanotubes (MWCNTs)**

Mechanical properties: Composite materials such as MWCNTs have significant importance for increasing mechanical properties. There are many studies to improve these properties. According to the a study, elastic properties of MWCNTs was examined and found that Young's modulus of MWCNT is 1.7-2.4 TPa. (Url-6)

- 1) Thermal properties: Thermal properties are important for materials that are used in wide variety of applications such as aerospace, under water studies. These applications are required the suitability for extreme temperature conditions. Therefore, MWCNTs are important materials. (Xie et al., 2007)
- 2) Optical properties: MWCNTs have more regular and uniform optical properties compared to the SWCNTs. The reason for this difference is that MWCNTs have larger size than SWCNTs. Due to the uniform optical properties of MWCNTs; each MWCNT can be seen as a homogeneous medium for many applications. (Bao et al., 2010)
- 3) Electrical properties: Volume fraction of the conductive phase is important for the electrical conductivity of the MWCNTs polymer nanocomposites. It affects the electrical conductivity directly. Percolation threshold is a limit for volume fraction of the filler. If MWCNTs disperses in polymer effectively, percolation threshold gets low value that provides good electrical conductivity. (Szentés et al., 2012)

#### **1.2.5 CNT-derived materials**

There are several composites with MWCNTs as a part of the materials. CNT/TiO<sub>2</sub> is one of them. Multiwall carbon nanotubes are used for starting material, titanium with different numbers used as titanium sources and solvent for this composite is benzene. Synthesis, characterization, and photocatalytic analysis of CNT/TiO<sub>2</sub> composites derived from MWCNTs and titanium sources. (Chen et al., 2009)

Another composite is MWCNT/Al<sub>2</sub>O<sub>3</sub> that consist of 1.wt % MWCNTs producing with precursor method. In this study, XRD results show that MWCNT/Al<sub>2</sub>O<sub>3</sub> is synthesized by the dehydration mixture of aluminum hydroxide-MWCNTs at 1500°C in vacuum successfully. The frictional properties were determined at carbon nanotube/alumina composites prepared by precursor method. (Y.Go et al)

### 1.3 Polymer Nanocomposites

Polymer nanocomposites are a combination of two parts. These parts are polymer matrix and inclusions in the nanometer size range. This combination has at least one dimension. It is classified depending on the number of dimensions such as one dimension is called nanowires, two dimensions are called nanosheets and three dimensions are called nanoparticles.

Nanocomposites are different from traditional composites. In traditional composites, fillers' length is micrometers scale. The magnitude of polymer coils and nanofillers are same diameter (40 nm) for some composites.

In polymer nanocomposites, the interaction between polymer and nanofillers enables composites to have different properties that conventional composites do not have. Kind of polymer matrix and nanofillers are different for different application materials. Polymer matrices can be classified thermoplastic resins, thermoset resins, and elastomers.

Thermoplastic resins: This structure has long chains. When heat is applied it can be soften easily. PVC, PC, PMMA are the examples of these groups. In this thesis study, PMMA is used for polymer matrix.

Thermoset resins: It has crosslinked chains that formed by resins. It does not melt. Epoxy and aminos can be given as an example for this matrix.

Elastomers: Natural and synthetic rubber are classified in this group matrix.

Another part of the polymer nanocomposites is nanofillers. It is also changeable for different applications. They can be divided many categories some of these are carbon nanofibers (CNFs), carbon nanotubes (CNTs), metallic nanoparticles. The nanofillers of this study are CNTs. (Carrandi, 2008)

To sum up; adding nanoparticles, nanosheets or nanowires increase the weak properties of the polymer matrix to have excellent materials. Therefore, polymer nanocomposites are chosen more than conventional composites.



## 2. BACKGROUND AND LITERATURE REVIEW

### 2.1 Synthesize of PMMA via ATRP

There are many polymerization techniques, which are radical polymerization, emulsion polymerization, solution polymerization, anionic polymerization, and bulk polymerization. Atom transfer radical polymerization (ATRP) is the one of the polymerization methods that provides producing well-defined polymers easily. ATRP is the effective method to preparation of polymers with controlled functionalities, topologies and compositions. Its functional groups are much more adaptable than ionic polymerization. This extends the range of unsaturated molecules that can be polymerized via ATRP method (Wojciech et al., nd). ATRP components were shown in Figure 2.1 with structures (Johnson & Jeremiah).

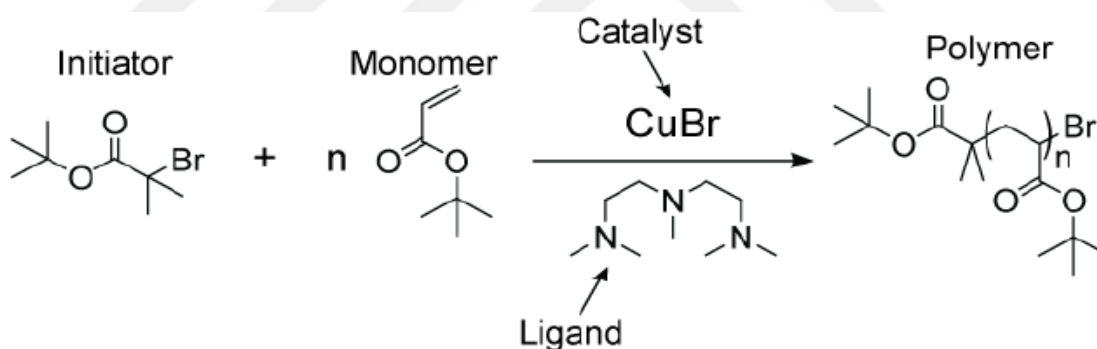


**Figure 2.1 :** Fundamental components of ATRP polymerization method.

ATRP mechanism consists of six main components to synthesize the PMMA using monomer. These components are monomer, initiator, catalyst, ligand, solvent, temperature. Properties and functions of these components are explained deeply afterwards.

- 1) Monomer : Methyl methacrylate (MMA).
- 2) Initiator: Alkyl halides R-X (X=Cl, Br) are the initiators in the ATRP method. Alkyl halides can comprise one or more halogen atoms in it.

- 3) Catalyst: It is used for lowering or increasing the oxidation states. Transition metal species ( $Mt^n$ ) have these two states.
- 4) Solvent: Solubility of catalysts complex is increased by using solvent.
- 5) Ligand: It is a metal complex in the ATRP mechanism that connected to the catalyst by a covalent or an ionic bond. It is important choosing suitable ligand for the reaction because of the fact that it has enormous impact on the controlled polymerization. It provides to solubilize the metal ion. Besides, it can also affect the reduction potential of the transition metal ion. (Tian et al., 2012)
- 6) Temperature: Temperature is the important factor that affects the polymerization rate directly.

### 2.1.1 MMA monomer

MMA is the monomer of PMMA polymerizing with ATRP method. It is colorless, liquid monomer which chemical formula is  $C_5H_8O_2$  that shown in Figure 2.2.

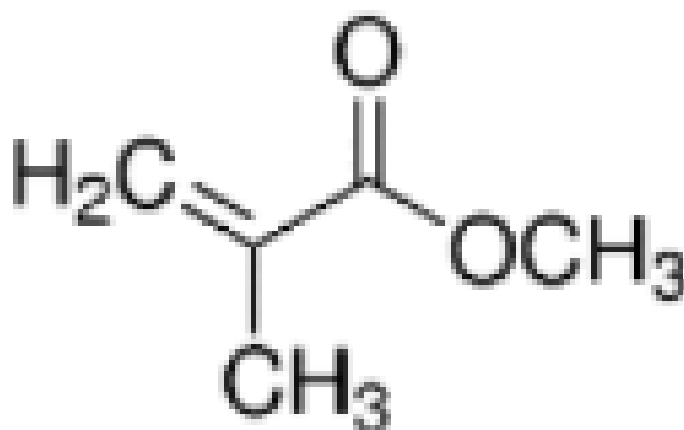


**Figure 2.2** : Chemical structure of MMA.

MMA has many significant properties that given in Table 2.1. It also has many benefits for new technology such as good durability, strength, transparency, UV, abrasive resistance.

**Table 2.1** : Significant properties of MMA.

<b>Properties</b>	<b>Value</b>
Density	0.94 g/cm <sup>3</sup>
Molar mass	100.12 g/mole
Boiling point	100.6°C
Melting point	-48°C
Flashpoint	8°C
Polymerization heat	2.97 J/mole

### 2.1.2 Initiator

The initiators for the polymerization of MMA by ATRP method are alkyl halides (RX). The concentration of RX determines the polymerization rate of the reaction. The properties of halide groups are very important to get high-quality polymers. Therefore, the complete initiator molecule is an essential part of the final material. (Matyjaszewski & Xia, 2001) Either RX group can be a monofunctional or a multifunctional initiator. Number of functional groups is important that they can provide a site for chain growth.

### 2.1.3 Catalyst

Catalysts consist transition metals with suitable metal. It is an essential part of the ATRP mechanism. Catalytic system is composed of both activating and deactivating components that must be presented at the same time. There are many requirements that catalysts must have to get efficient transition.

- 1) The metal complex must consist at least two accessible oxidation states separated by one electron.
- 2) The ligand should complex the metal relatively strongly.
- 3) The metal center should have reasonable affinity toward a halogen.
- 4) The coordination sphere around the metal should be expandable on oxidation to selectively accommodate a (pseudo) halogen.
- 5) The position and dynamics of the ATRP equilibrium should be appropriate for the particular system. To differentiate ATRP from the conventional redox-initiated polymerization and induce a controlled process, the oxidized transition metal should rapidly deactivate the propagating polymer chains to

form the dormant species. A variety of transition metal complexes with various ligands have been studied as ATRP catalysts.

### 2.1.4 Ligand

Ligand is an important part of the ATRP mechanism that has been used in conjunction with different transition metals. There is a wide variety of ligands in polymerization processes. They provide three main benefits for efficient polymerizations. The first benefit is that ligands can solubilize the metal in the reaction. Another benefit is that they control reaction via structural and electronic effects selectively. Third profit of the ligands is that they affect the oxidation-reduction chemistry of the final metal complex by their electronic effects. There are many ligands for copper-based ATRP. Copper is generally ligated with nitrogen-based ligands that are shown in Figure 2.3.

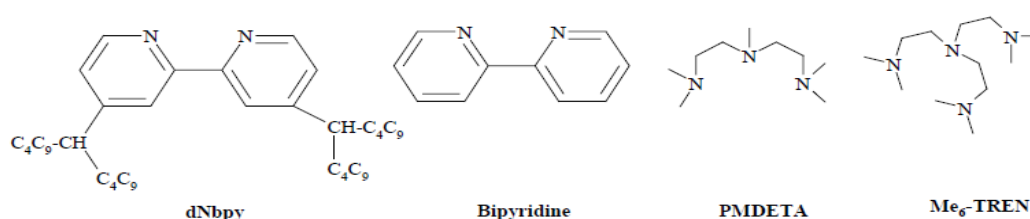


**Figure 2.3 :** Illustration of nitrogen-based ligands (C.Anna).

### 2.1.5 Solvent

Solvent effect on ATRP method is the important due to the structure of the catalyst complex that can change with different solvents. This changing affects the atom transfer equilibrium and rate of the polymerization. Thus, solvent choice is important for the effective polymerization. There are different solvents have been used for various monomers such as alcohol, toluene, ethyl acetate, ethylene carbonate, benzene, etc (Matyjaszewski et al.,2001).

### 2.1.6 Temperature

Temperature has significant role during the polymerization process. Temperature affects the polymerization rate directly. As the temperature increases, time to complete the reaction decreases. High temperature will increase the amount of heat



loss. Besides, high temperature increases the rate of reaction due to the increasing of collision frequency. This occurs more energy and reaction starts easily. (Wahab, 2013)

## 2.2 ATRP Mechanism

Matyjaszewski et al. (2001) found atom transfer radical polymerization (ATRP) in 1995. This mechanism consists of three reactions: initiation, propagation, termination respectively shown in Figure 2.4.

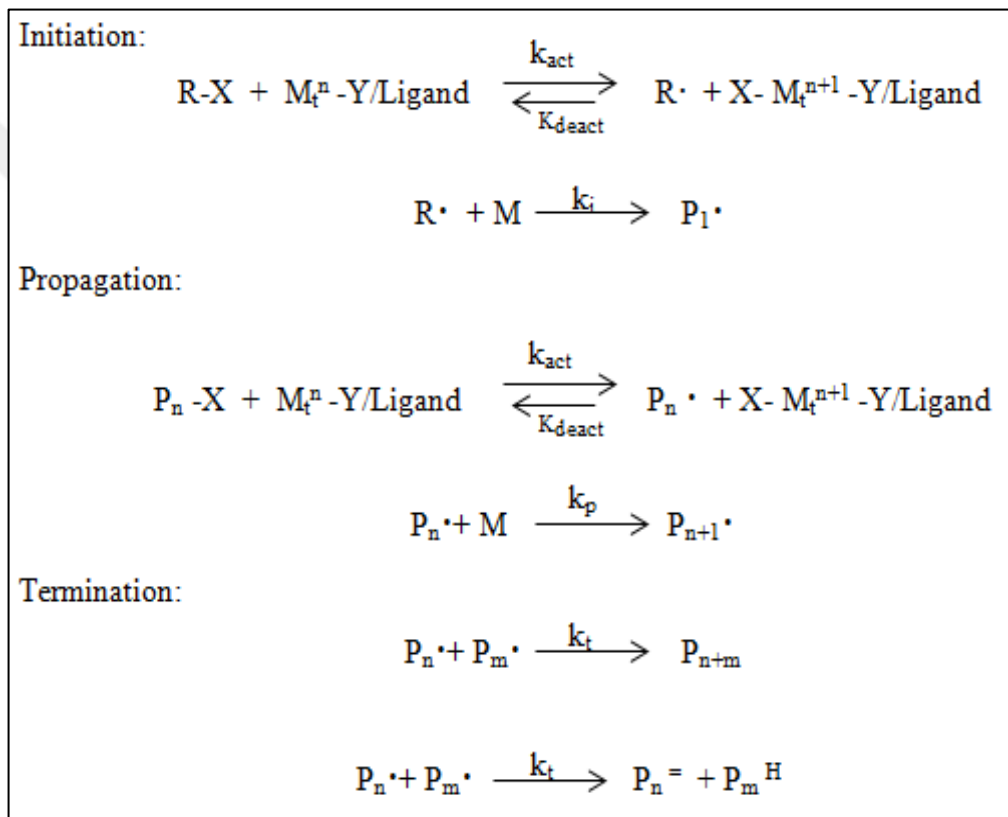


**Figure 2.4 :** Three main steps of ATRP mechanism.

Initiation: Thermal unstable part of this mechanism is initiator. It is needed to supply energy to split into two free radicals. These components carry unpaired electrons within it. Reaction temperature and solvents are the conditions for the rate of decomposition of initiators.

At this step, free radical must find another radical to couple with. This enables free radicals to get stabilized. Double bond in the monomer molecule will be attacked by highly reactive of free radical. Double bonds consist of two electrons one of them

occurs as sigma electrons the other one occurs as pi electrons. Pi electrons are far away from the nucleus so the pi electrons are weaker than the sigma electrons (Wahab, 2013).

**Propagation:** It is a second process of ATRP mechanism. In this step, new monomers are occurred due to the interactions between the fresh monomer to the first monomer. This situation occurs until the termination process.

**Termination:** It is a final step of the polymerization process. This part can be divided into two types are coupling termination and dis-proportionating termination. Two combined growing chains in the coupling termination occur electron pair. Therefore, coupling termination has longer chain length than dis-proportional termination.

Polymerization reactions should be living to be able to used as macroinitiators for continued polymerizations. With ATRP mechanism, this goal is achieved via the reversible halogen end capping. Thus, at the end of the polymerization, all polymer chains should possess a halogen atom and they can be used as macroinitiators for further polymerizations (Matyjaszewski et al., 2003)

## **2.3 Synthesize of Polymer/MWCNTs Nanocomposites**

There are different methods to obtain MWCNT-reinforced polymer nanocomposites including solution mixing, melt compounding, in-situ polymerization. The dispersion and distribution of MWCNTs in the polymer matrix are the significant during the polymerization process. Therefore, to obtain effective dispersion and distribution, most suitable method should used.

### **2.3.1 In-situ polymerization**

In this process, monomer and nanoparticles are premixed. This mixture process provides interaction between the monomer and nanoparticles that is MWCNTs in this study. Initiator is added after the homogeneous mixture is occurred. Heat is applied in this study to accelerate the polymerization process (Figure 2.5) .This method has excellent performance compared to the other methods. It provides good miscibility between the polymer and the nanotubes (Sankaran, 2016).

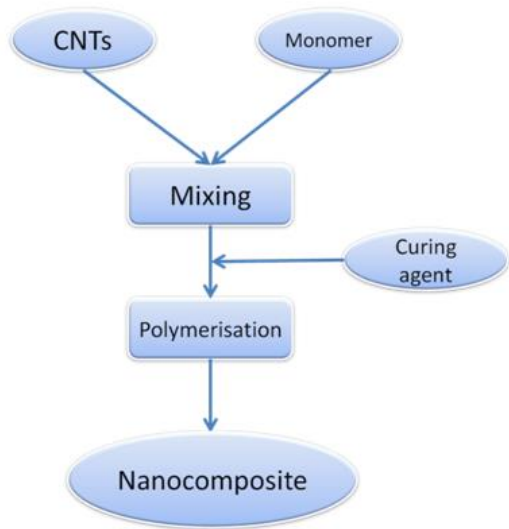


**Figure 2.5 :** The image of in-situ polymerization process with steps (Beyou et al).

### 2.3.2 Solution blending

Solution blending is the method to produce polymer nanotube composites. It is common method among others. Same solvent is added to the mixture of carbon nanotubes and polymer mixture stirres to get effective interaction between the polymer and carbon nanotube layers. There are both advantages and disadvantages of this method. This method works with small sample sizes very well and the dispersion is consistent in this polymerization method. The schematic illustration of this synthesis method is given in Figure 2.6. (Beyou et.al)

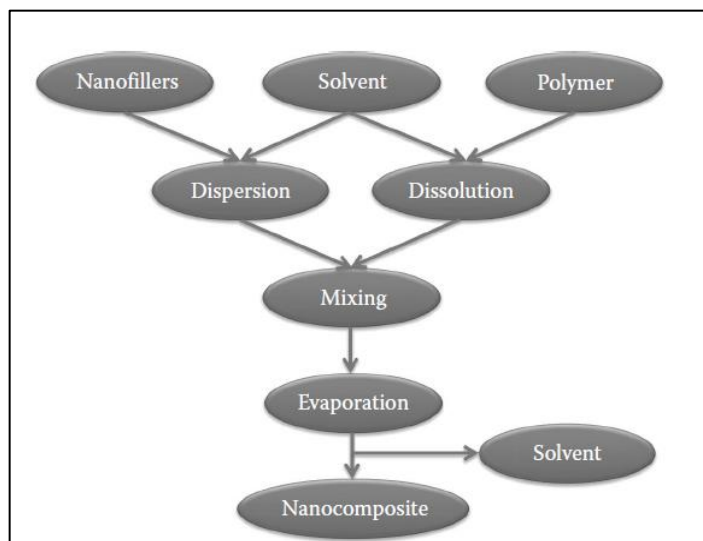


**Figure 2.6 :** Schematic representation of the solution blending process.

### 2.3.3 Melt compounding

It is an alternative method used in producing thermoplastic polymers. Nanofillers and polymers are used as the starting material and they are diluted in melt compounding step (Figure 2.7). For that matter, nanotubes and polymer matrix are combined efficaciously. However, this method is disabled at low MWCNT compositions due to their high aspect ratios. (Caroline et al., nd)

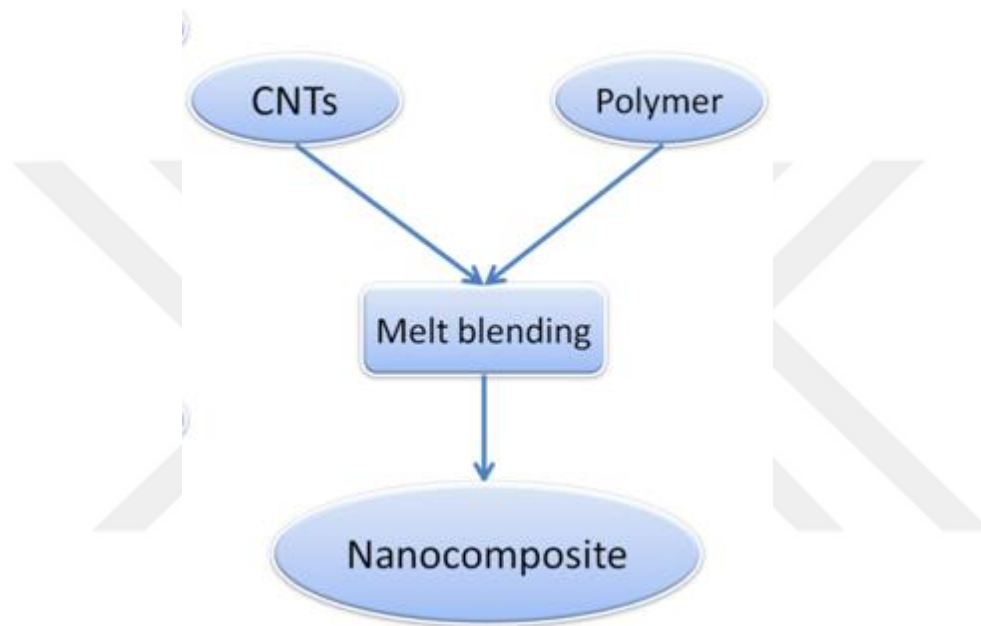


**Figure 2.7 :** Melt mixing process with its steps.

### 2.4 Thermal Properties of Polymers

Temperature affects the polymer's structure directly. At lower temperatures, polymer structure is frozen state that is also called glassy state that has hard and brittle nature. In this state, molecules can vibrate but they are not able to move importantly. Heat is the driving force to soften the polymer. When heat is applied to polymer, chains of the polymers can juggle around the each other. Thus, soft and flexible polymer is occurred. This satete is named as rubbery state. There is specific temperature that makes transition between the glassy states to rubbery state. This temperature is called the glass transition tempereture ( $T_g$ ). Glass transition temperature only affects the amorphous region of the polymers. Crystalline region does not affected by glass transition temperature. This situation was shown in the Figure 2.8.

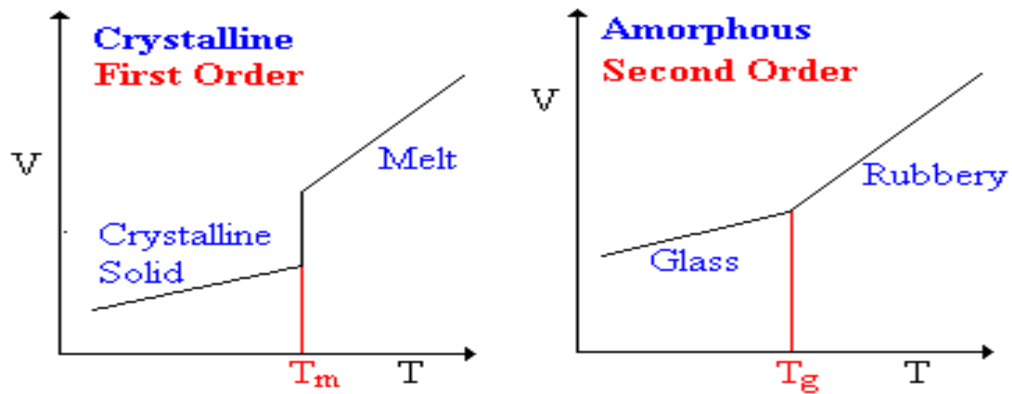


**Figure 2.8 :**  $T_G$  effects on crystalline and amorphous region (Url-7).

### 2.4.1 Thermogravimetric analysis

Amount of weight changes of materials are measured by TGA technique. This measurement can be as a function of time or as a function of raising temperature. This can be measured in an atmosphere of nitrogen, helium, air or in vacuum. With this technique, many types of materials can be analyzed such as inorganic materials, metals, polymers, ceramics, glasses and composites. Powder samples or small pieces are used to analyze the whole material. Temperature is changed from room temperature to 900°C steadily. The weight of sample can change from 1mg to 150 mg. Although 10 mg is preferred, for some situations, superior results are obtained using 1 mg from material.

## 2.5 Mechanical Properties of Polymer Nanocomposites

### 2.5.1 Hardness

Hardness is the resistance of materials against deformations. It is associated with its strength, wear and fatigue resistance. In other words, the bigger the hardness of the material, the better resistance it has to deformation. It is important to know the hardness of the materials, because it determines the mechanical properties of the materials. Hardness values of many materials such as metals, polymers, ceramics and coatings can be calculated by hardness test techniques. These techniques are special for different geometrical shapes of the indenter. The commonly used geometrical shapes were given below: (Url-8)

- 1) Brinell (hard steel, carbide sphere)

- 2) Vickers (pyramid-shaped diamond)
- 3) Rockwell (cone, sphere)

Some metals that are thin steel, cemented carbides, lead, aluminum, zinc, copper alloys, titanium and iron are characterized by using Rockwell hardness test method.

Force is applied to the sample measuring the permanent depth of indentation. Firstly, minor load is applied to a sample using a diamond or ball to notch. After applying the minor load for specified time, the depth of indentation is quantified. The amount of minor load is 10 kg; major load can divide three parts depending on nature of the indenter. These three types (Url-10) are classified as Rockwell (A), Rockwell (B), and Rockwell (C).

- 1) Rockwell hardness A is making with diamond and 60 kg load is applied.
- 2) Rockwell hardness B is making with 1/16 in ball, 100 kg major load is applied.
- 3) Rockwell hardness C is making with diamond and 150 kg is applied as major load. The C-scale is used for harder materials more load is applied with strong diamond indenter.

Rockwell hardness test technique is widely used to determine the hardness of the materials due to its some superior properties: it is faster than others, easy to perform, more appropriate.

Rockwell hardness test technique (Url-9) is occurred in several steps (Figure 2.9):

Firstly, penetration depth is determined by pressing the indenter to the specimen. This indenter-pressing step provides to get reference level ( $h_0$ ) for calculating the residual indentation depth ( $h$ ).

In the second step, the indenter enters into the specimen up to a maximum depth ( $h_1$ ) due to the additional test force applied for a dwell period.

In the last step, the additional test force is removed and the indenter moves up at the level of rest indentation depth.

After these steps, hardness values are calculated practically using the  $h$  value.

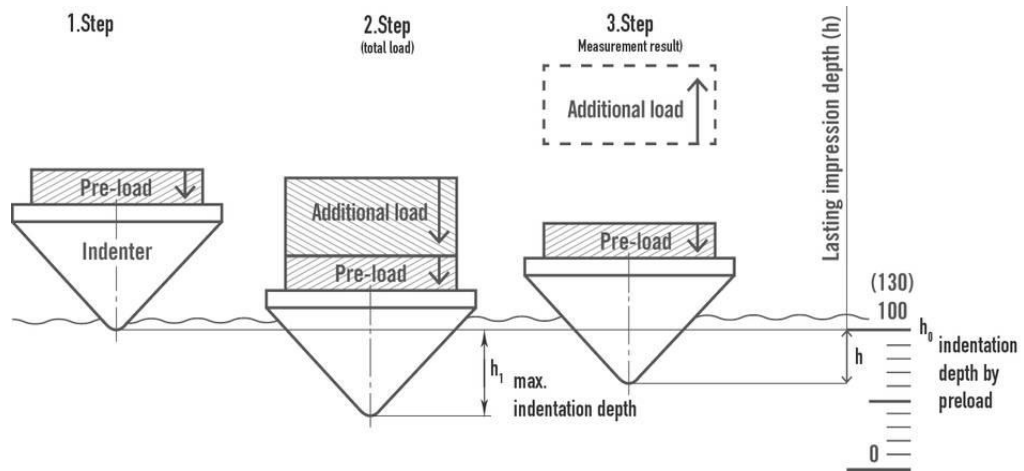


**Figure 2.9 :** The view of the Rockwell hardness test with steps (Hijazi, n.d).

## 2.6 Ultrasonic Test

To measure the imperfections in the materials, ultrasonic test can be used. This technique uses the high frequency sound waves. Ultrasonic test enables us to determine the speed of sound in a solid material. Additionally, it is useful for calculating the some important parameters such as Poisson's ratio, Young's modulus, shear modulus, microhardness of the materials.

In solids, there are four modes that sound can propagate. These modes are longitudinal waves, surface waves, shear waves, plate waves which occur in thin materials. Although there are four modes, only two modes of propagation are commonly used in ultrasonic testing method. These modes are longitudinal and shear waves that shown in the Figure 2.10. (Soffar, 2016)

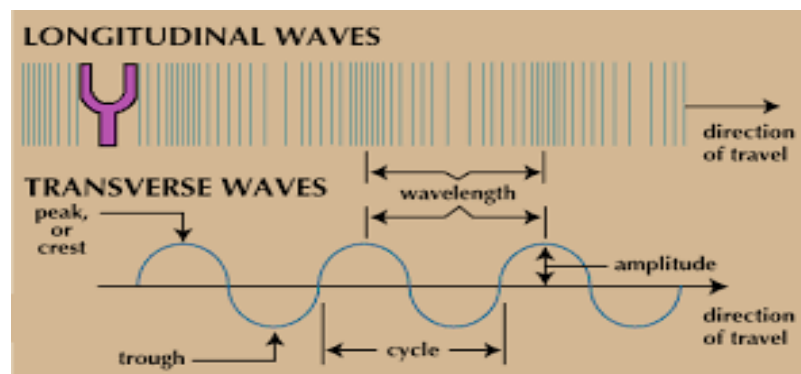


**Figure 2.10:** Longitudinal and transverse (shear) waves.

There are important formulas to analyze the longitudinal and transverse waves:

$$C_L = \sqrt{\frac{E(1 - \nu)}{\rho(1 + \nu)(1 - 2\nu)}} \quad (2.1)$$

$$C_T = \sqrt{\frac{E}{2\rho(1 + \nu)}} = \sqrt{\frac{G}{\rho}} \quad (2.2)$$

$C_L$ : velocity of the longitudinal wave

$C_T$ : velocity of the transverse wave

E: Young's modulus [N/m<sup>2</sup>]

$\rho$ : density [kg/m<sup>3</sup>]

$\nu$ : Poisson's ratio

G: shear modulus [N/m<sup>2</sup>]

To find E and  $\nu$  values, these two equations are solved for E and  $\nu$ :

$$\nu = \frac{1 - 2\left(\frac{C_T}{C_L}\right)^2}{2 - 2\left(\frac{C_T}{C_L}\right)^2} \quad (2.3)$$

$$E = 2\rho C_T^2(1 + \nu) \quad (2.4)$$

$$G = \rho C_T^2 \quad (2.5)$$

$$H = [(1 - 2\nu) * E] / [6(1 + \nu)] \quad (2.6)$$

H expresses microhardness that can be defined as the ratio of the load applied to the indenter force (kg) to the uncovered projected area A (mm<sup>2</sup>).

To sum up; E,  $\nu$ , G and H are found easily, if other parameters ( $\rho$ ,  $C_L$ ,  $C_T$ ) were given.

The speed of both longitudinal and transverse waves is found using the Equation 2.7 below:



$$c = \frac{2d}{\Delta t} \quad (2.7)$$

$d$  is the thickness of the material,  $\Delta t$  is the transit time and  $c$  is the speed of the waves. Using the both of these equations above, we can find Young's modulus, Poisson's ratio, shear modulus, microhardness of the solid materials. There are three kinds of the ultrasonic testing techniques:

Normal beam and angle beam: It depends on the angle that the sound energy enters the test article.

Contact and immersion: It relates to the method of coupling the transducer to the test article.

Pulse-echo and through transmission: In this technique, transducer produces an ultrasonic pulse at the surface of the solid material. This ultrasonic pulse travels inside the material and reflects echo with opposite direction. Echoes are taken by transducer to keep bouncing off the opposite faces of the material, decreasing with time.

## **2.7 The Use of Gamma Transmission Technique at Polymers**

Gamma rays are high energy photons that their wavelengths shorten than 10-11 m and frequencies above 10<sup>19</sup> Hz. Gamma rays are high-energy photons nearly 10000 times as much energy the visible photons. Gamma rays produced by decay of atomic nucleus from a high-energy state to a lower energy state. These photons have no mass and electrical charge so they cause indirect ionization. (Url-11)

There are so many interactions between the gamma rays and materials, only three key interactions were mentioned below.

Photoelectric effect: This event occurs at low energies of gamma rays. In this interaction, incident photon vanishes. Atom ejects the photoelectron from one of its bound shells.

The kinetic energy of the photoelectron (Equation 2.8) must be equal to energy differences between the incident photon energy ( $h\nu$ ) and binding energy of the photoelectron ( $E_b$ ).

$$E_e = h\nu - E_b \quad (2.8)$$

$h\nu$  is the energy of the incident gamma radiation ( $E_\gamma$ ). This interaction was illustrated in Figure 2.11. (Url-11)

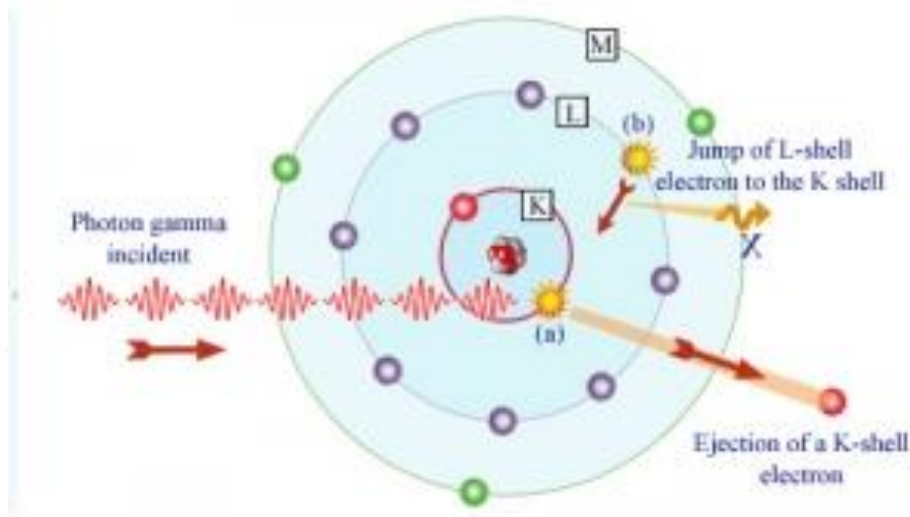


**Figure 2.11 :** The schematic view of the photoelectric effects.

Compton scattering: In this interaction, the incident gamma ray hits the target electron and it is deflected as a consequence an angle with respect to its original direction (Figure 2.12). This situation decreases the energy of the photon because it transfers a portion of its energy to the recoil electron. Due to there are many scattering angles, the transferred energy can change from zero to incident gamma ray energy values.

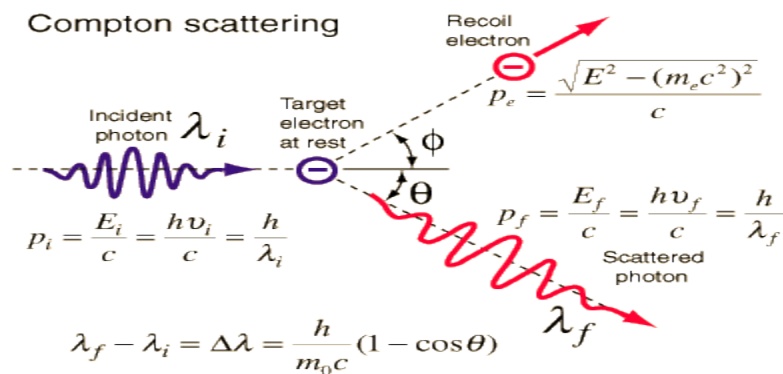


**Figure 2.12 :** The view of Compton scattering interaction with formulas (Url-11).

- 1) Pair Production: If the incident photon has at least 1.022 MeV, pair production occurs. When the photon passes near the nucleus, it interacts with the strong electric field around the nucleus. Photon is transformed into two

particles due to this electric field. Electron and positron are these two transformed particles. This specific interaction was given in Figure 2.13 schematically.



**Figure 2.13 :** The schematic view of pair production (Url-11).

These three interactions determine the total cross section of the interactions between gamma rays and atom. Cross-section of the interaction and intensity of the gamma ray are the important for finding the amount of attenuation. The sum of the linear absorption coefficients of the photoelectric effect, Compton scattering and pair production equals to the total attenuation coefficient ( $\mu_1$ ) (Equation 2.9).

$$\mu = \mu_{ph} + \mu_{Co} + \mu_{pp} \quad (2.9)$$

In this formula,  $\mu_{ph}$  determines the absorption coefficient of the photoelectric effect,  $\mu_{Co}$  gives the absorption coefficient of the Compton scattering, and  $\mu_{pp}$  is the absorption coefficients of the pair production.

The Lambert-Pierre law (Equation 2.10) provides to determine the  $\gamma$ -ray attenuation after interactions with materials.

$$I = I_0 \cdot e^{-\mu \cdot x} \quad (2.10)$$

$I$  is the intensity that passed through the material and reached the detector.  $I_0$  is the initial radiation intensity. It is the measurement of the air intensity without a sample.  $I/I_0$  ratio gives the gamma-ray transmission of the composite sample. The thickness of the absorbance expresses as  $x$  (cm). The linear attenuation coefficient labels as  $\mu$  in this equation. The value of  $\mu$  depends on both gamma-energy and density of the material. If thickness of the absorbent material increases, gamma-ray transmission decreases. On the other hand, gamma-ray transmission increases with increasing

gamma-ray energy. Another important expression is the mass attenuation coefficient depending on density of the material. It can be expressed as  $\mu/\rho$  and its unit is  $\text{cm}^2/\text{g}$ .

## 2.8 The Use of Howitzer with Pu-Be Neutron Source at Polymers

Neutrons are sub-atomic hadron particles. Neutrons do not have a net electric charge. The mass of neutrons is slightly more than the mass of the photon. There is at least one neutron in each atomic nucleus except hydrogen. Together with protons, neutrons form atomic nuclei together with nuclear force. It is symbolized with n. According to the standart model neutron is composed of two down and one upward quartzs (Figure 2.14) (Url-12).

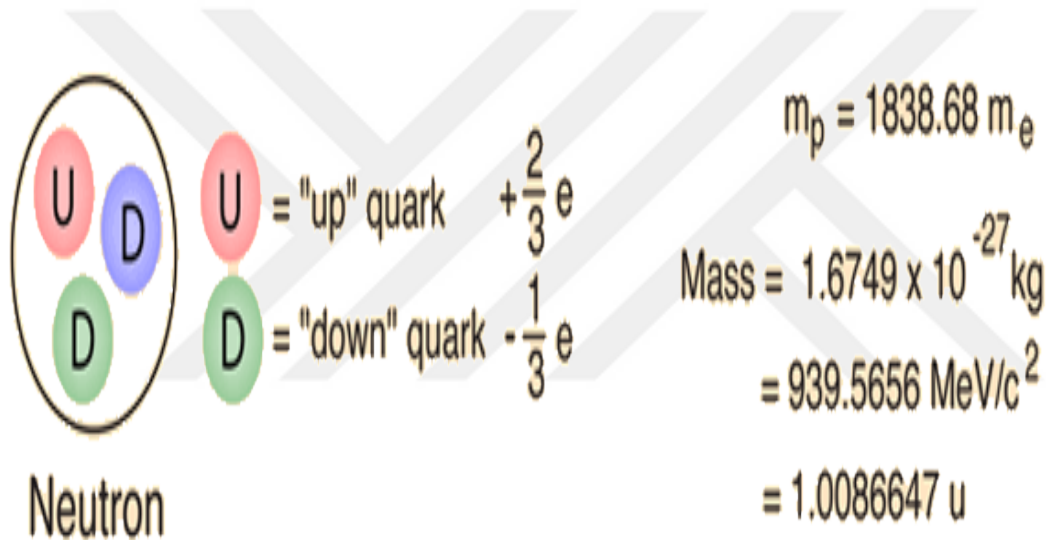


**Figure 2.14 :** The structure of a neutron according to the standart model.

Neutrons can be classified due to their energies as follows (L'Annunziata, 2003):

$E > 100 \text{ MeV}$ : High-energy neutrons

$10\text{-}20 \text{ MeV} > E > 100\text{-}200 \text{ keV}$ : Fast neutrons

$100 \text{ keV} > E > 0.1 \text{ eV}$ : Epithermal neutrons

$E \sim kT \sim 1/40 \text{ eV}$ : Thermal/slow neutrons

$E \sim \text{meV} \sim \mu\text{eV}$ : cold and ultracold neutrons

Neutrons can interact with matter in many ways. Five reactions can occur when a neutron interacts with a nucleus. These interactions were shown in Figure 2.15.

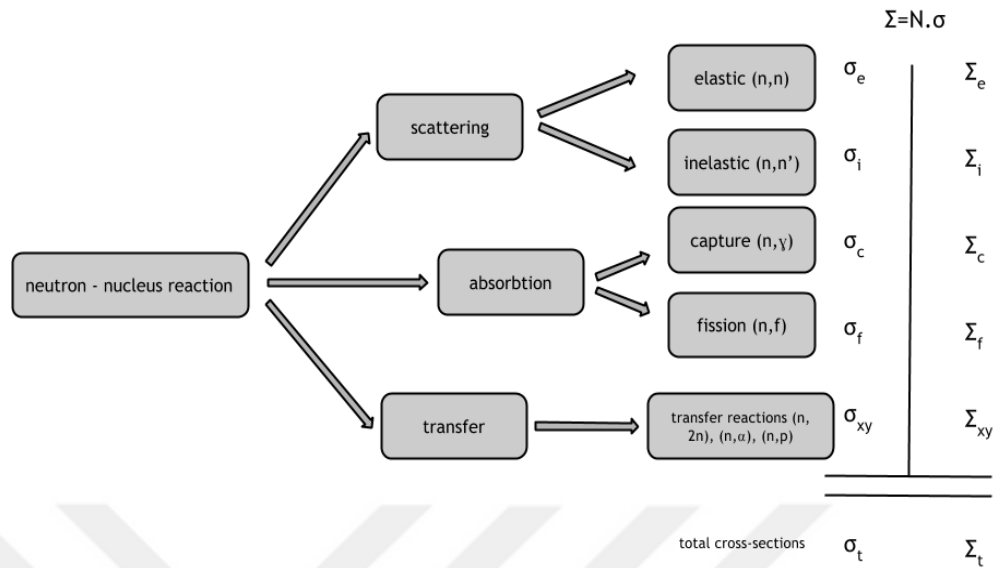


**Figure 2.15 :** The view of interactions between the neutron and nucleus (Url-15).

Elastic scattering (n, n): It seems like a billiard ball collision. When neutrons collide with a nucleus, they transfer their some energy to the nucleus. They go in a different direction. The target nucleus gains energy and moves at a raised speed.

Inelastic scattering (n, n<sub>γ</sub>): A neutron may hit a nucleus and it is absorbed temporarily. This forms compound nucleus that will be in an excited state. It goes to the initial position by emitting another neutron of lower energy in concert with a gamma photon. This situation is named inelastic scattering. (Url-13)

Neutron Absorption: This reaction happens in nuclear reactor. Neutron is fully absorbed in these reactions and compound nucleus is formed at the end of these reactions. There are two most important absorption reactions:

- 1) Radiative Capture: Capture reactions occur when neutron coupled with the production of one or more gamma rays. It is symbolized with  $\sigma_{\gamma}$ .
- 2) Neutron-induced Fission Reaction: For fissionable materials neutron can be captured or it can cause nuclear fission. Thus, absorption cross section divides two parts:  $\sigma_a = \sigma_{\gamma} + \sigma_f$ .

Neutron transfer reactions: In these reactions, neutron can absorb a neutron producing a compound nucleus. This producing compound nucleus emits charged particles that can be a photon or an alpha particle. At the end of these reactions, a nucleus of a different element occurs. There are three neutron transfer reactions which are (n, 2n), (n, α), (n, p).

Neutron- Proton Reaction (n, p): Nitrogen-16 is formed when Oxygen-16 captures a neutron and emits a photon (Figure 2.16) (Url-14).

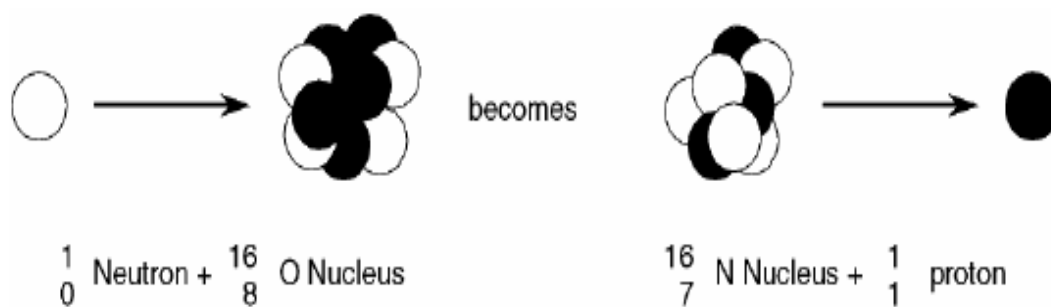


**Figure 2.16 :** The schematic illustration of neutron-proton reaction.

Neutron- Alpha Reaction (n, α): Boron-10 captures the neutrons to form the Li-7 nucleus (Figure 2.17) (Url-16).

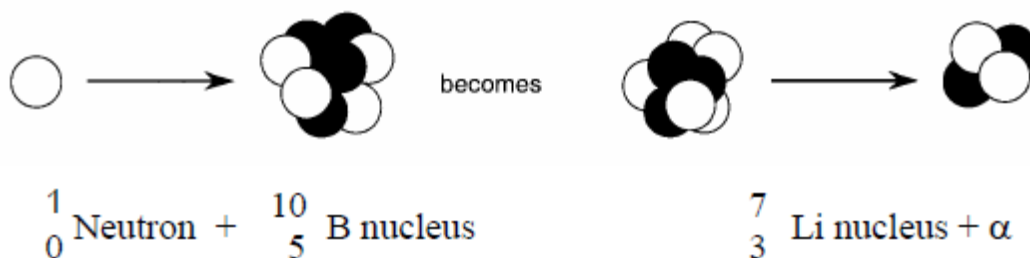


**Figure 2.17 :** The schematic illustration of neutron-alpha reaction.

The total probability for neutrons to interact with matter can be expressed as the sum of the cross-sections of these individual interactions mentioned above.

The attenuation coefficient for neutrons is expressed by the following formula (Equation 2.11).

$$I=I_0.e^{-\Sigma(\text{tot}).x} \quad (2.11)$$

$\Sigma_{\text{tot}}$  refers to the macroscopic cross section of neutrons. It looks like a linear attenuation coefficients of interactions between the matter and gamma photons.







### 3 EXPERIMENTAL

#### 3.1. Materials

Materials using this thesis study were listed with company names: Tetra-n-butylammonium bromide ( $\text{Bu}_4\text{NBr}$ ), 98+% (Alfa Aesar), copper bromide ( $\text{CuBr}$ ), Puratronic ®, 99.998% (metal basis) (Alfa Aesar), Methyl methacrylate (MMA), 99% stab. (Alfa Aesar), 1,1,4,7,7-Pentamethyldiethylenetriamine (PMDETA), 98% (Alfa Aesar), Ethyl 2-bromoisobutyrate (EBiB), 98+% (Alfa Aesar), Extra pure argon and regulator were received from Özvarış firm. Multi-wall carbon nanotubes (MWCNTs), purity > 92 %, outside diameter: 7-16 nm, is purchased from Nanografi.

#### 3.2. Preparation of PMMA/MWCNT Nanocomposite Samples

Chemicals were weighted inside two hands AtmosBag in an argon atmosphere. Before filling the argon gas, vacuum was applied to get air inside the AtmosBag that was shown in the Figure 3.1.



**Figure 3.1 :** The weight process was done inside this AtmosBag.

First, base samples were prepared. Solvent  $\text{Bu}_4\text{NBr}$  (1.211 g, 3.76 mmol) and catalyst (0.067 g, 0.47 mmol) were weighted then nanocomposite samples were prepared four different compounds of MWCNTs: 0.25 wt. %, 0.5 wt. %, 1 wt., %, 2

wt. %. All chemicals were added to the tubes. After the chemicals were weighted, they were taken out from the AtmosBag and put to the AtmosBag to start synthesis process shown in Figure 3.2. In this section, monomer MMA (28.2 g, 0.282 mol) was mixed with solid chemicals. Then, ligand PMDETA (0.081 g, 0.47mmol) was added to the mixture and mixture degassed with gas tight syringe for 5 minutes. Finally, initiator EBIB (0.092g, 0.47 mmol) was added in the tubes to start the polymerization and then tubes were closed and sealed with parafilm.



**Figure 3.2 :** The AtmosBag that synthesis process was done.

After these processes were finished, mixture was taken out and put on the magnetic stirrer with silicon bath. (Figure 3.3). This magnetic stirrer has also adjustable temperature property that provide us adjust the temperature manually. This stirring process continued until the polymerization was finished completely.



**Figure 3.3 :** The mixture is on the magnetic stirrer to complete the polymerization process fastly.

After the polymerization was completed, samples were prepared to test and determine the structural, mechanical, thermal and other properties. (Figure 3.4)



**Figure 3.4:** The view of PMMA/MWCNTs test samples.

### 3.3 SEM Characterization

SEM is an electron microscope type that acquires images by scanning the surface of the sample with a focused electron beam. Electrons contain different signals that interact with the atoms in the sample and contain information about the topography and composition of the surface. The electron beam scans the surface with the cellular scan plane, and the image is created by matching the beam's position with the perceived signal.

Higher resolution bigger than 1 nanometer is possible at SEM analysis. In order to form an image in the SEM, it is most useful to use secondary electrons emitted by the sample atoms excited by the electron beam. The change in the number of secondary electrons that are broken off from different regions of the sample depends primarily on the junction of the beam to the surface, that is, the surface topography of the surface. Besides secondary electrons; X-rays, light (cathode ray), sample current and transmitted electrons are also suitable for obtaining various signals from the sample.

#### Working Principle

High-energy beam electrons form low-energy Auger electrons due to the non-elastic interference with the outer orbital electrons of the sample atoms. These electrons carry information about the surface of the sample and form the working principle of the Auger spectroscopy.

Because of these interactions with the orbital electrons, electron beams emitted from their orbits are reducing from the surface of the sample. These electrons are called secondary electrons. The secondary electrons are collected in the scintillator that is made up of a crystal or matter that emits visible light in a charged particle excitation located in the sample chamber and converted into a secondary electron image signal. Secondary electrons are used to obtain a high resolution topographical image of the sample surface comes from a depth of 10 nm or less (Url-18).

In this study, FEI-Quanta FEG 250 Model scanning electron microscope was used to determine the morphological characterization of PMMA/MWCNTs nanocomposites. The image of the microscope was shown in Figure 3.5. The SEM Analysis was carried out at National Research Center on Membrane Technologies at ITU.



**Figure 3.5:** The scanning electron microscope using this study.

It is very important that knowing the dispersion of MWCNTs in the PMMA matrix. SEM allows us to see how amount of MWCNTs affect the microsize structures of PMMA/MWCNTs nanocomposites. It is significant property of dispersion of MWCNTs in the pure PMMA matrix since it affects the mechanical and physical properties of the PMMA/MWCNTs nanocomposites.

There are several steps to prepare the samples before characterization. First step was cleaning the polymer nanocomposites using deionized water, ethanol. After the cleaning process, samples were dried. Samples were coated with gold using plasma coating technique. This coating provided us having conductive samples. Continuity of electrons flow was provided with this coating process that provided high-quality morphology images. The thickness of the coated sample was about 0.2 nm to 0.3 nm. After the preparation steps, samples were placed into microscope chamber and 15 kV was applied from electron gun to generate the secondary electrons. These secondary electrons were coming from the top 5-15 nm of the sample surface. The morphology images of samples were forming by ejected secondary electrons.

### **3.4 Fourier Transform Infrared Spectroscopy (FTIR)**

FTIR is one of the useful methods that use the IR radiation to identify the unknown materials. In this method, IR radiation passed through a sample. There are two interactions between the sample and radiation. One of them is infrared radiation is absorbed and another interaction is some of its transmitted. These interactions provide to occur fingerprint of the sample. This trace is the unique for different molecular structures. Therefore, same infrared spectrum does not occur for the different molecules. This enables us easy way to determine the molecular structures clearly. (Url-19)

FTIR is useful to determine some properties of materials:

- 1) It provides us to determine the unknown materials.
- 2) It is also useful for identifying the amount of components in a mixture.
- 3) The quality of the material is easily determined by using FTIR.

The FTIR measurements were carried out using a Bruker ALPHA Spectrometer at ITU Faculty of Science and Letters Chemistry Laboratory.

Firstly, the PMMA/MWCNTs nanocomposite samples and base PMMA were cutting with abrasive cutting machine to get ~3 mm thickness. After that, cutting samples were grinded to have smooth surface. Finally, samples were ready to FTIR test to analyze the molecular structures of both pure PMMA sample and PMMA based MWCNTs nanofiller samples.

### 3.5 X-ray Diffraction (XRD)

An X-ray tube, an X-ray detector and a sample holder are the most important parts of the X-ray diffractometers. X-rays are produced in a cathode ray tube by heating a filament to produce electrons. Voltage is applied to accelerate the electrons through the target. These accelerating electrons interact with target and characteristic X-ray spectrum is formed in the screen. If incoming electrons do not have enough energy to dislodge inner shell electrons of the target material, X-ray spectrum will not occur. The produced spectrum has many components.  $K_{\alpha}$  and  $K_{\beta}$  radiations are the most important part of the spectra.  $K_{\alpha}$  has two parts that are  $K_{\alpha 1}$  and  $K_{\alpha 2}$ .  $K_{\alpha 2}$  has larger wavelength than  $K_{\alpha 1}$  but  $K_{\alpha 1}$  has twice intensity as  $K_{\alpha 2}$ . These special wavelengths give the main characteristic of the target material.

There are different target materials such as Cu, Fe, Mo, Cr but Copper (Cu) are the most usual targets for single-crystal diffraction, with  $CuK\alpha$  radiation which wavelength is 1.5418 Å. These rays can be collimated using the suitable filter to produce monochromatic X-rays eliminating brehmssthalung continuum radiation. (Dutrow & Clark, n.d)

There are many interactions between the X-rays and target material.

- 1) Absorption
- 2) Scattering
- 3) Transmitting

When materials subjected to X-rays, the X-rays are partly absorbed and partly scattered, and the rest of photons is transmitted.

Bragg's law (3.1) explains this mechanism clearly (Figure 3.6).

$$n\lambda = 2d\sin\theta \quad (3.1)$$

In this formula, theta is an incident angle, n is an integer number value,  $\lambda$  is the wavelength of the X-ray beam and d is the distance between the planes.

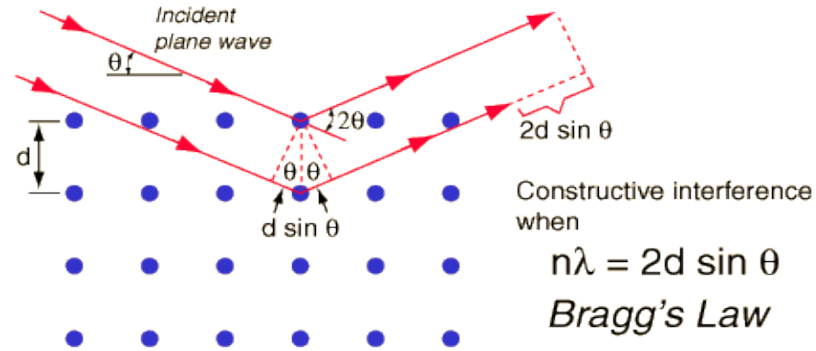


**Figure 3.6 :** Symbolic representation of Bragg's law (Url-17).

Two conditions satisfy the Bragg's law:

- 1) The incidence angle must be equal to scattering angle.
- 2) Wavelengths that have an integer number are equal to the pathlength difference.

These conditions enable us to calculate the details about the crystal structure of the polymers. To determine the crystal structure XRD diffractometer was used at ITU Prof.Dr.Adnan Tekin Materials Science and Production Technologies Applied Research Center (ATARC). XRD machine that was used for this study has scanning speed of 2°/min and operating at 40kV and 40 mA. The powder samples were prepared for XRD analysis. Manual milling agate martar was used to reduce particle size. After this process, samples were ready to XRD analysis.

### 3.6 Thermal Stability of PMMA/MWCNTs

In this characterization test, nearly 5 mg sample was placed in a platinum pan and it put into the insulated furnace. Nitrogen was used to obtain the inert atmosphere. Measurements were performed a temperature range from room temperature (25°C) to 600°C with a constant heating rate of 20°C per minute. TGA was performed at ITU Energy Institute Laboratory.

### 3.7 Ultrasonic Test

Ultrasonic test is especially useful for measuring homogeneity of the materials, to determine the homogeneity of PMMA/MWCNTs and find the mechanical properties of the materials such as Young modulus, shear modulus and microhardness of the samples, the ultrasonic test method was used. Pulse echo technique was used in the

ultrasonic test. It was used in ultrasonic test to observe echo amplitudes. To have different frequencies two different ultrasonic probes were used. These different frequencies enabled us to determine the changes in velocity of longitudinal and transverse waves in the PMMA/MWCNTs samples (Figure 3.7).



**Figure 3.7:** The pulse echo technique using this study.

The probes of ultrasonic test device (Krautkromer USM 25) measured the longitudinal and transverse waves at room temperature. Densities measured by using pichnometer. It was needed for finding elastic properties of the PMMA/MWCNTs with the different amounts of MWCNTs.

Before measurements of the longitudinal waves of the samples, device was calibrated with steel block and velocity of steel was found 5911 m/sn which was the reference for other samples. Range was 50 mm for reference material. To measure the longitudinal wave's velocity, B2S prob was used.

Before measurements of the velocity of the transverse waves, device was calibrated with steel block and velocity of steel was found 3248 m/sn which was the reference for other samples. Range was 50 mm for reference material.

To measure the longitudinal wave's velocity, B1Y prob was used. Measurements were taken with gel couplant and measurements were made by creating an ultrasonic bond with the gel couplant between the probe and the material.

This characterization test was performed at Çekmece Nuclear Research and Training Center at Küçükçekmece Istanbul.



### **3.8 Mechanical Properties of PMMA/MWCNTs**

#### **3.8.1 Rockwell hardness**

To find the hardness of the polymer nanocomposites, Rockwell hardness M scale was used. Steel ball that has 6.35 mm diameter was used in Rockwell hardness machine (Zwick Roell ZHR).

In Rockwell hardness test, major load (100 kg) and minor load (10 kg) were applied. Minor load was applied for seating the indenter and major load was applied for producing a permanent penetration.

Digital scale was on the machine that gave the hardness values of the materials directly. This mechanical test was performed at ITU Chemical and Metallurgical Engineering Faculty Sol-Gel Laboratory (Figure 3.8).



**Figure 3.8** : Rockwell hardness testing device.

#### **3.8.2 Density assesment of PMMA/MWCNTs nanocomposite by using pycnometer method**

The density values of the PMMA/MWCNTs nanocomposite samples and pure PMMA were determined using the pycnometer method. (Figure 3.9) The pycnometer

overflow glass jar which has 50 mL volume was weighted on a precision balance when it was empty. Then, it was filled with pure water and covered on the overflow lid and the excess volume was thrown out, then it was dried with towel. After that, it was measured again. At the end of these operations, the volume and mass of the pure PMMA and PMMA/MWCNTs nanocomposite samples were determined and density values of the all samples were calculated using the density: mass/volume. The temperature of the water bath was set to room temperature.

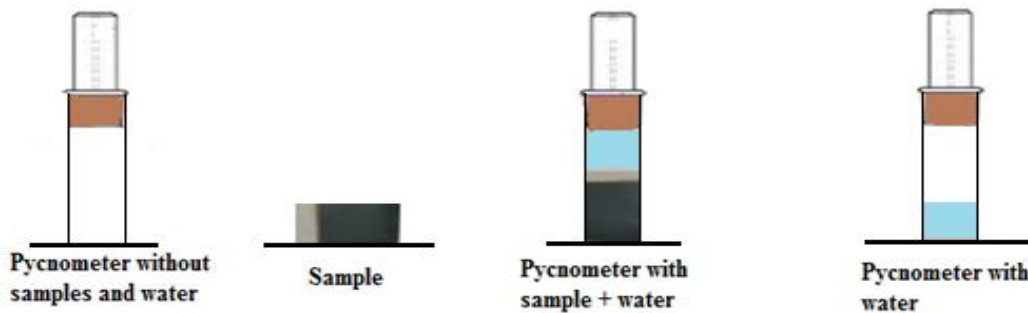


**Figure 3.9** : Schematic view of the application of the pycnometer method.

### 3.9 Application of Gamma Transmission Technique

To determine the attenuation coefficients of the PMMA/MWCNTs nanocomposites, two different radioisotopes were used in the gamma transmission technique. These radioisotopes are Cs-137 and Co-60 that have different gamma photon energies. Half-life of the Cs-137 radioisotope is 30.1 years and its gamma peak appears at 0.662 MeV.

The Co-60 radioisotope has two gamma peaks at 1.17 MeV and 1.33 MeV. It has short half-life (5.23 years) compared to the Cs-137. These two gamma radioisotopes were used to determine the relation between the amount of MWCNTs and linear attenuation coefficients.

Gamma rays that are passing through the materials were measured by gamma transmission technique. In this technique, detector and gamma source were put opposite sites on the same-axis. When the activation of detector was enabled, detector measured the gamma rays that reached the detector. The schematic view of the technique was showed in the Figure 3.10. This experiment was done at ITU Energy Institute Radiation Applications Laboratory-B.



**Figure 3.10 :** Experimental set up of gamma transmission technique.

At the first step, the intensity of the atmosphere was measured that can be called initial baseline ( $I_0$ ). Then, nanocomposite materials (MWCNTs) were placed at the detector side with the lead collimator that had 10 mm thickness. The intensity was counted 25 minutes for each PMMA/MWCNTs nanocomposite samples. This measurement was performed three times to get mean value.

Gamma spectrometer with a detector and a Multi-Channel Analyser was used in the experiments. The model of the detector was Canberra Bicron Model: 802-2x2. Multi-Channel Analyser has 1024 channel. The diameter of the detector was 20 mm. Cs-137 and Co-60 radioisotopes have same diameters values (6mm).

Diameter and thickness of the lead collimator were 7 mm and 10 mm respectively. The distance between the source and the detector was 190 mm for all measurements. However, the distance between the radiation source and materials was 140 mm due to using collimator to focus the intensity into the detector.

### **3.10 Application of Pu-Be Neutron Howitzer ( $\text{NH}_3$ )**

Neutron Howitzer ( $\text{NH}_3$ ) containing  $^{239}\text{Pu}$ -Be neutron source was used at the neutron transmission technique.  $^{239}\text{Pu}$ -Be neutron source ( $\alpha, n$ ), neutron detector (PM1401K), neutron collimator and neutron shielding equipment (boric acid) were carried out at the experiments. The properties of the  $^{239}\text{Pu}$ -Be neutron source were given in Table 3.1 (Url-20).

**Table 3.1** Properties of the Pu-Be Neutron Howitzer (NH<sub>3</sub>).

Properties	Value
Neutron Source	Pu-Be Neutron Source
Neutron Source Type	Nuclear Chicago Corporation
Neutron Production Reaction	( $\alpha$ ,n)
Activity	2 Ci
Neutron Flux	$10^4$ n/cm <sup>2</sup> s
Average Neutron Energy	53.97 kJ/mole
Number of The Irradiation Ports	2
Sizes of the Howitzer	Ø 60 cm x 90 cm
Thickness of the paraffin	25 cm

The neutron howitzer contains two radial beam ports of 29 cm long by 5 cm diameter:

One of the ports of the neutron howitzer is used for thermal neutrons. It can be accepted that this port is suitable to evaluate the total macroscopic cross section of the several materials such as the polymeric materials.

Another port of the neutron howitzer is utilized for epithermal neutrons. It can be accepted that this port at Neutron Howitzer (NH<sub>3</sub>) is suitable to evaluate the effective cross section of more dense material than polymer

Thermal neutron port of NH<sub>3</sub> was used to evaluate the changes in the total macroscopic cross sections of PMMA/MWCNTs nanocomposites. (Figure 3.11)

The neutron shielding performance of PMMA/MWCNTs nanocomposites was investigated with the rise of the MWCNTs compound in nanocomposite. Neutron tests were carried out at ITU Energy Institute.

Firstly, the initial count ( $I_0$ ) was measured without the nanocomposite samples. After measurement of the initial count, PMMA/MWCNTs nanocomposite samples that have different thickness were placed respectively at the experimental setup. This count took 100 seconds for each sample.

Counts were taken up to 100 seconds in every 10 seconds. Each count was performed three times to get mean value. This experiment was done for both irradiated PMMA/MWCNTs and unirradiated PMMA/MWCNTs.

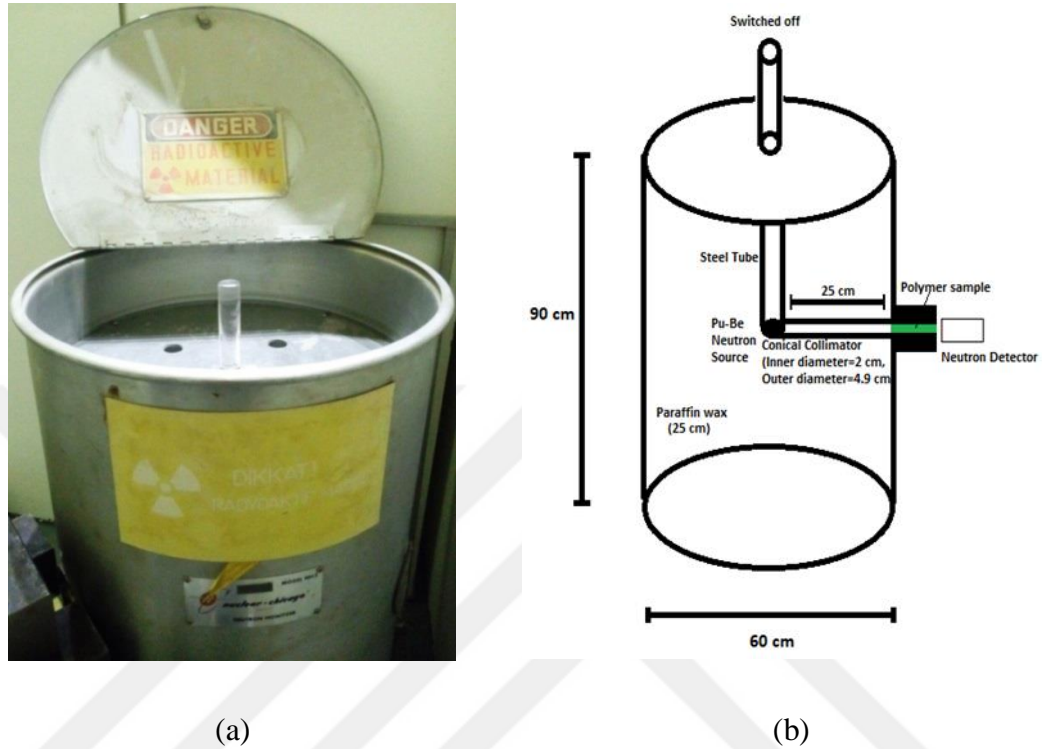


**Figure 3.11:** (a) The image of Neutron Howitzer (b) The schematic view of thermal neutron port of Neutron Howitzer.

### 3.11 Absorbed Dose of PMMA/MWCNTs Nanocomposite

The irradiation was performed by using Co-60 radioisotope in this study. PMMA/MWCNTs polymer nanocomposite samples produced by ATRP method at four different amounts of MWCNTs. 0.5 wt, 1 wt and 2.wt % PMMA/MWCNTs were irradiated.

#### 3.11.1 Irradiation conditions of the PMMA/MWCNTs nanocomposite

Properties of the Co-60 radioisotope were presented in Table 3.2. The irradiation settlement of the samples around the Co-60 radioisotope was presented in Figure 3.12. The irradiation tests place were performed in Gamma-Pak Sterilization Company and the date of tests was on August 14, 2017.

**Table 3.2 :** The properties of the Co-60 Radioisotope and irradiation conditions.

Properties	Value
Energy $E_{\gamma}$	1.17 and 1.33 MeV
Half-life of the radioisotope	5.26 years
Activity of the source	~ 1000000 Ci.
Dose rate	2.1 kGy/h
Irradiation time	23.81 hours

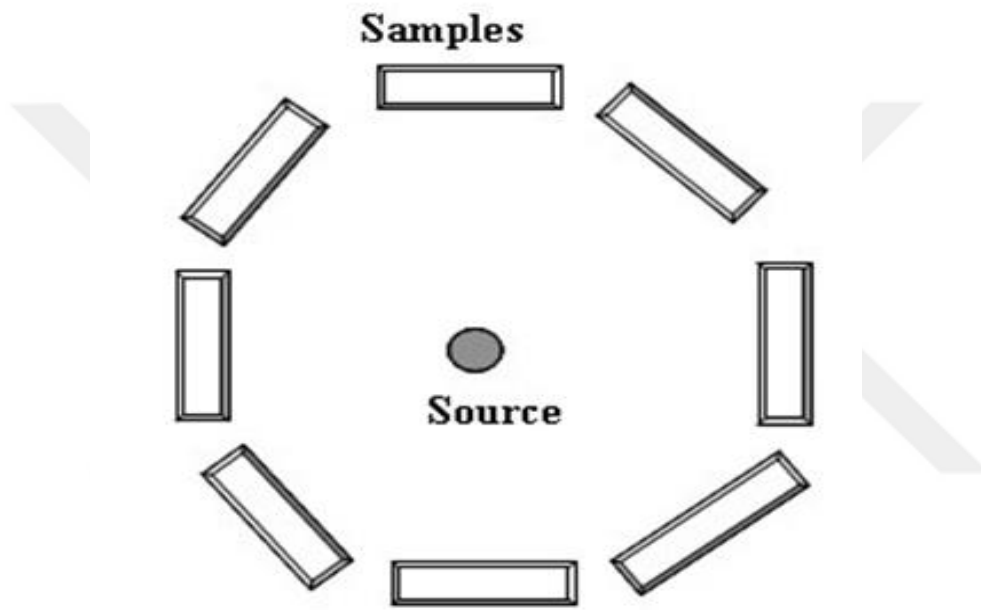


**Figure 3.12:** The settlement of the samples.

The powder/fragment has not appeared on the surface after irradiation treatment at 50 kGy in this study. This study was performed in Gamma-Pak Company at Tekirdağ.

## 4 RESULTS

### 4.1 SEM Characterization

The surface image of pure PMMA is relatively flat and smooth, shown in Figure 4.1(a-c).

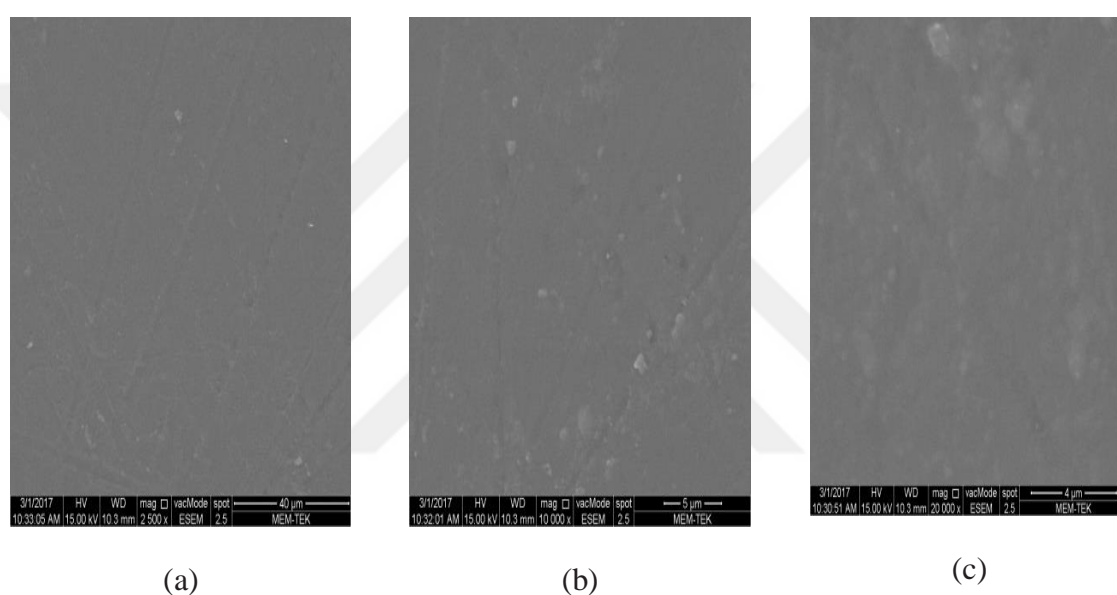


**Figure 4.1** : SEM images of pure PMMA at (a) 2 500x, (b) 10 000x, (c) 20 000x magnifications.

The surface morphologies of MWCNTs samples in SEM images were shown in Figure 4.2 with different magnifications that are 2 000x, 5 000x, 10 000x and 20 000x.

It can be seen from figure (20000x) that the MWCNTs are composed of nanotubes with surface diameter around 5 $\mu$ m. The SEM image of the 2 wt. % PMMA/MWCNTs were given at discussion section comparing with literature.

SEM images of 2 wt. %PMMA/MWCNTs provide to understand how nanofiller affects the morphology comparing with pure PMMA and pure MWCNTs.

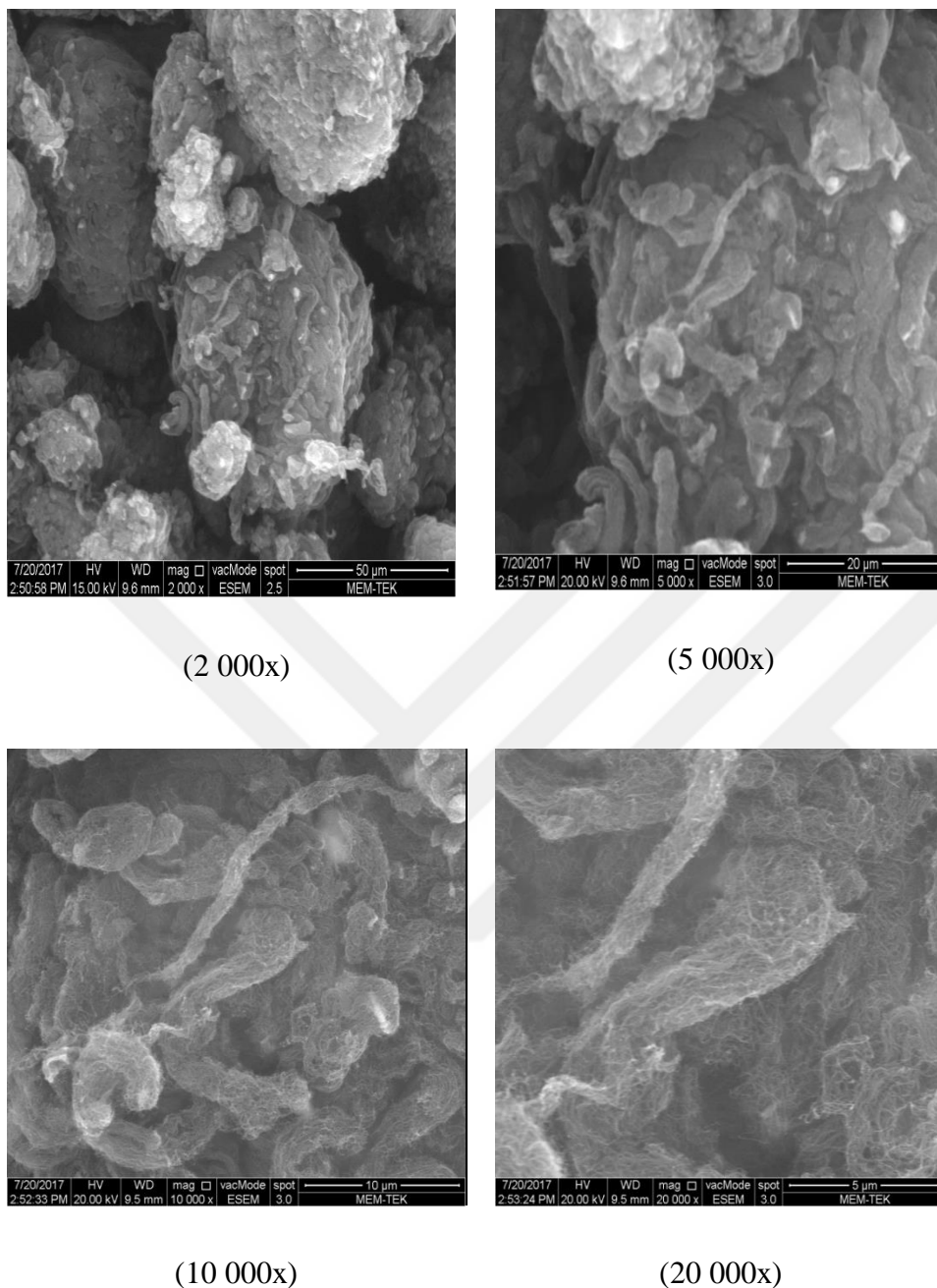


**Figure 4.2 :** SEM images of MWCNTs at 2 000x, 5 000x, 10 000x, 20 000x magnifications respectively.

#### 4.2 Fourier Transform Infrared Spectroscopy (FTIR) Characterization

FT-IR spectra of PMMA/MWCNTs and pure PMMA were examined in this study to investigate structural properties of PMMA based MWCNTs nanocomposites. According to the FT-IR spectra, the main absorption peaks were observed at  $\sim 2983$ ,  $2978$ ,  $2968 \text{ cm}^{-1}$  ( $-\text{CH}_2, -\text{CH}_3$ ) that represent stretch mode of a C-H bond vibration,



$\sim 1730\text{ cm}^{-1}$  (C=O band),  $\sim 1451\text{ cm}^{-1}$  ( $-\text{CH}_2$  bending),  $\sim 1381\text{ cm}^{-1}$  are due to bending vibrations of C-H bonds in  $-\text{CH}_3$  groups,  $\sim 1192$ ,  $\sim 1153\text{ cm}^{-1}$  absorption bands due to the C-H deformations.  $\sim 987\text{ cm}^{-1}$  represents C-H in plane bending deformation,  $\sim 753\text{ cm}^{-1}$  (C=O bending). All of these properties were shown in Figure 4.3. It can be easily seen that pure PMMA and PMMA based MWCNTs had similar FT-IR spectra, showing that interactions between the PMMA and MWCNTs were occurred effectively. (Brkovic et al., 2017)

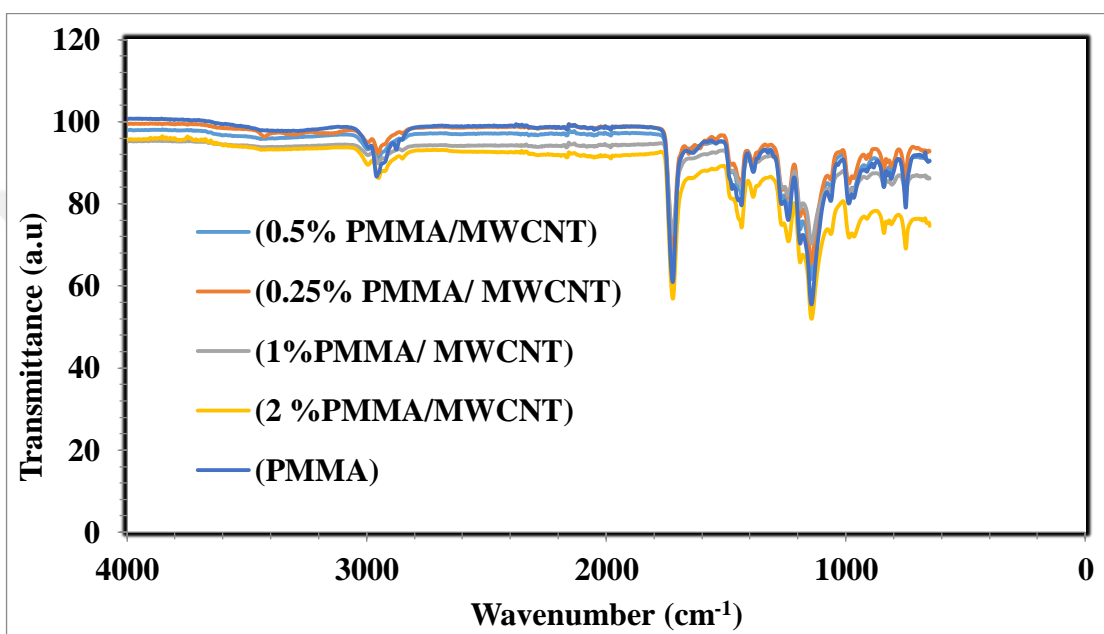


**Figure 4.3** : FT-IR spectra of pure PMMA and PMMA/MWCNTs nanocomposites.

### 4.3 XRD Characterization

The first most intense peak at  $2\theta$  values for PMMA is observed at  $\sim 13^\circ$  and this signal refers to the distribution and ordering of PMMA chains (Figure 4.4). PMMA produced by in situ polymerization technique presents a characteristic slight broad band at  $\sim 28^\circ$ . PMMA produced by ATRP method presents a slight peak at  $\sim 28^\circ$ . This peak at  $\sim 28^\circ$  may be attributed to the non-exchanged salt containing  $\text{Br}^-$  ions. The peak at  $\sim 28^\circ$  may indicate the salt containing  $\text{Br}^-$  ions (coming from  $\text{CuBr}$  and solvent  $\text{Bu}_4\text{NBr}$ ) in PMMA structure.

MWCNTs show a strong sharp diffraction peak (002) at  $\sim 25^\circ$ . The peak at  $\sim 25^\circ$  indicated 0.34 nm interplanar spacing of the diffraction planes of MWCNTs. MWCNTs had small peaks at  $\sim 42^\circ$ .

PMMA/MWCNTs nanocomposite presented three diffraction peaks. These are strong peak at  $\sim 13^\circ$ , indicated the distribution and ordering of PMMA chains. The second peak was determined as a broad band between  $25\text{-}30^\circ$  and it was centered  $\sim 28^\circ$ . The third one was distinguished as a small peak at  $\sim 42^\circ$ .

The diffraction peaks in XRD analysis are similar with the literature on Multiwall Carbon Nanotubes/Poly (Methyl Methacrylate) Nanocomposites prepared by using ultrasonication/solution casting technique to obtain free-standing nanocomposite films. (Brkovic' et.al., 2017)

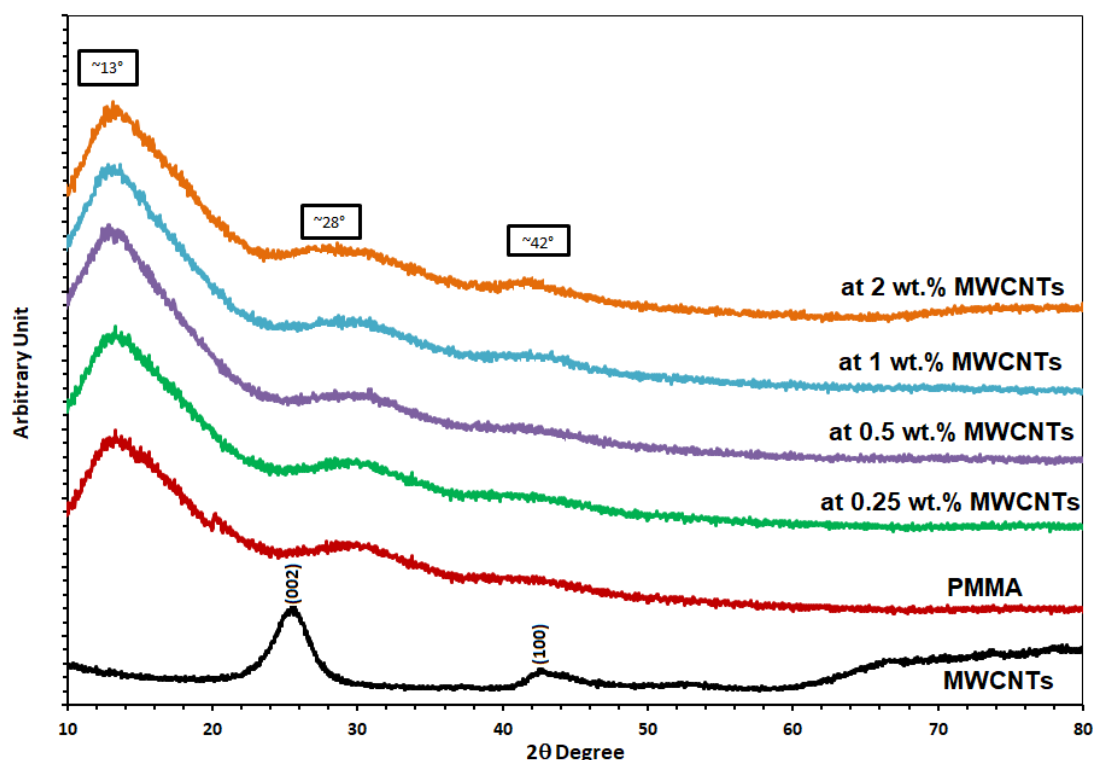


**Figure 4.4 :** The view of XRD pattern of PMMA, MWCNTs, and PMMA/MWCNTs.

#### 4.4 TGA Analysis of Unirradiated and Irradiated PMMA/MWCNTs Polymer Nanocomposite

Figure 4.5 showed the TGA curves of pure PMMA and PMMA/MWCNTs (irradiated), PMMA/MWCNTs (unirradiated) nanocomposites. Their 5% weight loss temperatures were given for the unirradiated (Table 4.1) and the irradiated (Table 4.2) states. Obviously, the thermal stabilities of the PMMA/MWCNTs nanocomposites were higher than that of the pure PMMA at 5% weight loss

temperature level. With the increase of amount of the MWCNTs, the 5% weight loss temperature were increased with the rise of the MWCNTs for 0.5, 1, 2 % wt. in the PMMA. With the addition of 2 wt. % MWCNTs, the 5% weight loss temperatures shifted from 191°C to 243°C. Hence, the thermal performance of the nanocomposite was improved by 52°C. The 5 % weight loss temperature was increased for irradiated 2 wt. % PMMA/MWCNTs nanocomposite from 243°C to 250°C. It can be seen that MWCNTs enhanced the thermal stability of PMMA by in situ polymerization method.

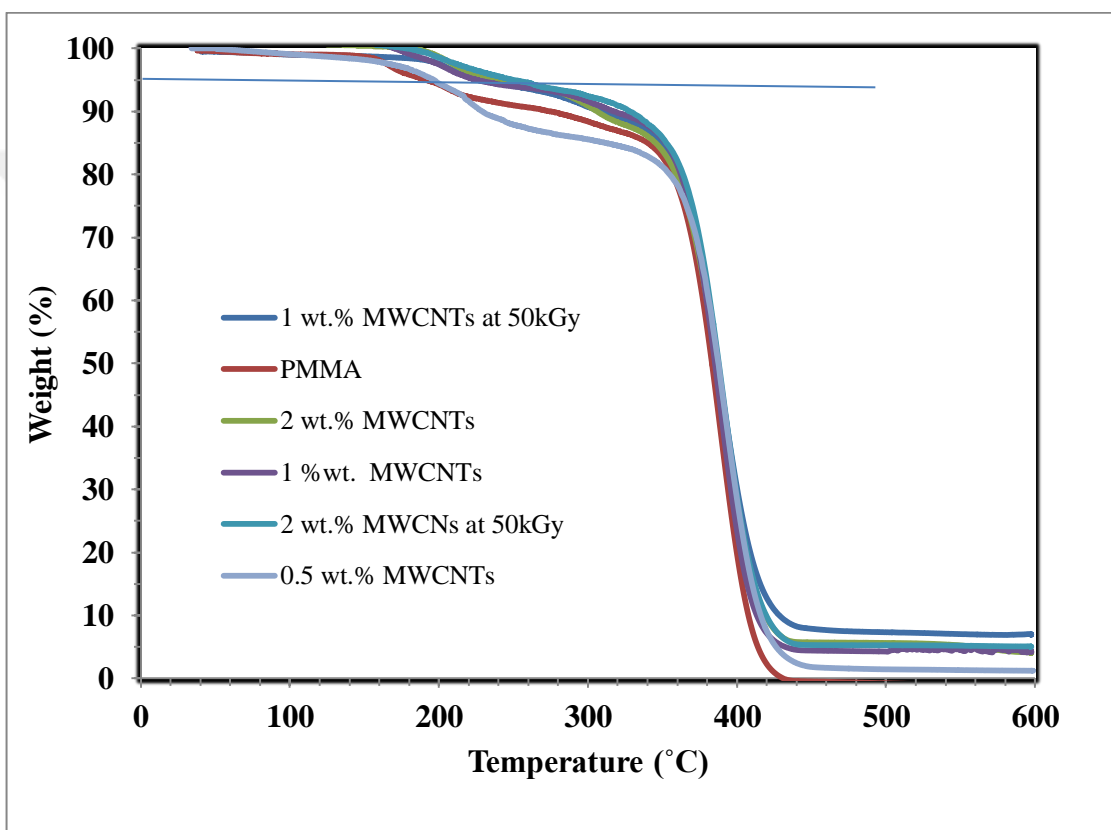


**Figure 4.5 :** The TGA results of PMMA and PMMA/MWCNTs nanocomposites for unirradiated and irradiated states.

**Table 4.1 :** 5% weight loss temperatures of pure PMMA and PMMA/MWCNTs nanocomposites for unirradiated state.

Samples	5% weight loss temperatures (°C)
PMMA	191.46
PMMA/MWCNTs 0.5%	196.73
PMMA/MWCNTs 1 %	225.37
PMMA/MWCNTs 2%	243.45

**Table 4.2 :** 5% weight loss temperatures of pure PMMA polymer and PMMA/MWCNTs polymer nanocomposites after irradiation process.

Samples (irradiated at 50 kGy)	5 % weight loss temperatures (°C)
PMMA	202.50
PMMA/MWCNTs 1 %	231.42
PMMA/MWCNTs 2%	250.08

#### 4.5 Mechanical Properties of PMMA/MWCNTs Nanocomposite

##### 4.5.1 Hardness tests results of unirradiated and irradiated PMMA/MWCNTs polymer nanocomposite

According to the hardness test results, as the amount of MWCNTs increased the hardness values also increased. This result showed that there is a relation between hardness and amount of MWCNTs. The hardness of the PMMA based carbon nanotubes was measured four different sections and average values were determined. Firstly, hardness was measured before irradiation, then irradiation (50 kGy) was applied and then hardness was measured again. The hardness differences between the before and after irradiation showed that irradiation affects the hardness of the materials. The hardness of composite samples were increased after irradiation. Another result that hardness values of MWCNTs with irradiation changed with amount of MWCNTs. The difference in hardness values between the pure PMMA and PMMA/MWCNTs nanocomposite at 2 wt. %. MWCNTs was approximately 11 %. The changes in hardness values of the PMMA/MWCNTs nanocomposite were compared with the irradiated and the unirradiated states of the PMMA/MWCNTs nanocomposite. The difference of hardness values between irradiated and unirradiated states is almost 3 % for 2 wt. % MWCNTs in PMMA/MWCNT nanocomposite.

All of these results were shown in Figure 4.6 graphically.

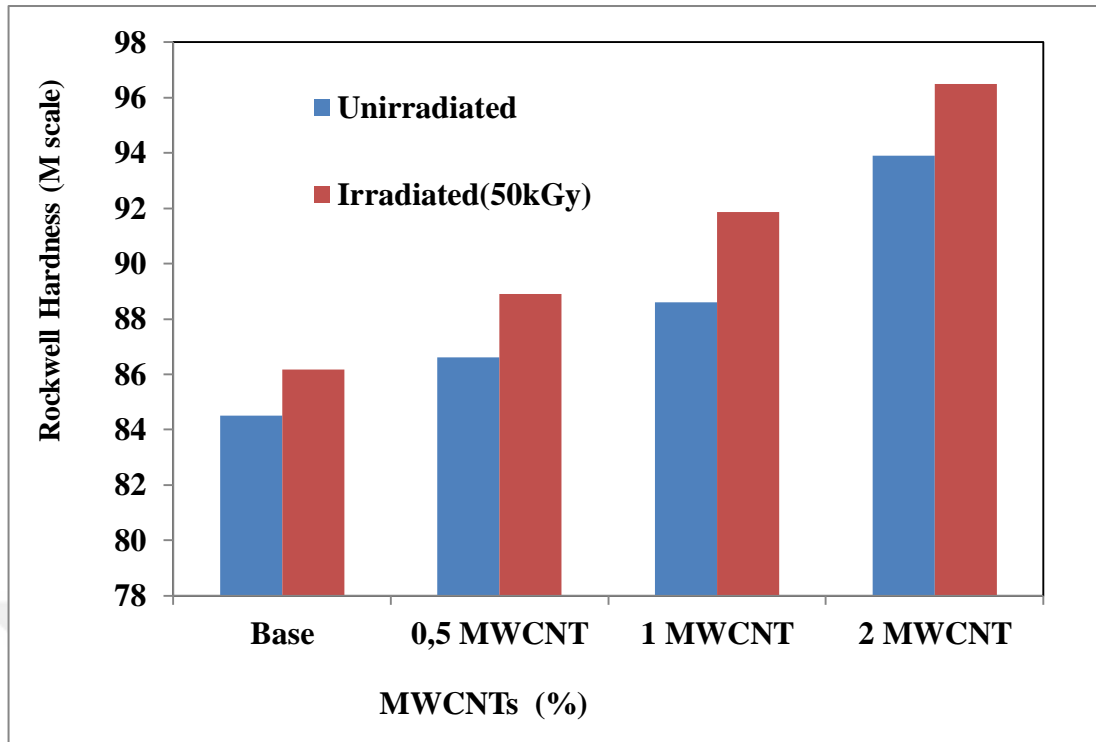


**Figure 4.6:** The Rockwell hardness values of PMMA and MWCNTs before and after irradiation.

#### 4.6 Gamma Transmission Technique and Pu-Be Neutron Howitzer

Two different gamma radioisotopes (Cs-137 and Co-60) were used to determine the changes in relative intensity of PMMA/MWCNTs nanocomposite samples were determined as a function of the thickness.

The slope of the thickness versus relative count gave information about the linear attenuation coefficient ( $\mu$ ) for Cs-137 and Co-60 radioisotopes. The slope of the thickness versus relative count gave the total macroscopic cross sections of neutron-material interaction ( $\Sigma_{total}$ ). The ratio of linear attenuation coefficient to density gave mass attenuation coefficient ( $\mu/\rho$ ) for Cs-137 and Co-60 radioisotopes.

##### 4.6.1 Radiation process by using Cs-137 radioisotope

One of the gamma sources used in the gamma transmission technique was Cs-137 radioisotope with a single gamma-peak at 0.662 MeV. The changes in the intensity values of the PMMA/MWCNTs nanocomposite samples were shown with the rise of the thickness in Table 4.3 for pure PMMA. The linear attenuation coefficient was shown in Figure 4.7.

**Table 4.3 :** Experimental results of pure PMMA against Cs-137 radioisotopes.

Thickness (cm)	Count 1	Count 2	Count 3	Average	Standard Deviation	Relative Count (I/I <sub>0</sub> )
0	13558	13515	13522	13532	23	1.000
0.308	13133	13158	13195	13162	31	0.973
0.613	12927	12832	12884	12881	48	0.952
0.922	12513	12560	12499	12524	32	0.926
1.237	12156	12197	12122	12158	38	0.899
2.045	11271	11236	11254	11254	18	0.832
3.277	9943	9864	9915	9907	40	0.732

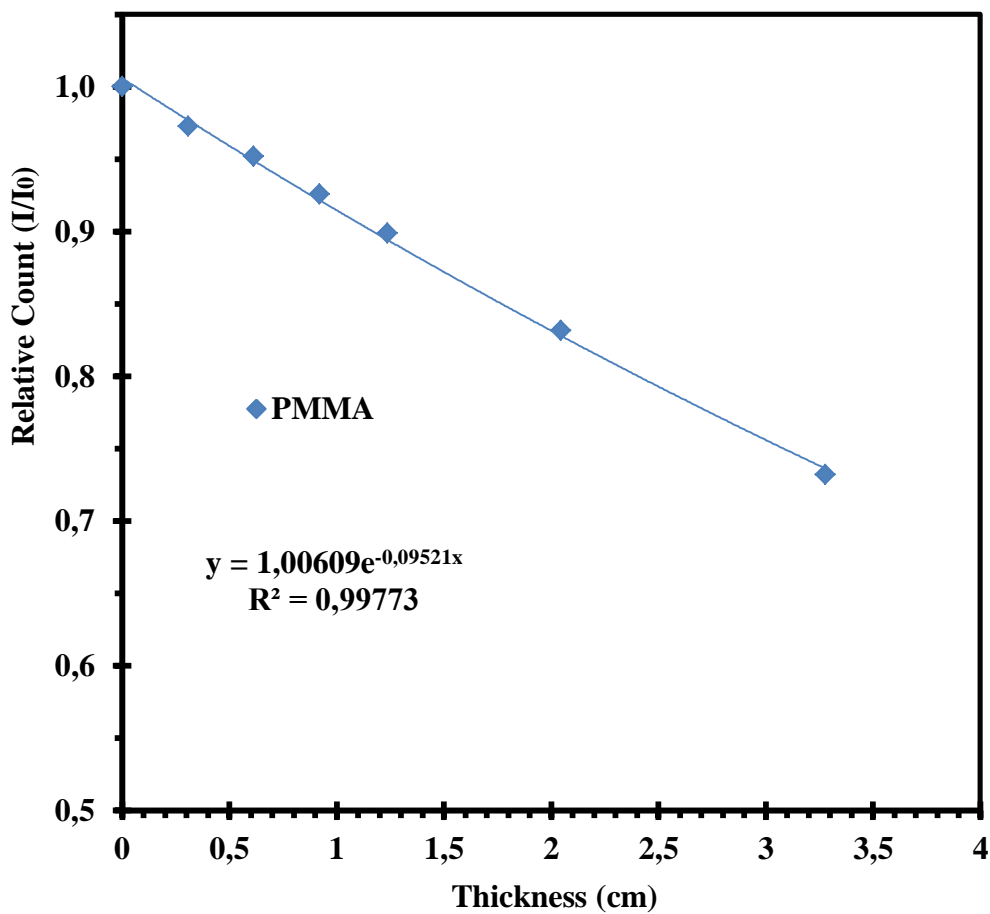


**Figure 4.7 :** The graph of thickness versus relative intensity in PMMA.

Experimental results of the gamma transmission properties of PMMA/MWCNTs at 0.25 wt. % against Cs-137 radioisotopes were given in Table 4.4.

The changes in relative intensity at 0.25 wt. % PMMA/MWCNTs nanocomposite sample depending on their thickness were given in Figure 4.8.

**Table 4.4 :** Experimental results of the gamma transmission properties of PMMA/MWCNTs 0.25 wt. % against Cs-137 radioisotopes.

Thickness (cm)	Count 1	Count 2	Count 3	Average	Standard Deviation	Relative Count (I/I <sub>0</sub> )
0	7172	7208	7276	7218	43	1
2.49125	6192	6108	6168	6156	35	0.8527
4.92765	4718	4771	4702	4730	29	0.6552
7.37545	3612	3628	3624	3621	6	0.5016
9.84455	2498	2472	2492	2487	11	0.3445

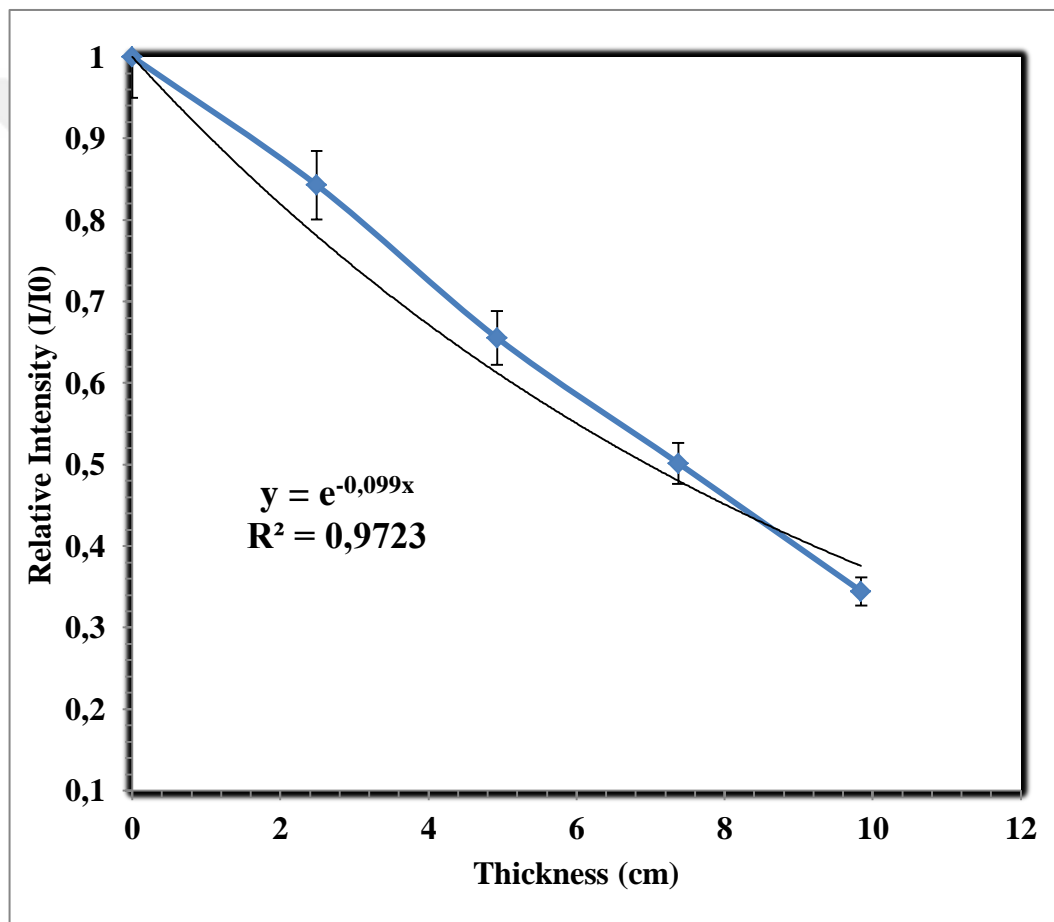


**Figure 4.8 :** Relative intensity versus thickness graph of 0.25 wt. % PMMA/MWCNTs against Cs-137.

Experimental results of the gamma transmission properties of 0.5 wt. % PMMA/MWCNTs against Cs-137 radioisotopes were given in Table 4.5. The linear attenuation coefficient was shown in Figure 4.9.

**Table 4.5 :** Experimental results of the gamma transmission properties of 0.5 wt % PMMA/MWCNTs against Cs-137 radioisotopes.

Thickness (cm)	Count 1	Count 2	Count 3	Average	Standard Deviation	Relative Count (I/I <sub>0</sub> )
0	7172	7208	7276	7218	43	1
3.29	5828	5886	5836	5850	25	0.8104
6.47	3646	3604	3628	3626	17	0.6198
9.74	3018	3098	3006	3040	40	0.4212
12.99	1894	1882	1875	1883	7	0.2609

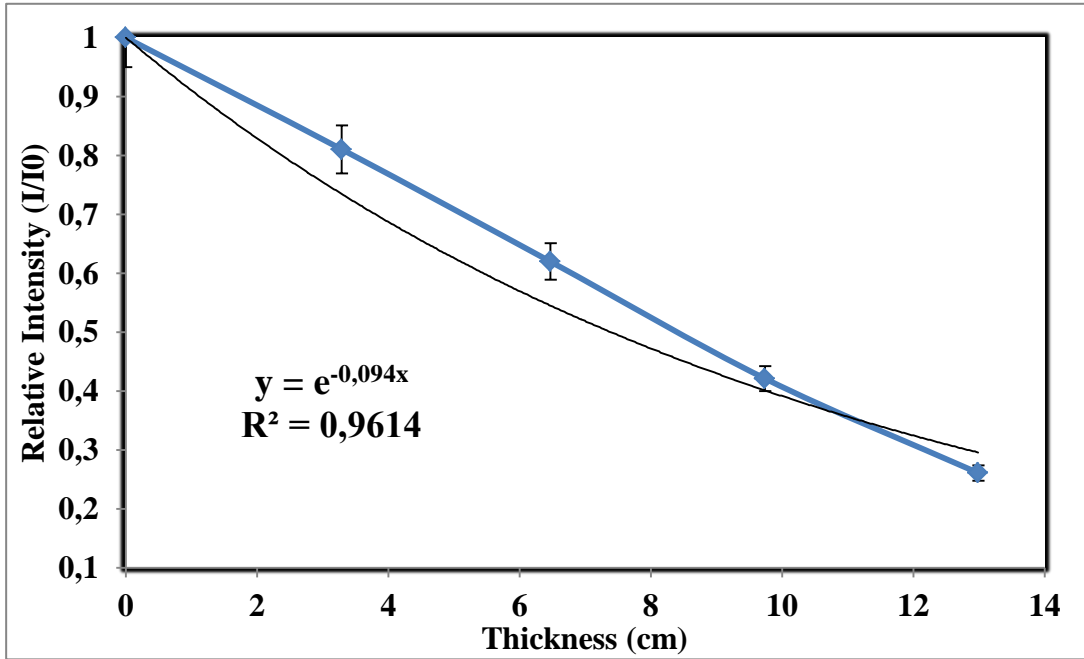


**Figure 4.9 :** Relative intensity-thickness graph of 0.5 wt.% MWCNTs

The experimental results of the gamma transmission properties of PMMA/MWCNTs 1 wt. % MWCNTs against Cs-137 radioisotopes were given in Table 4.6. The linear attenuation coefficient was presented in Figure 4.10.

**Table 4.6 :** Experimental results of the gamma transmission properties of PMMA/MWCNTs 1 wt. % MWCNTs against Cs-137 radioisotopes.

Thick.(cm)	Count 1	Count 2	Count 3	Average	Standard Deviation	Relative Count (I/I <sub>0</sub> )
0	7172	7208	7276	7218	43	1
2.436	5786	5760	5744	5763	17	0.7984
4.849	3448	3480	3432	3453	19	0.5992
7.278	1644	1608	1632	1628	14	0.4714
9.708	654	658	652	654	2	0.4021



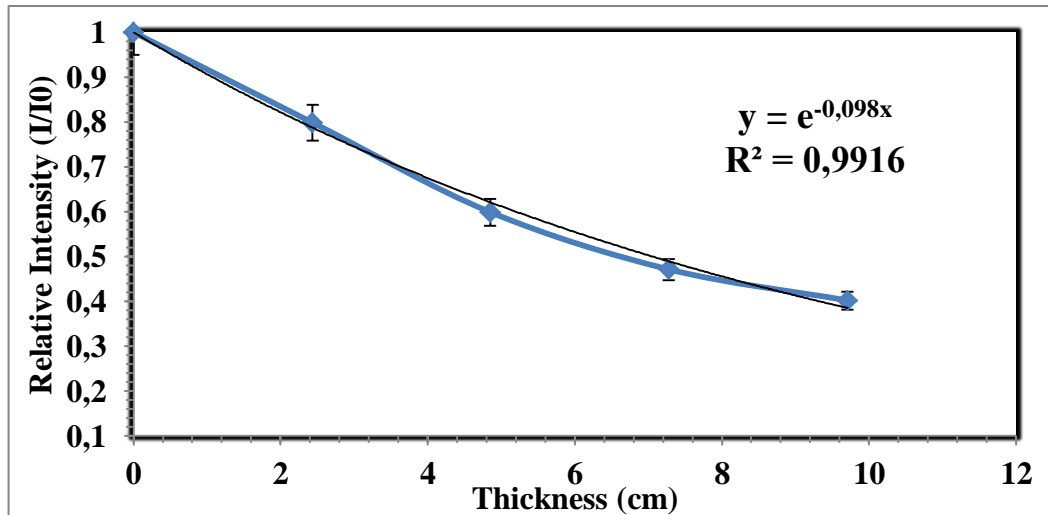


**Figure 4.10 :** Relative intensity-thickness graphs of 1 wt. % MWCNTs

The experimental results of the gamma transmission properties of PMMA/MWCNTs 2 wt. % against Cs-137 radioisotopes were given in Table 4.7. The linear attenuation coefficient of nanocomposite sample was given in Figure 4.11.

**Table 4.7 :** Experimental results of the gamma transmission properties of PMMA/MWCNTs 2 wt. % MWCNTs against Cs-137 radioisotopes.

Thick.(cm)	Count 1	Count 2	Count 3	Average	Standard Deviation	Relative Count (I/I <sub>0</sub> )
0	7172	7208	7276	7218	43	1
2.0495	5636	5640	5604	5626	16	0.7795
4.0898	3536	3598	3568	3567	25	0.6340
6.131	1996	1928	1912	1945	36	0.5453
8.1773	914	926	832	890	41	0.4578

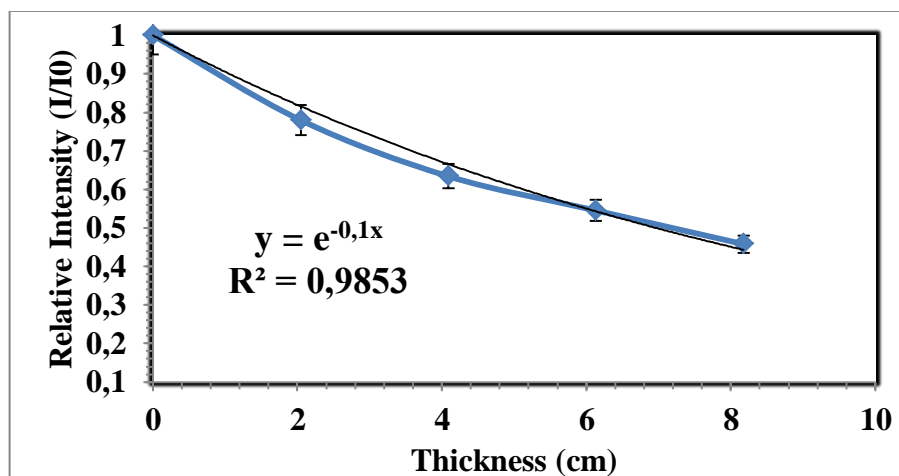


**Figure 4.11 :** Relative intensity-thickness graphs of 2 wt. %. PMMA/MWCNTs.

XCOM program was used to calculate the theoretical mass attenuation coefficients. This program uses the chemical compositions of each sample. Experimental linear attenuation coefficient was obtained from the slope of thickness-relative count graph. Mass attenuation coefficient was obtained via the formula of  $\mu/\rho$  were shown in Table 4.8.

**Table 4.8 :** The compositions of the PMMA nanocomposite samples at different MWCNTs.

Samples	C (Wt.%)	O (Wt.%)	H (Wt.%)	Cu (Wt.%)	Br (Wt.%)
PMMA	59.69	30.53	8.09	0.13	1.56
PMMA/MWCNTs 0.25%	59.79	30.46	8.07	0.13	1.56
PMMA/MWCNTs 0.5%	59.89	30.38	8.05	0.13	1.55
PMMA/MWCNTs 1%	60.09	30.23	8.01	0.13	1.54
PMMA/MWCNTs 2%	60.48	29.94	7.93	0.12	1.53

The changes in density of the samples with the rise of MWCNTs compounds were measured with pycnometer to calculate the experimental mass attenuation and their results were shown in Table 4.9. The difference between the linear and mass attenuation coefficients were given in Table 4.10.

**Table 4.9 :** The density values of the PMMA/MWCNTs samples.

Samples	Density (g/cm <sup>3</sup> )
PMMA	1.18089
PMMA/MWCNTs 0.25%	1.18242
PMMA/MWCNTs 0.5%	1.18566
PMMA/MWCNTs 1%	1.19314
PMMA/MWCNTs 2%	1.19788

**Table 4.10 :** The differences between linear and mass attenuation coefficients.

MWCNTs compounds at PMMA/MWCNTs (in wt.%)	Linear attenuation coefficients $\mu$ ( $\text{cm}^{-1}$ )	Density $\rho$ ( $\text{g}/\text{cm}^3$ )	Mass attenuation coefficients $\mu/\rho$ ( $\text{cm}^2/\text{g}$ )	Theoretical mass attenuation coefficients ( $\text{cm}^2/\text{g}$ ) (XCOM)	Difference (%)
PMMA	0.09521	1.18089	0.08063	0.08323	3.13
0.25%	0.099	1.18242	0.08372	0.08322	0.6
0.5%	0.094	1.18566	0.07928	0.08320	4.94
1%	0.098	1.19314	0.082136	0.08317	1.25
2%	0.1	1.19788	0.083480	0.08311	0.44

#### 4.6.2 Radiation process by using Co-60 radioisotope

Another gamma source that used in this study was Co-60 that has gamma-peak at ~ 1.25 MeV. Gamma transmission properties of both pure PMMA and PMMA/MWCNTs were examined in this study. The results of pure PMMA against Co-60 radioisotopes were given in Table 4.11. The changes in the linear attenuation coefficients were shown in Figure 4.12.

**Table 4.11 :** Experimental results of the pure PMMA against the Co-60 radioisotope.

Thickness (cm)	Count 1	Count 2	Count 3	Average	Standard Deviation	Relative Count ( $I/I_0$ )
0	25760	25679	25654	25698	55	1.000
0.308	25295	25190	25280	25255	57	0.983
0.613	24903	24837	24765	24835	69	0.966
0.922	24321	24453	24364	24379	67	0.949
1.237	23799	23739	23806	23781	37	0.925
2.045	22455	22419	22323	22399	68	0.872
3.277	20389	20456	20438	20428	35	0.795

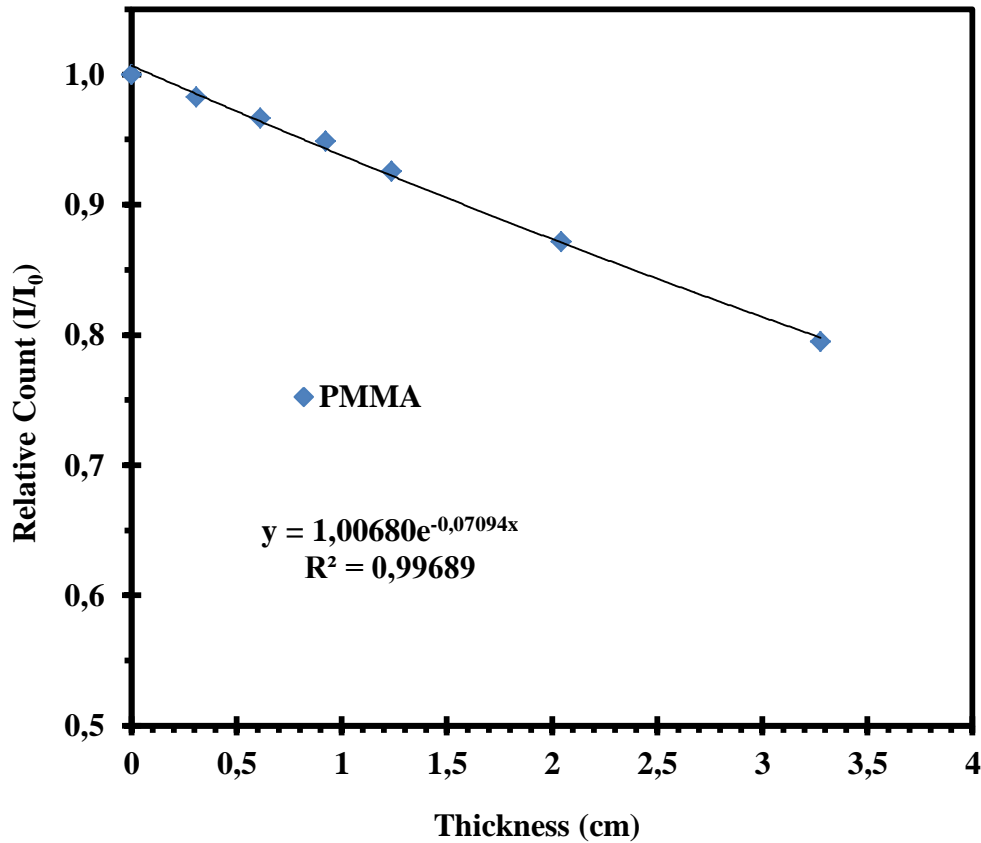


**Figure 4.12 :** The relative intensity of base PMMA for unirradiated state by using Co-60 radioisotope.

Experimental results of the gamma transmission properties of PMMA/MWCNTs 0.25 wt. % MWCNTs against Co-60 radioisotopes were given in Table 4.12. The linear attenuation coefficient was presented in Figure 4.13.

**Table 4.12 :** Experimental results of the gamma transmission properties of PMMA/MWCNTs 0.25 wt. % MWCNTs against Co-60 radioisotopes.

Thickness (cm)	Count 1	Count 2	Count 3	Average	Standard Deviation	Relative Count (I/I₀)
0	22668	22680	22656	22668	9	1
2.49125	19428	19484	19396	19436	36	0.8574
4.92765	15492	15424	15428	15448	31	0.6815
7.37545	13368	13328	13248	13314	49	0.5874
9.84455	11288	11264	11324	11292	24	0.4985

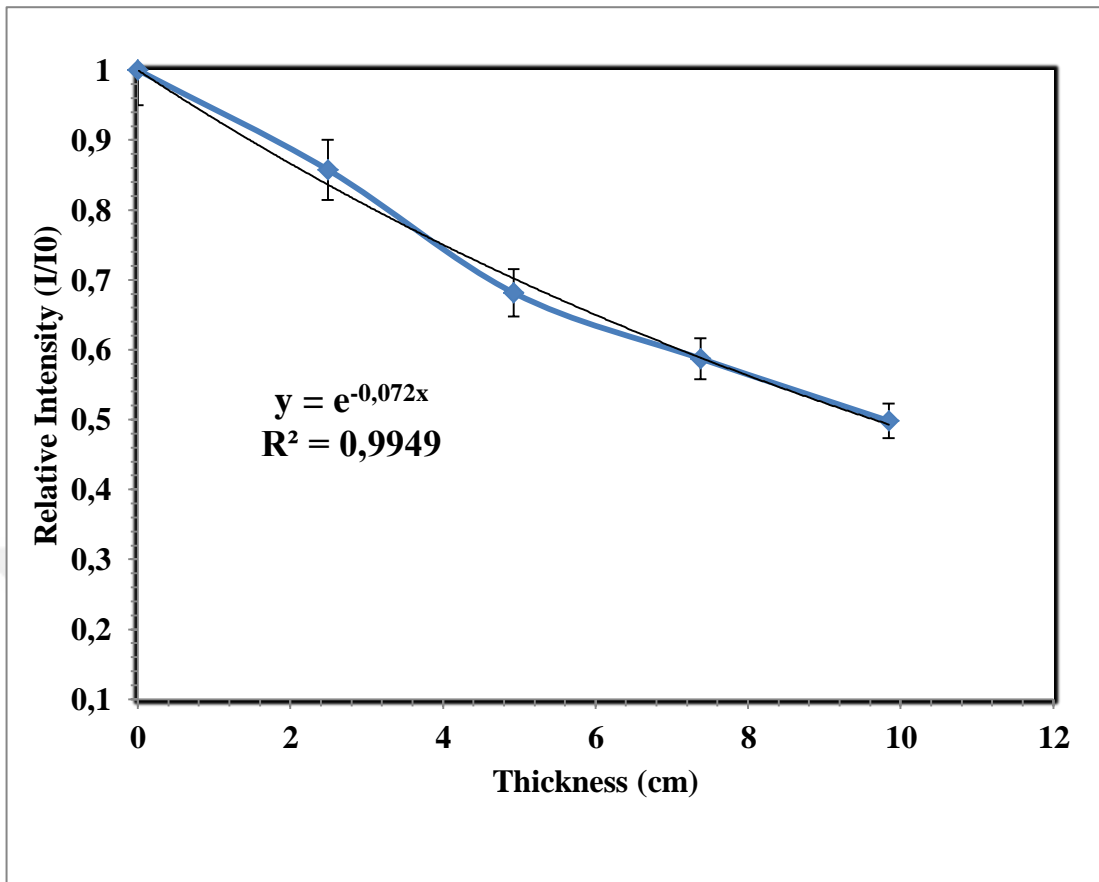


**Figure 4.13 :** The changes in the relative intensity of PMMA/MWCNTs nanocomposite at 0.25 wt. % MWCNTs with the rise of the thickness.

Experimental results of the gamma transmission properties of PMMA/MWCNTs 0.5 wt. % MWCNTs against Co-60 radioisotope were given in Table 4.13 and relative count versus thicknesses of the samples graph with linear attenuation coefficient was presented in Figure 4.14.

**Table 4.13 :** Experimental results of the gamma transmission properties of PMMA/MWCNTs 0.5 wt.% MWCNTs against Co-60 radioisotopes.

Thickness (cm)	Count 1	Count 2	Count 3	Average	Standard Deviation	Relative Count (I/I <sub>0</sub> )
0	22668	22680	22656	22668	9	1
3.29	18308	18306	18312	18308	2	0.8077
6.47	14504	14568	14548	14540	26	0.6414
9.74	11504	11540	11532	11525	15	0.5084

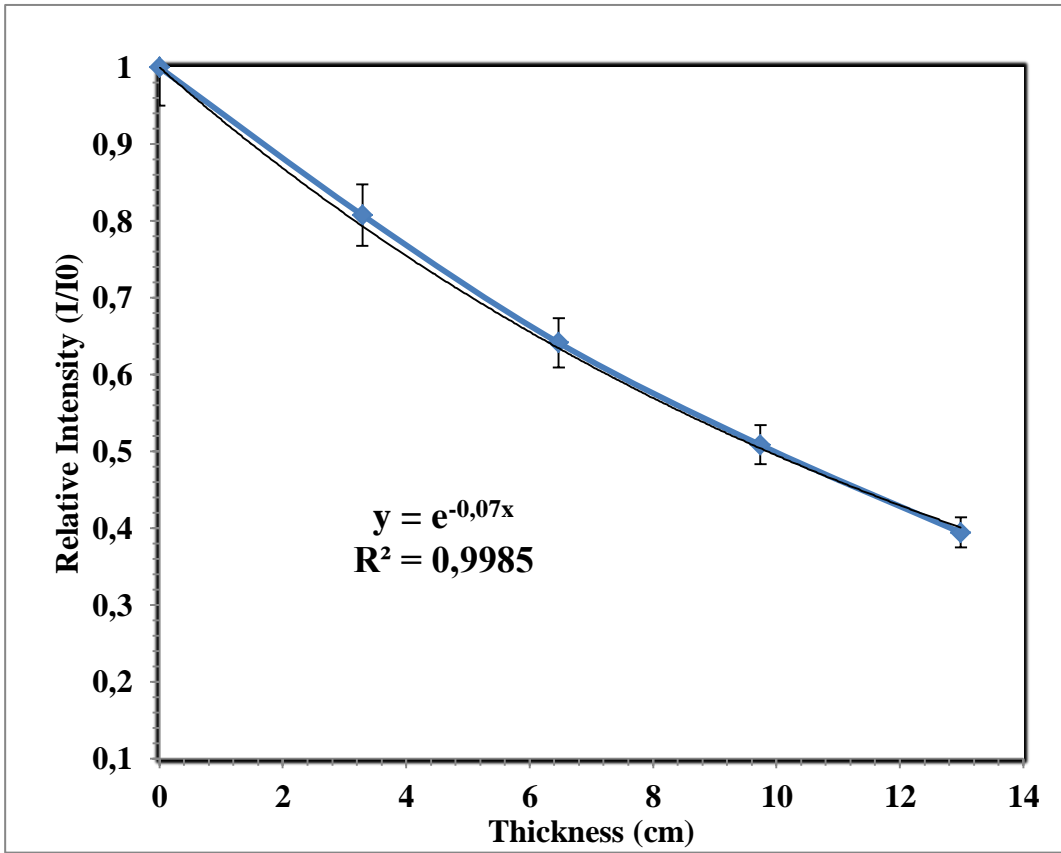


**Figure 4.14 :** The changes in the relative intensity of PMMA/MWCNTs nanocomposite at 0.5 wt. % MWCNTs with the rise of the thickness.

Experimental results of the gamma transmission properties of PMMA/MWCNTs 1% MWCNTs against Co-60 radioisotope were given in Table 4.14. The linear attenuation coefficient was presented in Figure 4.15.

**Table 4.14:** Experimental results of the gamma transmission properties of PMMA/MWCNTs 1 wt. % MWCNTs against Co-60 radioisotopes.

Thickness (cm)	Count 1	Count 2	Count 3	Average	Standard Deviation	Relative Count (I/Io)
0	22668	22680	22656	22668	9	1
2.436	18084	18024	18004	18037	33	0.7957
4.849	15304	15348	15303	15318	20	0.6757
7.278	13028	13084	13004	13038	33	0.5752

9.708      10444      10492      10468      10468      19      0.4618

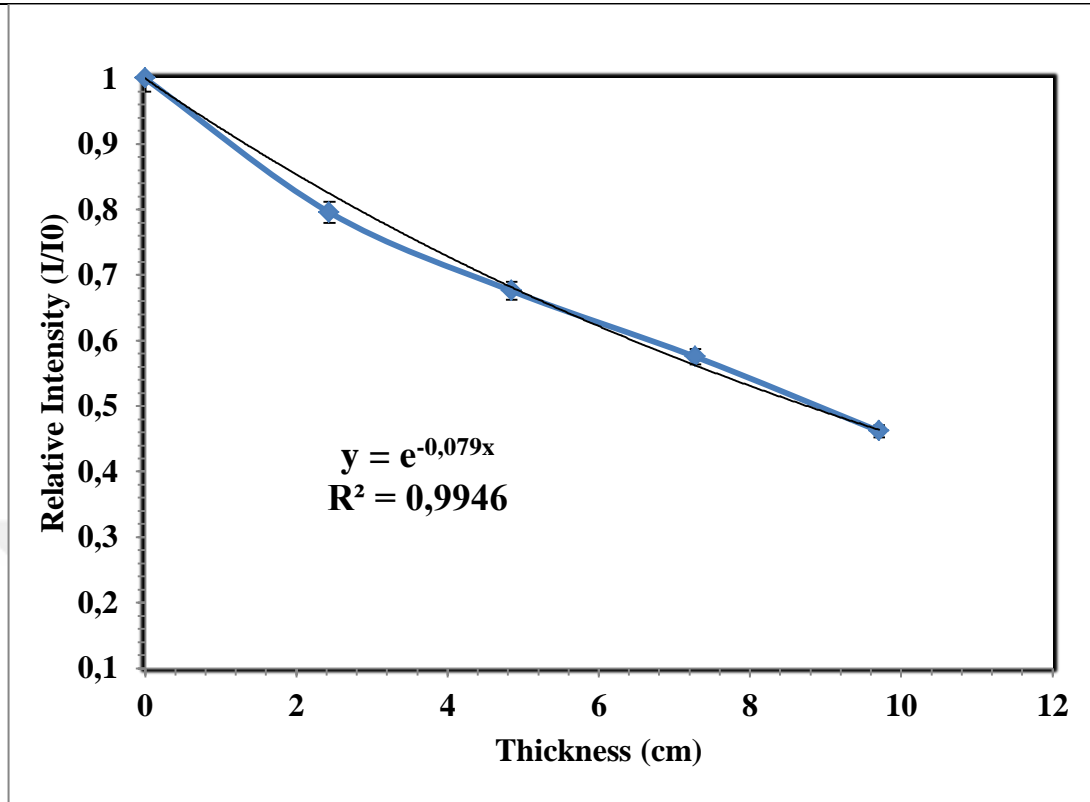


**Figure 4.15:** The changes in the relative intensity of PMMA/MWCNTs nanocomposite at 1 wt. % MWCNTs with the rise of the thickness.

Experimental results of the gamma transmission properties of PMMA/MWCNTs 2 wt. % against Co-60 radioisotopes were given in Table 4.15. The linear attenuation coefficient was presented in Figure 4.16. Differences between experimental and theoretical mass attenuation coefficients for Co-60 radioisotope were given in Table 4.16.

**Table 4.15:** Experimental results of the gamma transmission properties of PMMA/MWCNTs 2 wt. % MWCNTs against Co-60 radioisotopes.

Thickness (cm)	Count 1	Count 2	Count 3	Average	Standard Deviation	Relative Count (I/I <sub>0</sub> )
0	22668	22680	22656	22668	9	1
2.0495	17796	17776	17752	17774	17	0.7841
4.0898	14786	14756	14784	14775	13	0.6518
6.131	11940	11988	11960	11962	19	0.5277

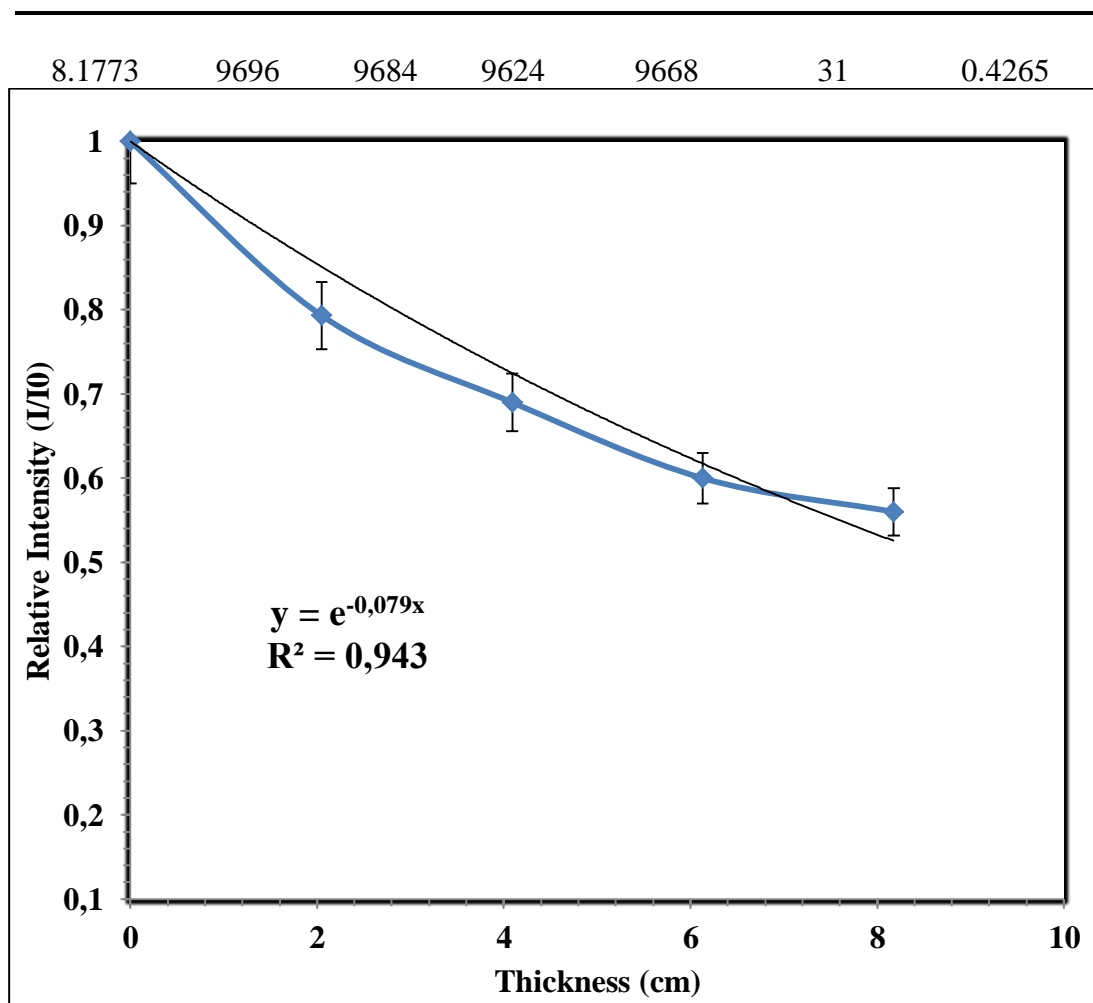


**Figure 4.16 :** The changes in the relative intensity of PMMA/MWCNTs nanocomposite at 2 wt. % MWCNTs with the rise of the thickness.

**Table 4.16 :** Differences between experimental and theoretical mass attenuation coefficients. against Co-60 radioisotope.

MWCNTs (in wt %) PMMA/MWCNTs	Linear attenuation coefficients $\mu$ ( $\text{cm}^{-1}$ )	Density $\rho$ ( $\text{g}/\text{cm}^3$ )	Mass attenuation coefficients $\mu/\rho$ ( $\text{cm}^2/\text{g}$ )	Theoretical mass attenuation coefficients ( $\text{cm}^2/\text{g}$ ) (XCOM)	Difference (%)
Base PMMA	0.07094	1.18089	0.06007	0.06135	2.08
0.25%	0.07200	1.18242	0.06089	0.06134	0.77
0.5%	0.07000	1.18566	0.06081	0.06133	0.85
1%	0.07900	1.19314	0.06621	0.06131	7.9
2%	0.07900	1.19788	0.06594	0.06127	7.6



### 4.6.3 Application of the gamma transmission technique for the irradiated PMMA/MWCNTs nanocomposites at 50 kGy.

The irradiation (50 kGy) was applied some PMMA/MWCNTs nanocomposite samples which are 0.5 % wt. MWCNTs, 1 % wt. MWCNTs, 2 % wt. MWCNTs.

The changes in relative intensity of the PMMA/MWCNTs nanocomposite at 0.5 wt. % MWCNTs with the rise of the thickness were given in Figure 4.17. Experimental results of the gamma transmission properties of the irradiated PMMA/MWCNTs at 0.5 wt. % MWCNTs for Cs-137 radioisotopes were given in Table 4.17.

**Table 4.17 :** Experimental results of the gamma transmission for the irradiated PMMA/MWCNTs at 0.5 wt. % MWCNTs for Cs-137 radioisotope.

Thickness (cm)	Count 1	Count 2	Count 3	Average	Standard Deviation	Relative Count (I/I <sub>0</sub> )
0	7188	7148	7164	7166	16	1
2.856	5960	5952	5960	5957	2	0.8312
5.709	4509	4542	4556	4535	19	0.6328
8.553	3292	3264	3208	3254	34	0.4541
11.000	2368	2328	2313	2336	23	0.3260

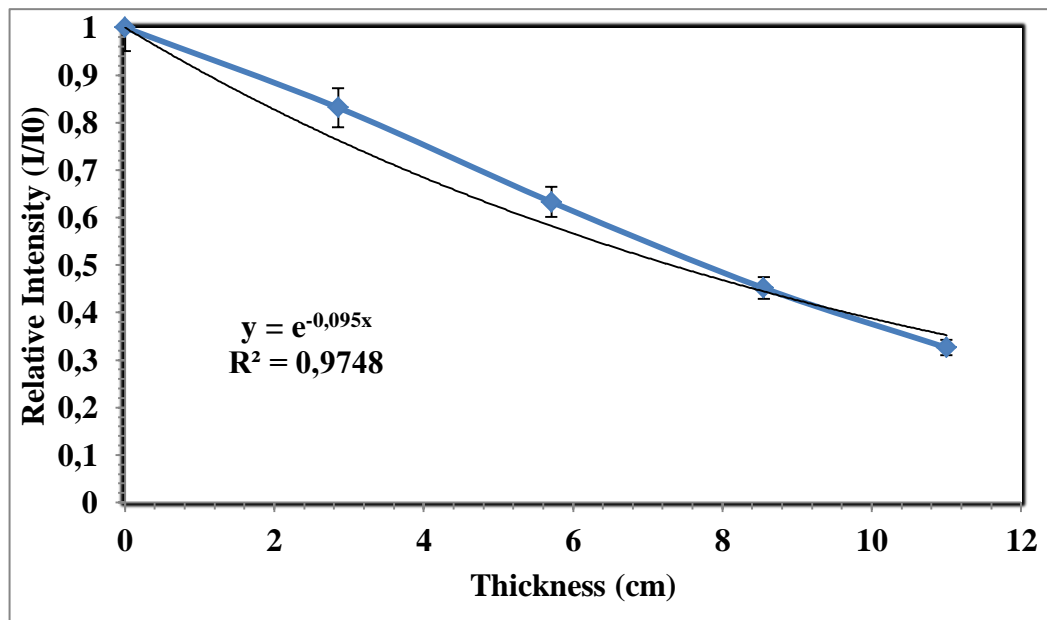


**Figure 4.17:** The changes in the relative intensity of PMMA/MWCNTs nanocomposite at 0.5 wt. % MWCNTs with the rise of the thickness.

The changes in relative intensity at 1 wt. % PMMA/MWCNTs depending on their thickness were given in Figure 4.18.

The relative count ( $I/I_0$ ) was determined at four different thicknesses of the PMMA/MWCNTs nanocomposite by using Cs-137 radioisotope. The addition of MWCNT as nanofiller into PMMA synthesized by Atom Transfer Radical Polymerization (ATRP) method performed a slight variations in relative count ( $I/I_0$ ) of the nanocomposite samples. The reason of this result was explained that MWCNT nanofillers at 1 wt. % MWCNT amount was dispersed in PMMA polymer matrix. Experimental results of the gamma transmission properties of irradiated 1 wt. % PMMA/MWCNTs nanocomposite samples with different thickness values against Cs-137 radioisotopes were given in Table 4.18.

Average counts and standard deviations were calculated for all different thickness values.  $I/I_0$  gives the relative count that calculated in table below.

**Table 4.18:** Experimental results of the gamma transmission technique of the irradiated PMMA/MWCNTs at 1 wt. % MWCNTs for Cs-137 radioisotope.

Thickness (cm)	Count 1	Count 2	Count 3	Average	Standard Deviation	Relative Count ( $I/I_0$ )
0	7188	7148	7164	7166	16	1
1.703	5916	5928	5956	5933	16	0.8279
3.415	4842	4804	4816	4820	15	0.6726
5.137	4056	4048	4012	4038	19	0.5635
7.000	3286	3268	3276	3276	7	0.4572

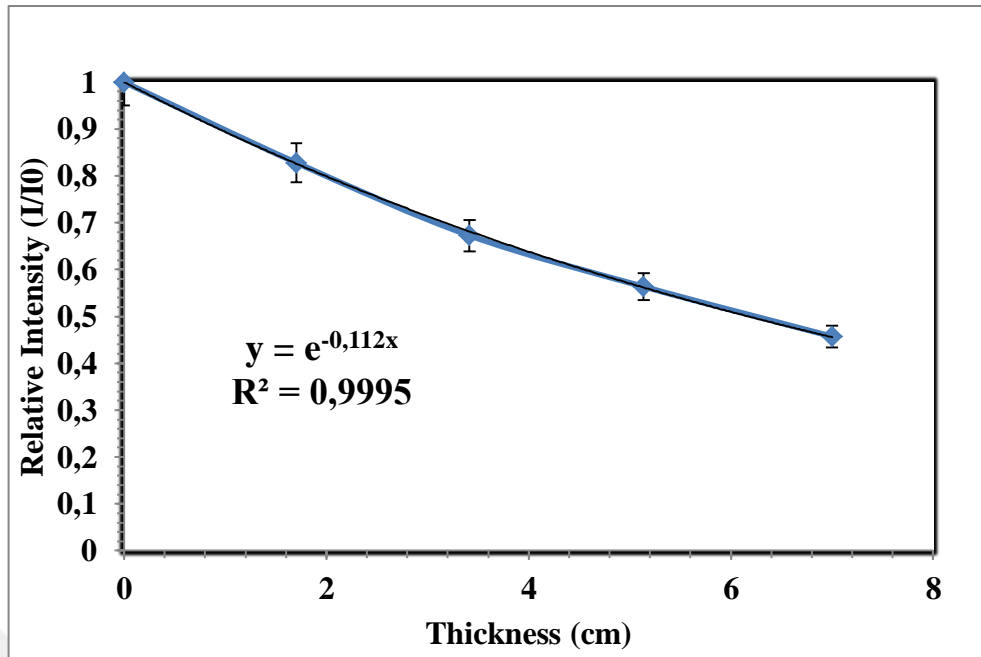


**Figure 4.18 :** The changes in the relative intensity of PMMA/MWCNTs nanocomposite at 1 wt. % MWCNTs with the rise of the thickness.

Experimental results of the gamma transmission properties of the irradiated PMMA/MWCNTs at 2 wt. % MWCNTs for Cs-137 radioisotope were given in Table 4. 19.

**Table 4.19:** Experimental results of the gamma transmission technique of the irradiated PMMA/MWCNTs at 2 wt. % MWCNTs.

Thickness (cm)	Count 1	Count 2	Count 3	Average	Standard Deviation	Relative Count (I/I <sub>0</sub> )
0	7188	7148	7164	7166	16	1
3.05425	5140	5108	5128	5125	13	0.7152
6.10336	4128	4148	4120	4132	11	0.5765
9.14878	3072	3048	3048	3056	11	0.4264
12	2284	2204	2292	2260	39	0.3153

The changes in relative intensity at 2 wt. % PMMA/MWCNTs were given with the rise of the thickness in Figure 4.19. The density values of the irradiated PMMA/MWCNTs determined by using pycnometer were presented in Table 4.20 after the irradiation treatment at 50 kGy.

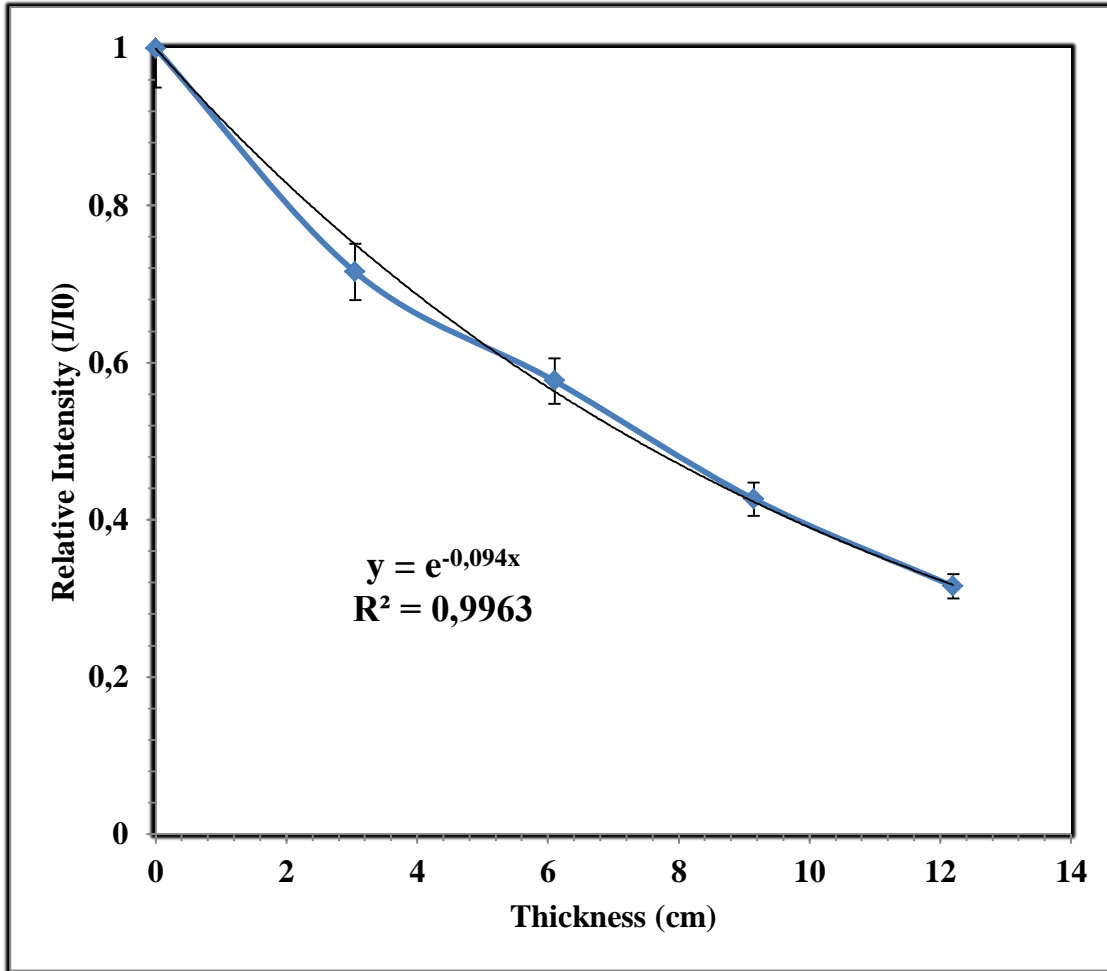


**Figure 4.19:** The changes in the relative intensity of PMMA/MWCNTs nanocomposite at 2 wt. % MWCNTs with the rise of the thickness.

**Table 4.20:** Density values of the irradiated PMMA/MWCNTs at 50kGy.

MWCNTs (in wt.%) PMMA/MWCNTs Nanocomposite	Density Values (g/cm <sup>3</sup> )
0.5	1.134
1.0	1.152
2.0	1.171

The linear and mass attenuation coefficients of the irradiated samples were given at Table 4.21.

**Table 4.21:** The linear and mass attenuation coefficients of the irradiated PMMA/MWCNTs nanocomposite samples for Cs-137 radioisotope.

MWCNTs (in wt.%)	Linear attenuation coefficients $\mu_l$ (cm <sup>-1</sup> )	Density $\rho$ (g/cm <sup>3</sup> )	Mass attenuation coeffic. $\mu_p/\rho$ (cm <sup>2</sup> /g)
0.5	0.095	1.134	0.08377
1.0	0.112	1.152	0.09722
2.0	0.094	1.171	0.08027

According to the results, the density of the PMMA/MWCNTs polymer nanocomposites was decreased after 50 kGy irradiation was applied.

Results of Gamma Transmission Technique with Co-60 Radioisotope:

The changes in relative intensity of the PMMA/MWCNTs at 0.5 wt. % MWCNTs were given depending on their thickness in Figure 4.20. Experimental results of the gamma transmission technique of the irradiated PMMA/MWCNTs at 0.5 wt. % MWCNTs against Co-60 radioisotopes were given in Table 4.22.

**Table 4.22 :** Experimental results of the gamma transmission technique of the irradiated PMMA/MWCNTs at 0.5 wt. % MWCNTs.

Thick. (cm)	Count 1	Count 2	Count 3	Average	Standard Deviation	Relative Count (I/I <sub>0</sub> )
0	25788	25760	25740	25762	19	1
2.856	21544	21544	21576	21554	11	0.8366
5.709	16860	16816	16748	16808	46	0.6524
8.553	14368	14304	14308	14326	29	0.5561
11	11356	11368	11256	11326	50	0.4396

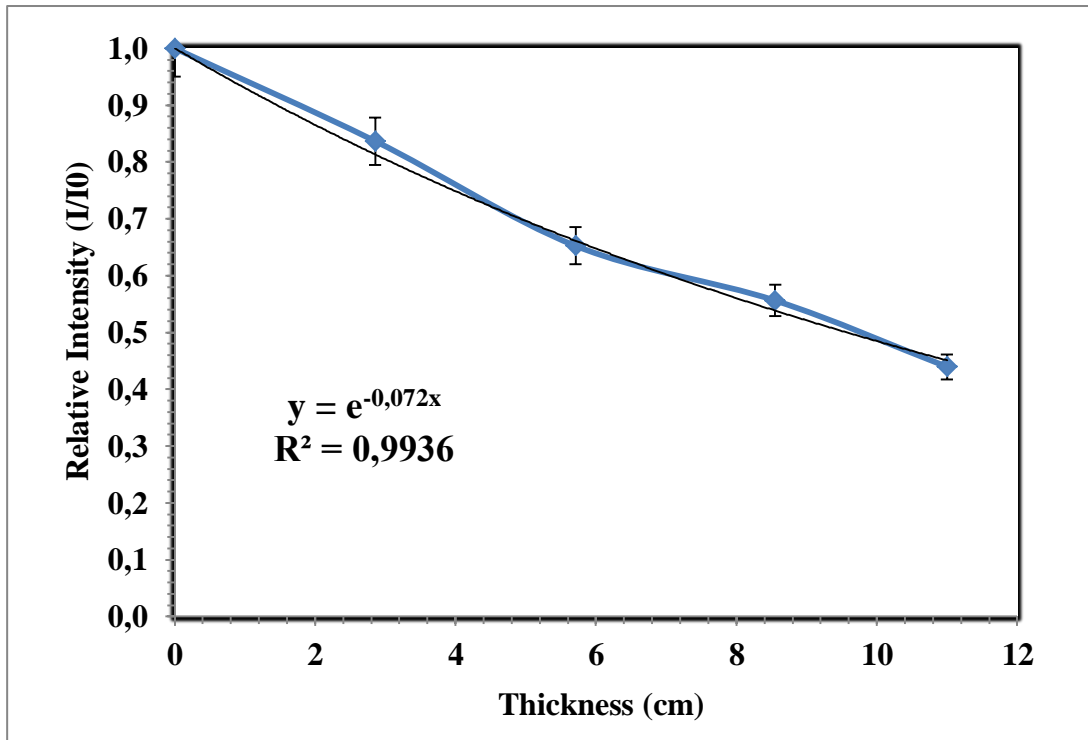


**Figure 4.20:** The changes in the relative intensity of the irradiated PMMA/MWCNTs at 0.5 wt. % MWCNTs with the rise of thickness.

The changes in relative intensity at 1 wt. % PMMA/MWCNTs depending on their thickness were given in Figure 4.21. Experimental results of the gamma transmission properties of irradiated PMMA/MWCNTs (at 1 wt. % MWCNTs) against Co-60 radioisotopes were given in Table 4.23.

**Table 4.23:** Experimental results of the gamma transmission technique of the irradiated PMMA/MWCNTs at 1 wt. % MWCNTs against Co-60 radioisotope.

Thick n. (cm)	Count 1	Count 2	Count 3	Average	Standard Deviation	Relative Count (I/I <sub>0</sub> )
0	25788	25760	25740	25762	19	1
1.703	21328	21332	21202	21287	60	0.8262
3.415	15512	15548	15554	15538	18	0.7299
5.137	9656	9658	9643	9652	6	0.6212
7	5392	5368	5376	5378	9	0.5572

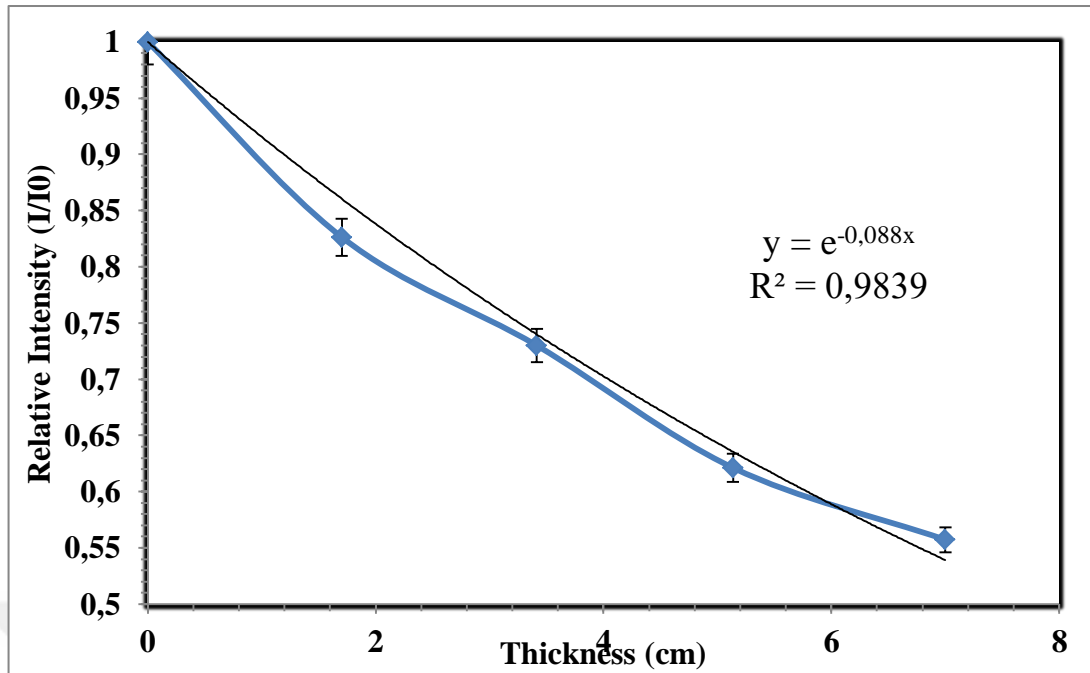


**Figure 4.21:** The changes in the relative intensity of the irradiated PMMA/MWCNTs nanocomposite at 1 wt. % MWCNTs with the rise of the thickness.

The changes in relative intensity at 2 wt. % PMMA/MWCNTs depending on their thickness were given in Figure 4.22. Experimental results of the gamma transmission properties of irradiated 2 wt. % PMMA/MWCNTs against Co-60 radioisotopes were given in Table 4.24.

**Table 4.24:** Experimental results of the gamma transmission technique of the irradiated PMMA/MWCNTs at 2.wt % MWCNTs.

Thick. (cm)	Count 1	Count 2	Count 3	Average	Standard Deviation	Relative Count (I/Io)
0	25788	25760	25740	25762	19	1
3.054	19208	19256	19228	19230	19	0.8047
6.103	15808	15840	15816	15821	13	0.6621
9.149	12932	12948	12996	12958	27	0.5423
12	10138	10140	10128	10135	5	0.4241

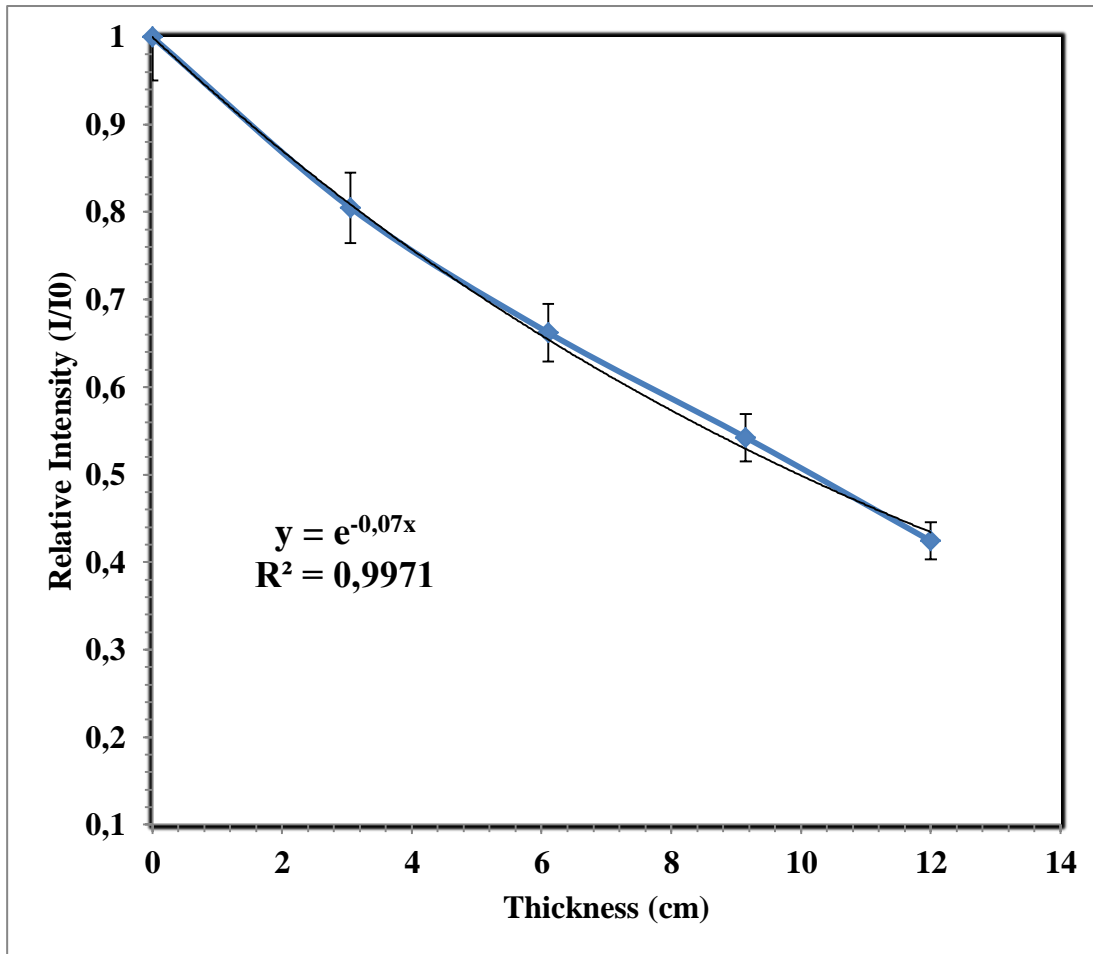


**Figure 4.22:** The changes in the relative intensity of the irradiated PMMA/MWCNTs nanocomposite at 2 wt. % MWCNTs with the rise of the thickness.

The linear and mass and linear attenuation coefficients of the irradiated PMMA/MWCNTs nanocomposites samples were given at Table 4.25.

**Table 4.25:** The linear attenuation coefficient,  $\mu_l$  and mass attenuation coefficient,  $\mu_p$  of the irradiated PMMA/MWCNTs nanocomposite samples against Co-60.

MWCNTs (in wt.%)	Linear attenuation coefficients $\mu_l$ (cm <sup>-1</sup> )	Density $\rho$ (g/cm <sup>3</sup> )	Mass attenuation coefficients $\mu_p/\rho$ (cm <sup>2</sup> /g)
0.5	0.072	1.134	0.0694
1.0	0.088	1.152	0.076
2.0	0.07	1.171	0.06



#### 4.6.4 The Application of the neutron transmission technique for the unirradiated PMMA/MWCNTs nanocomposite by using neutron Howitzer

The attenuation curves were plotted against the neutrons, based on the results obtained for the PMMA/MWCNTs nanocomposite materials studied by experiments with the Pu-Be neutron Howitzer ( $\text{NH}_3$ ) neutron source. The linear and mass attenuation coefficients of irradiated PMMA/MWCNTs nanocomposite samples and unirradiated PMMA/MWCNTs nanocomposite samples provide to observe irradiation effects on attenuation properties. Pu-Be neutron experiment results enable us to compare the linear attenuation coefficients values for gamma radioisotopes and total macroscopic cross sections for neutron source after irradiation treatment. The changes in relative intensity at 0.25 wt. % PMMA/MWCNTs depending on their thickness were given in Figure 4.23. The relative count ( $I/I_0$ ) was determined at four different thicknesses of the PMMA/MWCNTs nanocomposite by using the Pu-Be neutron Howitzer ( $\text{NH}_3$ ) neutron source. The addition of MWCNT as nanofiller into PMMA synthesized by Atom Transfer Radical Polymerization (ATRP) method performed the variations in relative count ( $I/I_0$ ) of the nanocomposite samples. The reason of this result was explained that MWCNT nanofillers at 0.25 wt. % MWCNT amount was dispersed in PMMA polymer matrix. Experimental results of the PMMA/MWCNTs 0.25 wt. % against Pu-Be neutron source were given in Table 4.26.

**Table 4.26 :** Experimental results of the PMMA/MWCNTs 0.25 wt. % against Pu-Be neutron source.

Thick. (cm)	Count 1	Count 2	Count 3	Average	Standard Deviation	Relative Count ( $I/I_0$ )
0	6642	6638	6644	6642	2	1
2.4913	5734	5728	5738	5734	4	0.8633
4.9277	4644	4628	4632	4635	6	0.6978
7.3755	3611	3612	3620	3614	4	0.5442
9.8446	3167	3166	3163	3166	1	0.4766

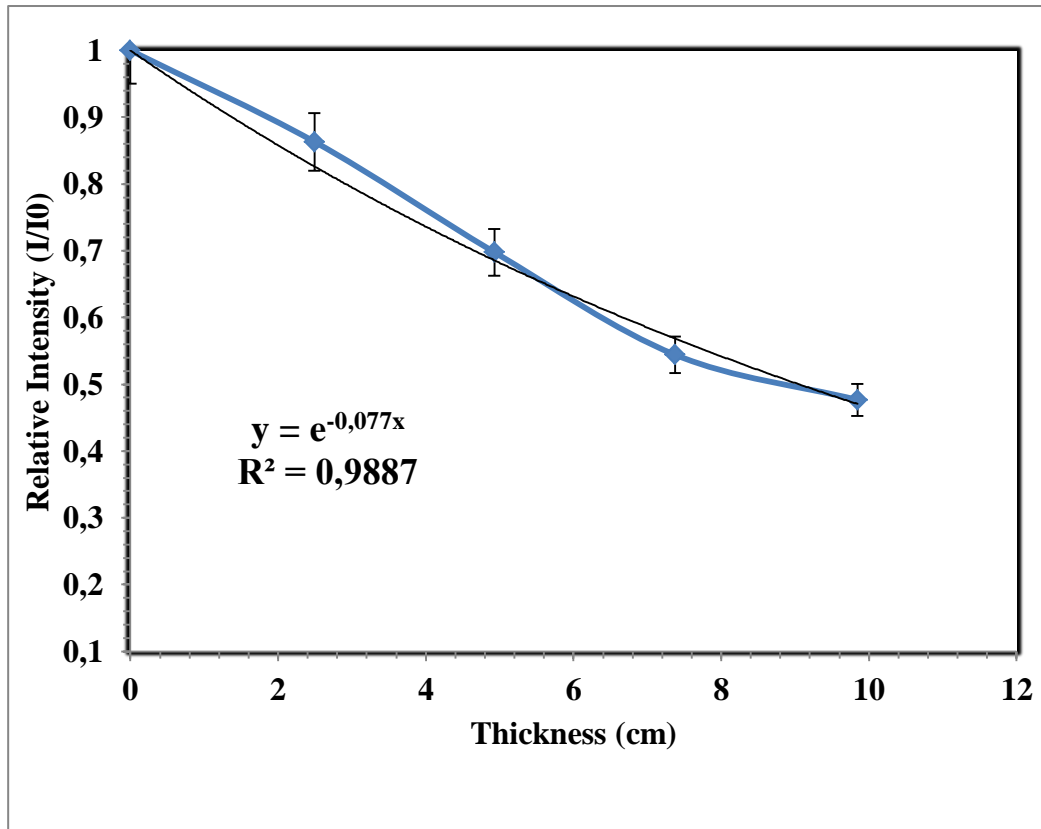


**Figure 4.23:** The changes in relative intensity at 0.25.wt.%PMMA/MWCNTs with the rise of the thickness.

The changes in relative intensity at 0.5.wt.% PMMA/MWCNTs depending on their thickness were given in Figure 4.24.

Experimental results of the PMMA/MWCNTs 0.5.wt.% against Pu-Be neutron source were given in Table 4.27.

**Table 4.27:** Experimental results of the PMMA/MWCNTs 0.5.wt. % against Pu-Be neutron source.

Thicknes s (cm)	Count 1	Count 2	Count 3	Averag e	Standard Deviatio n	Relative Count (I/Io)
0	6642	6638	6644	6641	2	1
3.29	5282	5275	5280	5279	3	0.7949
6.47	4267	4234	4257	4252	13	0.6403
9.74	3289	3176	3191	3218	49	0.4846
12.99	2727	2722	2719	2722	3	0.4099

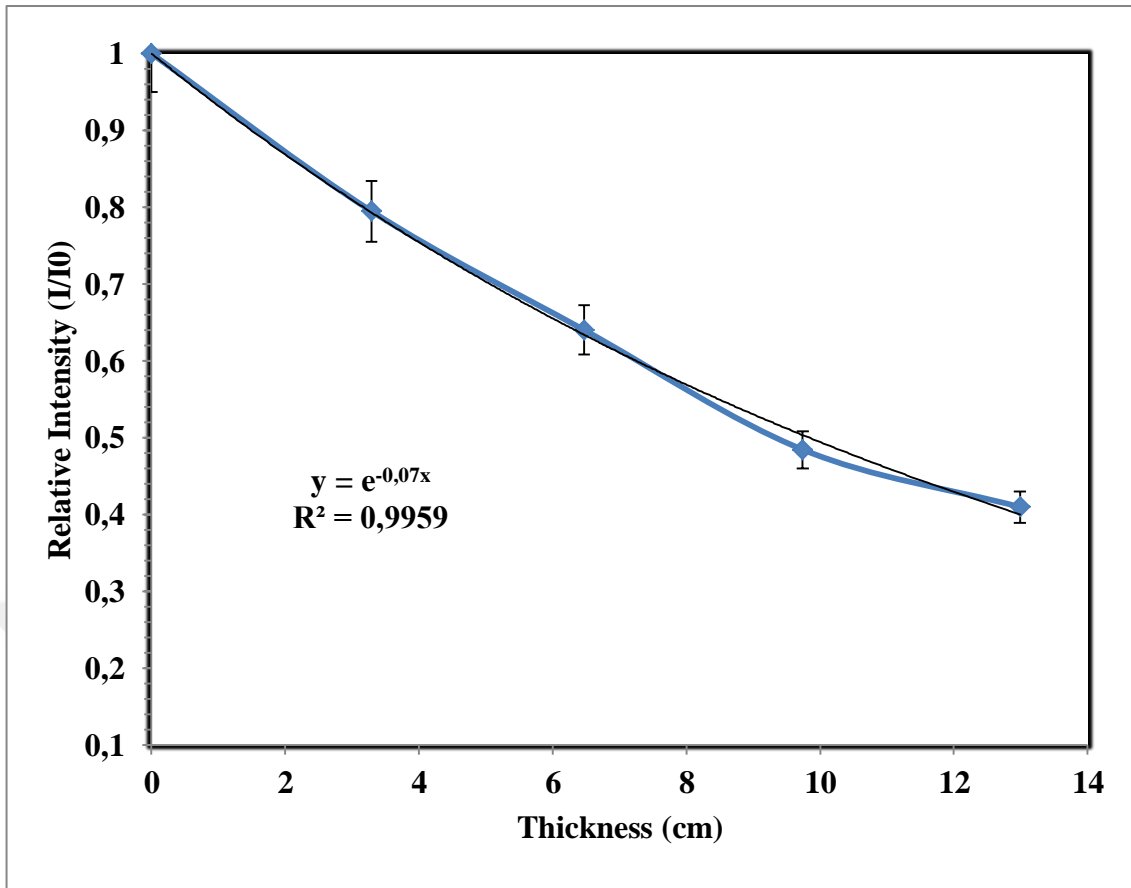


**Figure 4.24:** The changes in relative intensity at 0.5 wt. % PMMA/MWCNTs depending on their thickness.

The changes in relative intensity at 1.wt.%PMMA/MWCNTs depending on their thickness were given in Figure 4.25. Experimental results of the PMMA/MWCNTs 1.wt. % against Pu-Be neutron source were given in Table 4.28.

**Table 4.28:** Experimental results of the PMMA/MWCNTs 1.wt. % against Pu-Be neutron source.

Thickness (cm)	Count 1	Count 2	Count 3	Average	Standard Deviation	Relative Count (I/I <sub>0</sub> )
0	6642	6638	6644	6641	2	1
2.436	5243	5241	5242	5242	1	0.7893
4.849	4337	4332	4335	4334	2	0.6526
7.278	3609	3612	3619	3613	4	0.5441
9.708	2930	2936	2928	2931	3	0.4414

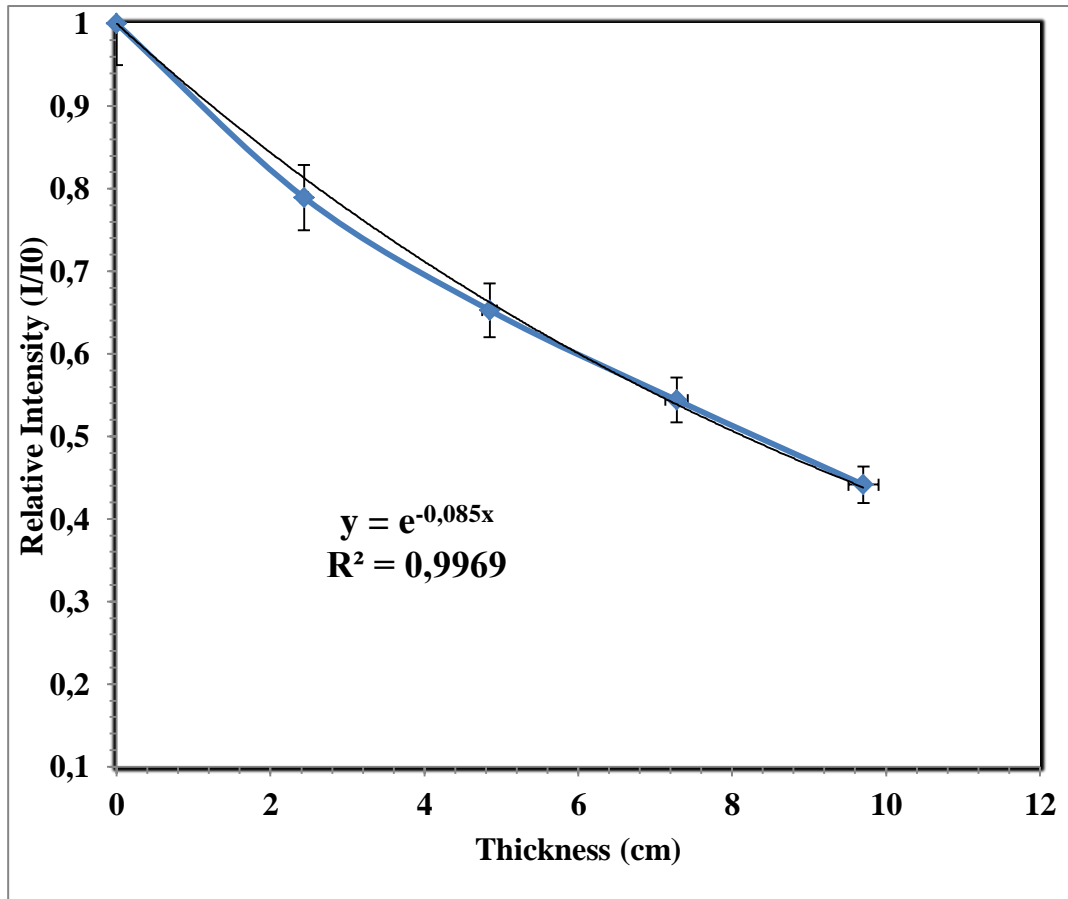


**Figure 4.25 :** The changes in relative intensity at 1.wt.%PMMA/MWCNTs depending on their thickness.

The changes in relative intensity at 2.wt.%PMMA/MWCNTs depending on their thickness were given in Figure 4.26.

Experimental results of the PMMA/MWCNTs 2.wt. % against Pu-Be neutron source were given in Table 4.29.

**Table 4.29 :** Experimental results of the PMMA/MWCNTs 2.wt. % against Pu-Be neutron source.

Thickness (cm)	Count 1	Count 2	Count 3	Average	Standard Deviation	Relative Count (I/I <sub>0</sub> )
0	6642	6638	6644	6641	2	1
2.0495	5112	5106	5115	5111	3	0.7695
4.0898	4461	4457	4462	4460	2	0.6715
6.131	3588	3577	3584	3583	4	0.5395
8.1773	2800	2812	2808	2807	4	0.4226

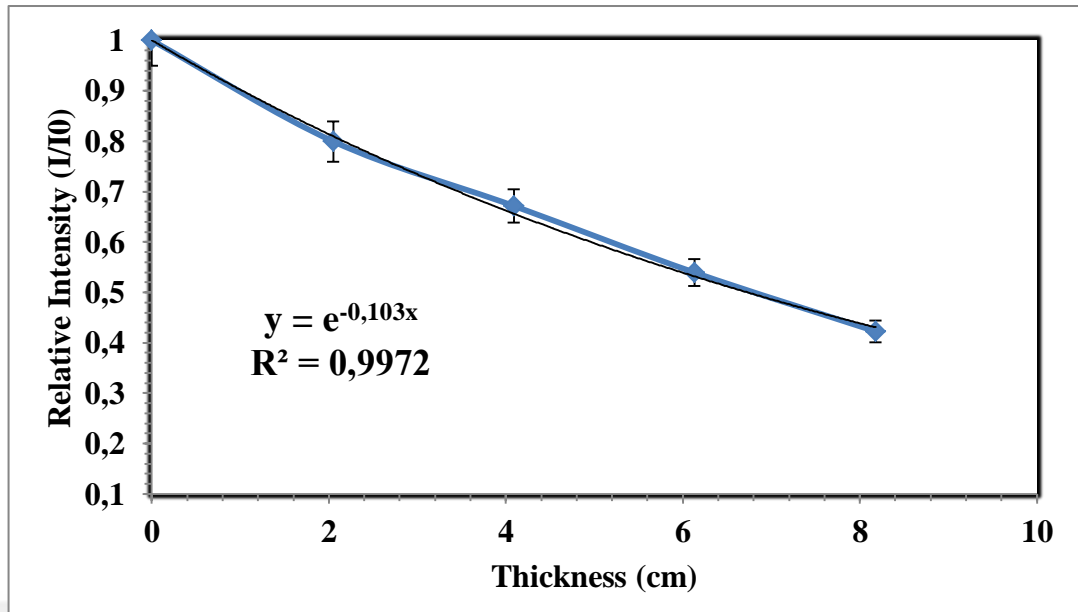


**Figure 4.26 :** The changes in relative intensity at 2.wt.%PMMA/MWCNTs depending on their thickness.

#### 4.6.5 The Application of the neutron transmission technique for the irradiated PMMA/MWCNTs nanocomposites by using neutron Howitzer

The irradiation (50 kGy) was applied some PMMA/MWCNTs which are 0.5.wt. % MWCNTs, 1.wt. % MWCNTs, 2.wt. % MWCNTs. The changes in relative intensity at 0.5.wt. % PMMA/MWCNTs depending on their thickness were given in Figure 4.27.

Experimental results of the irradiated 0.5.wt. % PMMA/MWCNTs against Pu-Be neutron source were given in Table 4.30.

**Table 4.30 :** Experimental results of the irradiated PMMA/MWCNTs 0.5.wt. % for Pu-Be neutron source.

Thickness (cm)	Count 1	Count 2	Count 3	Average	Standard Deviation	Relative Count (I/I <sub>0</sub> )
0	6774	6764	6771	6769	4	1
2.856	5804	5817	5827	5816	9	0.8591
5.709	4742	4740	4741	4741	1	0.7003
8.553	3859	3850	3887	3859	15	0.5700
11	2987	2980	2988	2985	3	0.4409

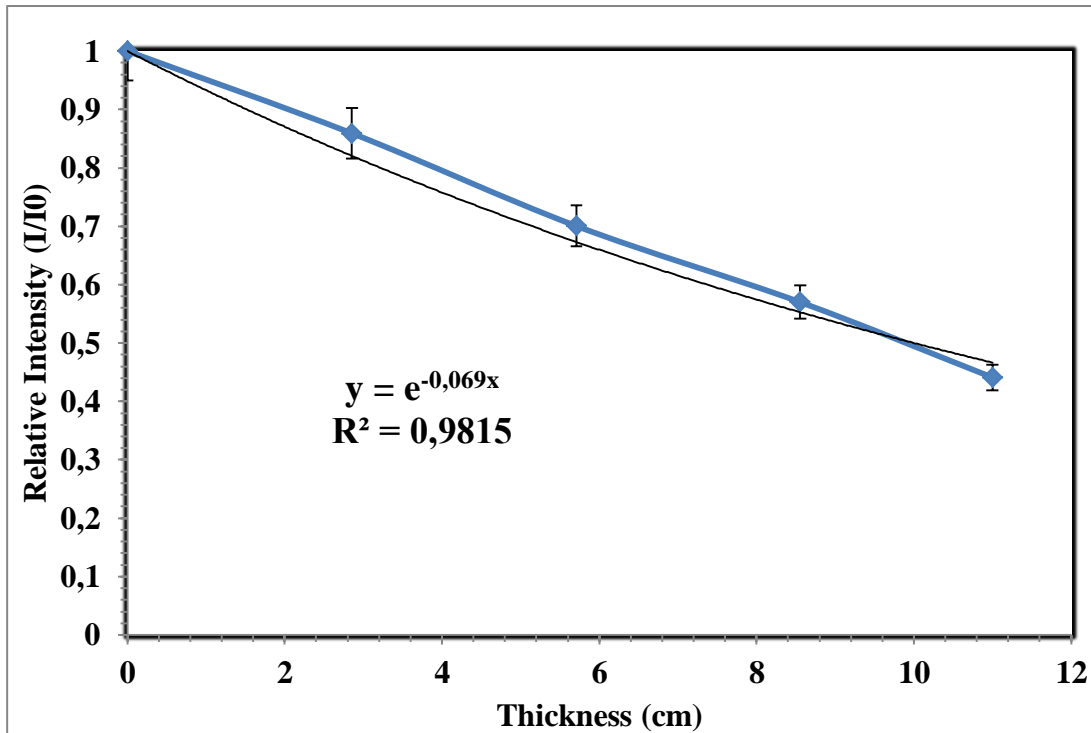


**Figure 4.27 :** The changes in relative intensity at irradiated 0.5.wt.%PMMA/MWCNTs depending on their thickness.

The changes in relative intensity at 1.wt.%PMMA/MWCNTs depending on their thickness were given in Figure 4.28. Experimental results of the irradiated 1.wt.%PMMA/MWCNTs against Pu-Be neutron source were given in Table 4.31.

**Table 4.31 :** Experimental results of the irradiated PMMA/MWCNTs 1 wt. % against Pu-Be neutron source.

Thickness (cm)	Count 1	Count 2	Count 3	Average	Standard Deviation	Relative Count (I/I <sub>0</sub> )
0	6774	6764	6771	6769	4	1
1.703	5726	5742	5730	5733	6	0.8468
3.415	5149	5134	5131	5138	8	0.7589
5.137	4375	4381	4375	4377	2	0.6465
7	3851	3835	3828	3838	9	0.5669

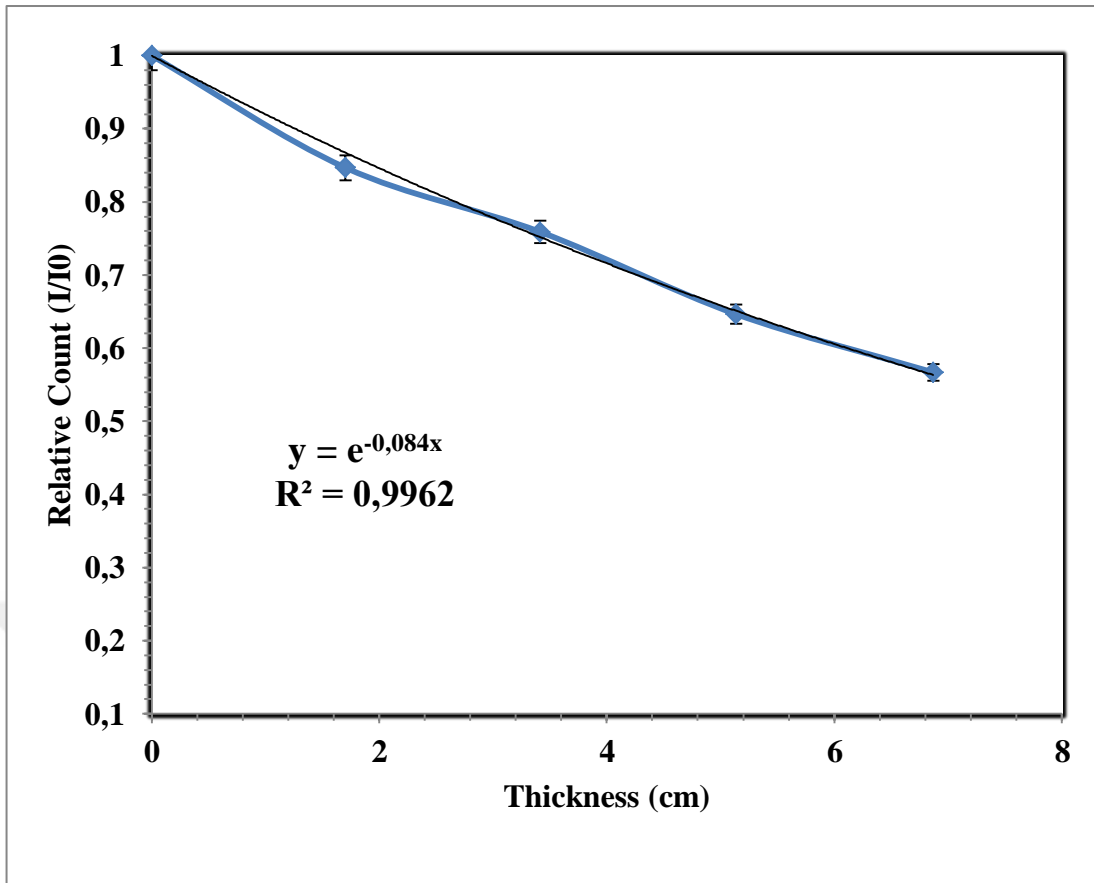


**Figure 4.28 :** The changes in relative intensity at irradiated 1.wt.% PMMA/MWCNTs depending on their thickness.

The changes in relative intensity of the PMMA/MWCNTs nanocomposite at 2.wt.%PMMA/MWCNTs depending on their thickness were given in Figure 4.29. Experimental results of the irradiated 2.wt.% PMMA/MWCNTs against Pu-Be neutron source were given in Table 4.32.

**Table 4.32 :** Experimental results of the irradiated PMMA/MWCNTs at 2.wt.%PMMA/MWCNTs against Pu-Be neutron source.

Thickness (cm)	Count 1	Count 2	Count 3	Average	Standard Deviation	Relative Count (I/Io)
0	6774	6773	6770	6773	1	1
2.0495	5684	5683	5679	5682	2	0.8389
4.0898	4755	4754	4752	4754	1	0.7018
6.131	3842	3841	3847	3843	2	0.5674
8.1773	2855	2854	2852	2854	1	0.4214

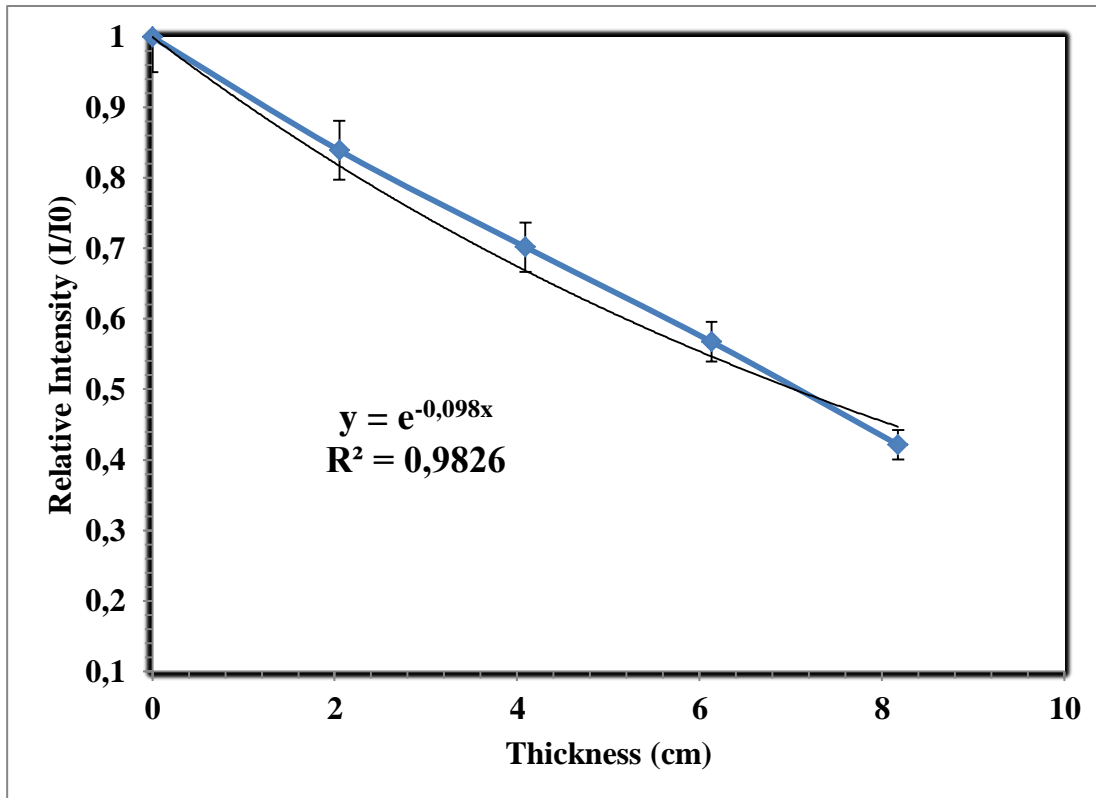


**Figure 4.29 :** The changes in relative intensity at irradiated 2.wt.%PMMA/MWCNTs depending on their thickness.

The total macroscopic cross-sections ( $\Sigma_T$ ) of the PMMA/MWCNTs nanocomposite for Pu-Be neutron source was used to evaluate the attenuation of neutrons at the nanocomposite with the rise of the amount of MWCNTs. The total macroscopic cross-section ( $\Sigma_T$ ) of the PMMA/MWCNTs nanocomposite was derived from the relative intensity curve by utilising  $I=I_0.e^{-\Sigma_{tot}.x}$  equation. Total macroscopic cross-sections of the unirradiated (Table 4.33) and irradiated (Table 4.34) PMMA/MWCNTs nanocomposite samples were given below.

**Table 4.33 :** The changes total macroscopic cross-sections ( $\Sigma_T$ ) ( $\text{cm}^{-1}$ ) of the unirradiated PMMA/MWCNTs nanocomposite samples for Pu-Be neutron source.

MWCNTs (in wt.%)	The total macroscopic cross-sections ( $\Sigma_T$ ) ( $\text{cm}^{-1}$ )	Mean free path $1/\Sigma_T$ (cm)
0.25	0.077	12.98
0.50	0.07	14.28
1.00	0.085	11.76
2.00	0.103	9.708



**Table 4.34 :** The changes total macroscopic cross-sections ( $\Sigma_T$ ) ( $\text{cm}^{-1}$ ) of irradiated PMMA/MWCNTs nanocomposite samples for Pu–Be neutron source.

MWCNTs (in wt.%)	The total macroscopic cross-sections ( $\Sigma_T$ ) ( $\text{cm}^{-1}$ )	Mean free path $1/\Sigma_T$ (cm)
0.5	0.069	14.492
1.0	0.084	11.905
2.0	0.098	10.204

Half-value layer (HVL) was considered as a required thickness to stop half of the incoming radiation. The experimental values of linear attenuation coefficients ( $\mu_1$ ) for Cs-137 and Co-60 radioisotopes (Equation 4.1) and total macroscopic cross-sections ( $\Sigma_T$ ) values for neutrons (Equation 4.2) were used to determine the half value thickness of PMMA/MWCNTs nanocomposite with the rise of the amount of MWCNTs.

$$HVL = \frac{\log(0,5)}{\mu} = \frac{0.693}{\mu} \quad (4.1)$$

$$HVL = \frac{\log(0,5)}{\Sigma_{total}} = \frac{0.693}{\mu} \quad (4.2)$$

The results of the Half-Value-Layer for unirradiated (Table 4.35) and irradiated (Table 4.36) PMMA/MWCNT nanocomposite samples were calculated using above equations.

**Table 4.35 :** Half-value layer (HVL) of unirradiated PMMA, PMMA/MWCNTs for Cs- 137, Co-60 Radioisotopes and Pu–Be ( $\text{NH}_3$ ).

MWCNTs (in wt.%)	HVL (cm) for Cs-137 radioisotope	HVL (cm) for Co-60 radioisotope	HVL (cm) for Pu-Be $\text{NH}_3$
0.25	7	9.63	9
0.50	7.37	9.9	9.9
1.00	7.07	8.77	8.15
2.00	6.93	8.772	6.72

**Table 4.36 :** Half-value layer (HVL) of the irradiated PMMA, PMMA/MWCNTs for Cs- 137, Co-60 Radioisotopes and Pu–Be (NH<sub>3</sub>).

MWCNTs (in wt.%)	HVL (cm) for Cs-137 radioisotope	HVL (cm) for Co-60 radioisotope	HVL (cm) for Pu-Be NH <sub>3</sub>
0.5	7.29	9.62	10.04
1.0	6.18	7.87	8.25
2.0	7.37	9.9	7.07

#### 4.7 Ultrasonic Test

Figure 4.30 indicated that nanocomposite material is a homogeneous due to the relative smooth region between two echos.



**Figure 4.30 :** The picture of homogeneity of the 2.wt. % PMMA/MWCNTs nanocomposite sample.

The longitudinal waves velocity and transverse waves velocity were measured after the measurement of the thickness of the materials.

Using the results of the velocities and density values some materials properties that are Poisson's ratio, Shear modulus (G), Young's modulus (E) and Microhardness (H) were calculated. All calculations were done using the formulas that was given at background and literature review section. These calculations were done for pure PMMA, unirradiated 2 wt.% PMMA/MWCNTs and irradiated 2 wt. % PMMA/MWCNTs. The difference between these values also calculated to understand the changes after irradiation effect. All calculations were given in Table 4.37.

Furthermore, ultrasonic test results showed importance of the homogeneity of the material that related with production steps. Production steps of the PMMA/MWCNTs nanocomposite supported to produce the homogenous polymer nanocomposite and to obtain the polymer nanocomposite with the suitable elastic properties in the ultrasonic test results at the experiments. These production steps of the polymer nanocomposite are using pure chemicals weighted inside two hands AtmosBag in argon atmosphere and the synthesis step in the argon.

The determined ultrasonic test results indicated that the details of the production steps of the PMMA/MWCNTs nanocomposite were the key parameters to obtain the suitable elastic properties and homogeneity at the produced nanocomposite. The details of the production steps were declared to obtain the suitable mechanical properties: It was tried to obtain a vacuum ambient and the air was removed to outside at the AtmosBag by using a vacuum pump.

**Table 4.37 :** The changes in Poisson's ratio, Shear modulus (G), Young's modulus (E) and Microhardness (H) with the rise of the MWCNTs in PMMA/MWCNTs nanocomposite samples.

Samples at 2 wt.% MWCNTs amount	$\rho$ Density (kg/m <sup>3</sup> )	$C_L$ Longitudina l velocity (m/s)	$C_T$ Transverse velocity (m/s)	$\nu$ Poisson's ratio	G Shear modulus (GPa)	E Young's modulus (GPa)	H Microhardness (GPa)
Base PMMA	1180.890	2663.5	1322	0.3370	2.0640	5.517	0.225
Unirradiated PMMA/MWCNTs	1197.88	2711.0	1340	0.3383	2.1510	5.757	0.231
Irradiated PMMA/MWCNTs	1171.00	2738.0	1334	0.3444	2.0840	5.598	0.215
Difference (%) between unirradiated and irradiated states of PMMA/MWCNTs nanocomposite samples	2.24	0.98	0.44	1.7700	3.1100	2.760	6.920

## 5. DISCUSSIONS

CNT within polymer matrices under tensile stress align themselves parallel to the direction of the applied load, enabling crack bridging behind a crack tip. Andrews et al (2002) explained that this phenomenon reduced the stress concentration in the region surrounding the crack tip, and ultimately reduced crack propagation. Key reinforcement mechanisms identified in CNT polymer systems are nanotube pullout, bending of nanotubes (often due to surface defects such as iron oxide catalyst inclusions from the CNT production process) and telescopic fracture of nanotubes in Figure 5.1. The disintegration of MWCNT in the MMA liquid monomer can be possible by ultrasonication and MWCNT can bridge a micro-crack across the polymer surface. (Dunne & Ormsby, n.d)

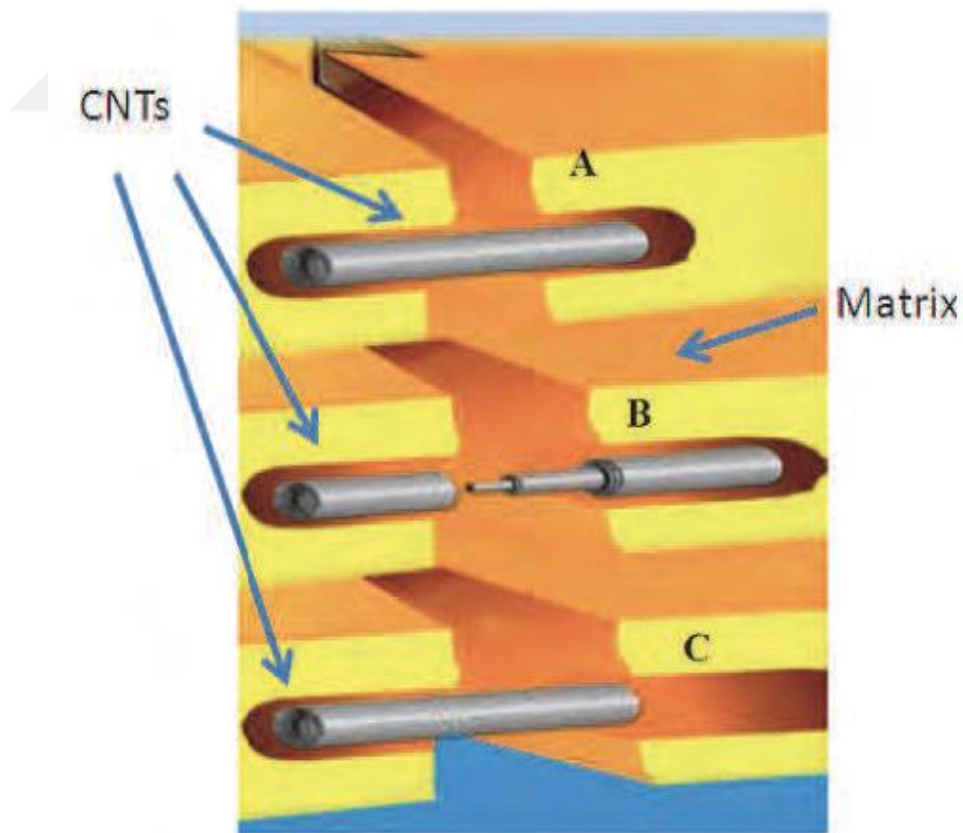
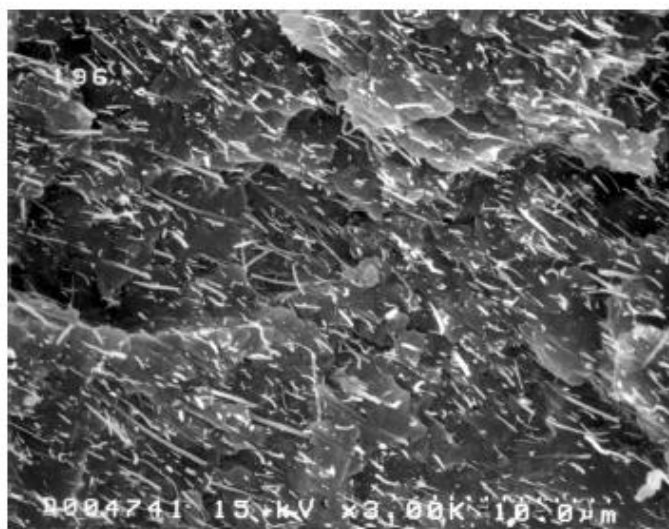
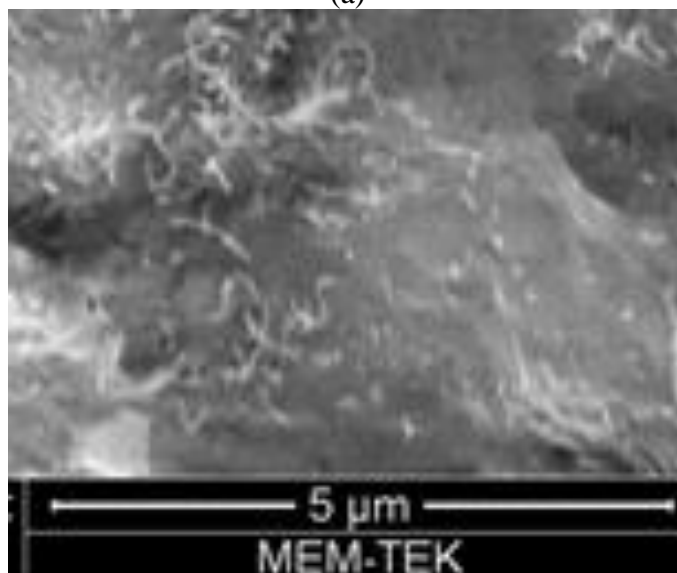


**Figure 5.1** : Schematic illustration of (A) a CNT bridging a crack, (B) telescopic failure of a CNT and (C) CNT fibre pullout experienced in CNT-reinforced polymers.

SEM technique was used to examine the surface morphology of the PMMA/MWCNTs. The dispersion was assigned the uniformity of MWCNTs distribution across the specimen in this study. MWCNT is dispersed a suitable way in polymer nanocomposite with the absence of agglomerates and a uniform fiber density distribution across the field of view in Figure 5.2. (A. Rodney et al.). SEM image for well-dispersed MWCNT in polymer nanocomposite at this study was similar with the literature (A.Rodney et al.). In this study, the dispersion was assigned the uniformity of fiber distribution across the specimen avoiding agglomeration in the matrix.



(a)



(b)

**Figure 5.2 :** SEM image of PMMA/MWCNTs nanocomposite in (a) the literature and (b) this study at 2.wt % PMMA/MWCNTs.

The structural characterization of PMMA/MWCNTs nanocomposite structure was carried out to examine the effect of MWCNTs nanofiller on PMMA using XRD analysis. XRD diffraction patterns of PMMA/MWCNTs nanocomposites presented a pick at  $\sim 13^\circ$ . The intensity of the pick increased with the rise of the amount of the MWCNTs. There was the similar shifts was determined with the rise of the amount of MWCNTs in the literature (Brkovic, et al., 2017).

Further, it was focused on in-situ polymerization method depending on the suitable dispersion of multi-wall carbon nanotubes (MWCNTs) at PMMA effectively In this study.

The addition of MWCNT as nanofiller into PMMA was performed to enhance the physical properties of the polymer and it was synthesized by Atom Transfer Radical Polymerization (ATRP) method supported to the improve the nanocomposite structure. MWCNT nanofillers at four different MWCNT amounts (such as 0.25, 0.5, 1.0 and 2.0 wt. %) was dispersed in PMMA polymer matrix via in situ polymerization technique. The dispersion quality of MWCNT in PMMA polymer was examined with SEM analysis. The changes in the characteristic properties of PMMA were examined several characterization tests such as XRD, FTIR, TGA/DSC and hardness test.

The chemical structure was investigated by FTIR analysis. The FTIR spectra of PMMA/MWCNTs nanocomposite presented similar spectra with pure PMMA, showed that interaction occurred between MWCNTs nanocomposite and PMMA polymer matrix. The changes in FTIR characteristics were similar with the literature (Brkovic, et al., 2017).

Thermal stability was examined with the Thermogravimetric Analysis. TGA results for unirradiated samples showed that with the addition of 2% MWCNTs, the 5% weight loss temperatures shifted from  $191^\circ\text{C}$  to  $243^\circ\text{C}$ , improved by  $52^\circ\text{C}$ . The thermal stability of PMMA improved with the rise of the amount of the PMMA/MWCNTs. The 5 % weight loss temperatures increased after irradiation was applied.

The improvements in Rockwell Hardness (M scale) values were examined to investigate the mechanical performance. The differences between Rockwell Hardness values for unirradiated and irradiated states indicated that the irradiation

treatment affected the Rockwell Hardness of the nanocomposite after irradiation at 50 kGy. The changes in Rockwell Hardness (M scale) value of the irradiated nanocomposite samples addressed to lead the variations in microscopic structure of the nanocomposite.

Ultrasonic test results supported to the dispersion of PMMA/MWCNTs nanocomposite at 2wt. % PMMA/MWCNTs nanofiller homogeneously in PMMA polymer matrix.

Besides, ultrasonic test results indicated that the elastic parameters improved slightly with the rise of MWCNTs nanofiller. Shear modulus and Young's modulus of the irradiated PMMA/MWCNTs nanocomposite at 2wt. % PMMA/MWCNTs decreased after irradiation at 50 kGy. The decrease in elastic properties such as Shear modulus and Young's modulus indicates the variations in the flexible property of the polymer nanocomposite with the same geometry but with lower elastic modulus, the resulting forward speed is significantly greater than that of the more rigid material. (Shyy et.al, 2013)

Comparison with literature of the produced PMMA/MWCNTs nanocomposites in this study and the details on improvement in the thermal properties and mechanical performance of the irradiated PMMA/MWCNTs nanocomposites in this study was presented in Table 5.1.

There are three important temperatures for polymer nanocomposites: glass transition temperature, melting temperature and degradation temperature. Degradation temperature is important to know up to which temperature value polymer can preserve its structure. There are four studies provide to know this temperature value with different dispersion methods.

Besides, mechanical properties are also important subject to determine the mechanical performance of the material against external effects. Hardness property is one of them. Hardness values of the PMMA based MWCNTs can be compared with two studies with same dispersion method but different amounts of MWCNTs in PMMA matrix.



**Table 5.1** : Comparison with literature of the produced PMMA/MWCNTs nanocomposites in this study.

Researchers	Dispersion method	Thermal properties	Mechanical properties
Mohd.Shadab Alam & K.K.Verma	In-situ polymerization	PMMA/MWCNTs were degraded at 328°C. The melting temperature was increased from 369.8 °C to 372.68°C.	Hardness value was 88 for pure PMMA It was 45 for PMMA/MWCNTs 0.1 wt.% MWCNTs.
Tomova, et al	Casting solution tech.	Degradation temperature increased by five degrees (at 339°C, sample PMMA/MWCNTs at 1 wt. % MWCNTs).	-
Logakis, et al.	Melt mixing	Glass transition temperature for PMMA was 107.9°C. It was 108.9°C for PMMA/MWCNTs at 8.0 wt.% MWCNTs.	Storage modulus of PMMA was 3.72 GPa. It was 3.99 GPa for 1.0 wt. % PMMA/MWCNTs. However, it decreased for 5.0 wt. % PMMA/MWCNTs that were 3.25 GPa.
S. Ulag (in this thesis study)	In-situ polymerization	Unirradiated PMMA/MWCNTs degraded at 340 °C wt. % MWCNTs. Irradiated PMMA/MWCNTs started to degrade at ~360 °C wt.% MWCNTs.	Hardness value was 84.5 for unirradiated base PMMA. Hardness value was 86 for irradiated base PMMA. Hardness value was 94 for unirradiated PMMA/MWCNTs at 2.wt. %PMMA/MWCNTs. Hardness value was 97 for irradiated PMMA/MWCNTs at 2. wt.% MWCNTs.



## 6. CONCLUSIONS

Dispersion of the MWCNTs in the matrix is one of the key parameter in polymer nanocomposite. It was determined that “in-situ polymerization method” was an efficient method to get homogeneous dispersion at PMMA/MWCNTs nanocomposite in this study.

SEM image of the PMMA/MWCNTs nanocomposite at 2 wt. % PMMA/MWCNTs indicated that MWCNTs nanofillers dispersed homogeneously in the PMMA polymer matrix. XRD patterns of PMMA, MWCNTs and PMMA/MWCNTs nanocomposites explained that there were three characteristic diffraction peaks. One of them centered at  $\sim 13^\circ$ , and two small peaks placed at  $\sim 28^\circ$  and  $\sim 42^\circ$ . The changes in the Rockwell hardness values of the nanocomposite were examined before and after the irradiation treatment at 50 kGy. The Rockwell hardness values of the pure PMMA increased with the addition of MWCNTs nanofiller. The addition of MWCNTs at 2 wt. % amount supported to improve the Rockwell hardness value of the PMMA/MWCNTs nanocomposite. The difference of the Rockwell hardness value was  $\sim 11\%$  between pure PMMA and PMMA/MWCNTs nanocomposite with 2 wt. % PMMA/MWCNTs amount. Besides, the irradiation process improved the hardness value of the PMMA/MWCNTs nanocomposite. The difference in the Rockwell hardness values between the unirradiated and the irradiated states was  $\sim 3\%$  for PMMA/MWCNTs. The ultrasonic inspection as a nondestructive testing was used to examine the detailed information on the structural changes and the elastic properties of pure PMMA and PMMA/MWCNTs nanocomposite. The ultrasonic test results of the PMMA/MWCNTs nanocomposite at 2wt. % PMMA/MWCNTs amount indicated that MWCNTs nanofiller has dispersed homogeneously in PMMA polymer matrix. The ultrasonic test results of the PMMA/MWCNTs nanocomposite asserted that the addition of MWCNTs at 2 wt. % amount into the PMMA improved the elastic properties of its structure. However, the irradiation process at 50 kGy addressed to decrease in the elastic modulus of the PMMA/MWCNTs nanocomposite and this change supported to the enhancement in the flexible property of the polymer nanocomposite with the same geometry but with lower elastic modulus. After the irradiation of the PMMA/MWCNTs nanocomposite, the decrease in elastic properties (such as Shear modulus and Young's modulus) of the

nanocomposite with the rise of Rockwell Hardness (M scale) value addressed to lead the enhancement of the resulting forward speed at high speed applications of the vehicles containing PMMA/MWCNTs nanocomposite. The decrease in the Shear modulus and Young's modulus values and the enhancement in Rockwell Hardness value of the irradiated nanocomposite addressed to use this nanocomposite at the high-speed applications.

The application of the gamma transmission technique performed to examine the variations in the radiation shielding performance of the PMMA/MWCNTs nanocomposite against to gamma radiation by using two different gamma sources (such as Cs-137 and Co-60 radioisotopes). The linear attenuation coefficient of PMMA/MWCNTs nanocomposite changed slightly with the rise of the amount of the MWCNTs nanofiller. The experimental attenuation coefficient values were compared with the theoretical attenuation coefficient values. The comparison of their results addressed to a similarity between the experimental and theoretical attenuation coefficient values. The use of Pu-Be Neutron Howitzer supported to examine the details on the structural characteristics of PMMA/MWCNTs nanocomposites and to evaluate the effect of MWCNTs on PMMA/MWCNTs nanocomposite. These results indicated that PMMA/MWCNTs nanocomposite produced by ATRP method was a suitable lightweight material to use several industrial areas such as the aviation and aerospace industries.

## REFERENCES

- A. Szentes, Á. Kukovecz, Cs. Varga, G. Horváth, L. Bartha, H. Haspel, J. Szél, Z. Kónya** (2012). *Electrical resistivity and thermal properties of compatibilized multi-walled carbon nanotube/polypropylene composites*. 15 January 2012.
- A. Rodney, J. David, M. Mickael, R. Terry.** (2002). *Fabrication of Carbon Multiwall Nanotube/Polymer Composites by Shear Mixing*, *Macromol. Meter Eng.* Pages:287,395-403.
- B. Y. Tian, P. J. Hu, M. Yuan, E. J. Tang, S. J. Liu, X. Y. Zhao, D. S. Zhao** (n.d.). *Effects of different ligands on the controlled polymerization of monodisperse polystyrene nanospheres by atom transfer radical polymerization in an aqueous emulsion*.
- B. Emmanuel, A. Sohaib, C. Philippe, Ca. Phippe.** (n.d). *Polymer Nanocomposites Containing Functionalized Multiwalled Carbon Nanotubes:a Particular Attention to Polyolefin Based Materials*.
- B.V. Danijela, P.B. Vladimir, P.P. Vera, O. Nina, M. Miodrag, S. Sanja, V. Branislav, U.S. Petar, M.D. Aleksandar.** (2017). *Structural Properties of the Multiwall Carbon Nanaotubes/Poly (Methyl methacrylate) Nanocomposites: Effect of the Multiwall Carbon Nanaotubes Covalent Functionalization*, *POLYMER COMPOSITES*. Press.
- B. Hua, R. Xiulin, F.S. Timothy.** (2010). *Optical properties of ordered vertical arrays of multiwalled carbon nanotubes from FDTD simulations*. Brick and NCN Publications. Paper 688.
- C. Anna.** (2002) *Atom Transfer Radical Polymerization Multifunctional Substrates*. Department of Polymer Technology. Royal Institue of Technology.
- C. Ming-liang, Z Feng-Jun, O. Won-chun.** (2009). *Synthesis, characterization, and photocatalytic analysis of CNT/TiO<sub>2</sub> composites derived from MWCNTs and titanium sources*. Pages 159-166.
- C.Lourdes del Valle.** (2008). *Polymer Nanocomposites Master in Nanoscience. Low dimensional systems and nanostructures*.
- D. Nicholas, O.W. Ross.** (n.d). *MWCNT Used in Orthopaedic Bone Cements, Carbon Nanotubes-Growth and Applications*.
- D.L. Barbara, C.M. Christine.** (n.d). *Geochemical Instrumentation and Analysis, X-Ray Powder Diffraction (XRD)*.
- E. Bryan, S. Ray.** (2008). *Polymers: A Property Database*, Second Edition, and CRC Press Book. October 29, 2008. Reference - 1052 Pages.
- E. Logakis, Ch. Pandis, P. Pissis, J. Pionteck, P. Pötschke.** (2011). *Highly conducting poly (methyl methacry-late)/carbon nanotubes composites:*

*Investigation on their thermal, dynamic-mechanical, electrical and dielectric properties. Composites Science and Technology*, Elsevier, 2011, 71 (6), pp.854-861. <10.1016/j.compscitech.2011.01.029>. < hal-00736298 >

- H. Ala.** (n.d). *Introduction to Non-Destructive Testing Techniques*.
- J. Wojciech, T.V.Nicolay, M. Patrick.** (n.d) *ATRP:Complete Tools for the Synthesis of Well-Defined Functionalized Polymers*.
- J. Gwyn Morgan, K. Kiyoshi.** (1976). *Polymeric carbons-carbon fibre, glass and char*. Cambridge University Press, 6 May 1976-pages 178.
- K. Matyjaszewski, J. Xia.** (2001). *Atom transfer radical polymerization*, Chemical reviews, 101, 2921-2990.
- K. Matyjaszewski, T.P.Davis.** (2003). *Handbook of Radical Polymerization*, Wiley.
- K.H. Joseph.** (2006). *Polymer Nanocomposites Processing, Characterization, and Applications*. Nanoscience and Technology Series.
- L'A. F. Michael** (2003). *Handbook of Radioactivity Analysis*. Elsevier Science, 2nd Ed, ABD.
- M. Caroline, M. Tany, B. Werner, R. Manuel, P. Petra.** (n.d). *Composites of Poly (methylmethacrylate) and Multi-walled carbon nanotubes by melt blending*. The Polymer Processing Society 23<sup>rd</sup> Annual Meeting.
- O. Olagoke, A. Kolapo.** (2015). *Handbook of Thermoplastics*, Second Edition, CRC Press.
- P. Vladimir, L. Rynno, H. Irina, P. Alex, V. Sergey.** (2007). *Introduction to nanomaterials and nanotechnology*. University of Tartu. 225p.
- R.S. Rodney, Q. Dong, L.K. Wing, R.S. Ruoff.** (2003). *Mechanical properties of carbon nanotubes: theoretical predictions*
- S. Sowmya.** (2016). *Synthesis and characterization of nanocomposites for potential applications*.
- S. Heba.** (2016). *What is the difference between the transverse waves and longitudinal waves?*
- S. Wei, A. Hikaru, K. Chang-kwon, L.Hao.** 2003. *An Introduction to Flapping Wing Aerodynamics*, Cambridge University Press, Printed in USA.
- T. Atsuya, H. Akihiko, F. Mitsuru, T. Hiroyuki, K. Junno.** (2012). *Dose-dependent mesothelioma induction by intraperitoneal administration of multi-wall carbon in p53 heterozygous mice*. *Cancer Sci/August 2012/vol.103 /no.8/1440-1444*.
- T. Kübra.** (2016). *PMMA (Polimetilmetakrilat)* Selcuk University.
- Y. Abdullah.** (2011). *Karbon nano tüpler Çukurova Üniversitesi Fen Bilimleri Enstitüsü*. Pages 69.
- Y.Go, O.Mamoru, Y.Kenji, H.Toshiyuki, A.Koshi .** (2008). *Structural characterization and frictional properties of carbon nanotube/alumina composites prepared by precursor method*. Pages 265-269.

**W. B. H. Noor.** (2013). *Temperature effect on polymerization kinetics of Poly methylmethacrylate (PMMA)*. Faculty of Chemical & Natural Resources Engineering. Universiti Malaysia Pahang.

**X. Huaqing, C. An, W. Xinwei.** (2007). *Thermal diffusivity and conductivity of multiwalled carbon nanotube arrays*.

**Url-1**<<http://www.recycledplastic.com/index.html%3Fp=10288.html>> date retrieved 11.09.2017.

**Url-2**<[https://www.news-medical.net/life-sciences/Properties-of\\_Nanoparticles.aspx](https://www.news-medical.net/life-sciences/Properties-of_Nanoparticles.aspx)> date retrieved 20.09.2017.

**Url-3**<<https://www.sigmaaldrich.com/materials-science/polymer-science/learning-center-library.html>> date retrieved 23.09.2017.

**Url-4**<[http://webhotel2.tut.fi/projects/caeds/tekstit/plastics/plastics\\_PMMA.pdf](http://webhotel2.tut.fi/projects/caeds/tekstit/plastics/plastics_PMMA.pdf)> date retrieved 23.09.2017.

**Url-5**<<http://www.pharmainfo.net/book/emerging-trends-nanotechnology-pharmacy-1introduction-nanotechnology/physical-and-chemical>> date retrieved 26.09.2017.

**Url6**<[http://web.mit.edu/mbuehler/www/SIMS/Adhesion%20of%20Carbon%20Nanotube\\_files/CARBON%20SP.png](http://web.mit.edu/mbuehler/www/SIMS/Adhesion%20of%20Carbon%20Nanotube_files/CARBON%20SP.png)> date retrieved 10.10.2017.

**Url7**<<http://faculty.uscupstate.edu/llever/polymer%20resources/glasstrans.htm>> date retrieved 15.10.2017.

**Url-8**<<https://www.calce.umd.edu/TSFA/Hardnessa.htm>> date retrieved 18.10.2017.

**Url-9**<<http://www.wmtr.com/en.rockwellscale.html>> date retrieved 19.10.2017.

**Url-10**<<https://www.emcotest.com/en/the-world-of-hardness-testing/hardness-know-how/theory-of-hardness-testing/rockwell/rockwell-test-procedure/>> date retrieved 21.10.2017.

**Url-11**<<http://www.nuclear-power.net/nuclear-power/reactor-physics/atomic-nuclear-physics/fundamental-particles/photon/gamma-ray/characteristics-gamma-rays/>> date retrieved 23.10.2017.

**Url-12**<<http://hyperphysics.phy-astr.gsu.edu/hbase/Particles/lepton.html>> date retrieved 26.10.2017

**Url-13**<<http://hyperphysics.phy-astr.gsu.edu/hbase/Particles/proton.html>> date retrieved 27.10.2017.

**Url-14**<<http://www.nuclear-power.net/nuclear-power/reactor-physics/atomic-nuclear-physics/fundamental-particles/neutron/interactions-neutrons-matter/>> date retrieved 28.10.2017.

**Url-15**<<http://sites.ifi.unicamp.br/mabernal/files/2014/09/NeutronInteractions.pdf>> date retrieved 01.11.2017.

**Url-16**<<http://www.nuclear-power.net/nuclear-power/reactor-physics/atomic-nuclear-physics/fundamental-particles/neutron/interactions-neutrons-matter/>> date retrieved 03.11.2017.

**Url-17**<<http://hyperphysics.phy-astr.gsu.edu/hbase/quantum/bragg.html>> date retrieved 28.09.2017.

**Url-18**<<http://www.nanokon.yildiz.edu.tr/nanoteknoloji/taramali-elektron-mikroskopu-scanning-elektron-microscope-sem/>> date retrieved 17.10.2017.

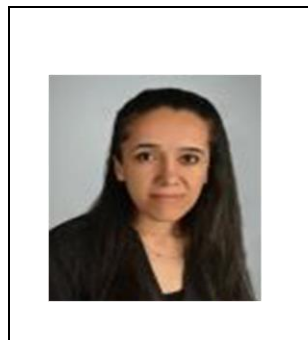
**Url-19**< [http://www.niu.edu/analyticallab/\\_pdf/ftir/FTIRintro.pdf](http://www.niu.edu/analyticallab/_pdf/ftir/FTIRintro.pdf)> date retrieved 15.09.2017.

**Url-20**<[www.polimaster.com](http://www.polimaster.com)> date retrieved 13.11.2017.





## CURRICULUM VITAE



**Name Surname:** Songül ULAĞ

**Place and Date of Birth:** Tunceli- 26/10/1990

**E-Mail:** ulag@itu.edu.tr

**Education:** Istanbul Technical University

**B.Sc.:** Physics Engineering

### PUBLICATIONS AND PRESENTATIONS:

1. T.Bel, S.Ulag, M.Muhammettursun, H. Cimenoglu, N.Baydogan, Preparation and Characterization of PMMA/MWCNT Polymer Nanocomposite, NanoTR-13 2017 - 13th Nanoscience & Nanotechnology Conference, Abstract Book, TUBES (Nanotubes) P-07-2811, pp.403.
2. T.Bel, M.Muhammettursun, S.Ulag, M.Ba Dughaiş, N. Yahya, H. Cimenoglu, N.Baydogan, Preparation And Characterization Of Pmma/Graphene Nanoplatelets Polymer Nanocomposite, 13th International Conference on Diffusion in Solids and Liquids - DSL2017, Mass Transfer, Heat Transfer, Microstructure & Properties, Nanodiffusion & Nanostructured Materials, Alternative Energy, Abstract Book, pp. 103-104, 26-30 June, 2017 – Vienna, Austria. (Invited Presentation)
3. T.Bel, H. Cakar, M.Muhammettursun, S.Ulag, M.Ba Dughaiş, N. Yahya, H. Cimenoglu, N.Baydogan, Investigation of the Bubble Effect in Lightweight PMMA Polymer, 13th International Conference on Diffusion in Solids and Liquids - DSL2017, Mass Transfer, Heat Transfer, Microstructure & Properties, Nanodiffusion & Nanostructured Materials, Alternative Energy, Abstract Book, pp. 101, 26-30 June, 2017 – Vienna, Austria.
4. T.Bel, M.Muhammettursun, S.Ulag, H. Cimenoglu, N.Baydogan, Physical Properties of Poly(Methyl Methacrylate)/Graphene Nanoplatelets Nanocomposite, NanoTR-13 2017 - 13th Nanoscience & Nanotechnology Conference, Abstract Book, GRAP OR-01-2840 pp. 144Antalya, Turkey, 2017.

## **RESEARCH PROJECTS:**

1. Responsibility: Scholarship, TUBITAK 1001 Research Project, Project No: 115R017, “Multy Phase Self Healing Nanocomposite Shielding Material Development and Investigation of Mechnical Properties”, 2015-Scientific and Technological Research Projects Funding Program
2. Responsibility: Researcher, ITU BAP MSc. Thesis Project, Project No: MYL-2017-40886, Istanbul Technical University Scientific Research Project; MSc. Thesis Project of Songul Ulag, 2017, “The Investigation of The Irratiation Effect on PMMA/MWCNTs Polymer Nanocomposites”.

